METABOLIC EFFECTS OF HYPOXIA AND CHRONIC HEPATITIS C

By

Dr TEEGAN REINA LIM

MBChB, MRCP, Postgrad (dip) in Gastroenterology

Student ID No: 1209946

A thesis submitted to the University of Birmingham for the degree of DOCTOR OF PHILOSOPHY

NIHR Liver Biomedical Research Unit

& Centre for Liver Research

Immunology and Immunotherapy

University of Birmingham

June 2017

Abstract

Hypoxia has been linked to the pathogenesis of hepatic steatosis in murine and human models. There is an abundance of data suggesting that HIFs play a central role in regulating hepatic lipid metabolism. This study suggested that hypoxia-induced hepatic lipid accumulation is through *de novo* lipogenesis and free fatty acid uptake, and is dependent on hypoxia inducible factors 1α and 2α. On the contrary, hepatitis C infection reduced *de novo* lipogenesis and free fatty acid uptake in both normoxic and hypoxic conditions *in vitro*, and this inhibition is viral strain-dependent. In the clinical setting, chronic hepatitis C (CHC) and non-alcoholic fatty liver diseases (NAFLD) are associated with hepatic steatosis and insulin resistance. Using an integrative physiological approach that measures lipid and carbohydrate flux *in vivo* we demonstrated that patients with CHC had modest increase in insulin resistance and that the relative contribution of tissue specific insulin sensitivity in patients with CHC and NASH varied. Furthermore, curing HCV infection improved hepatic and subcutaneous adipose tissue insulin resistance. The improvement in hepatic and adipose tissue insulin resistance was more pronounced in patients infected with genotype 3 HCV, whilst the improvement in skeletal muscle insulin resistance was more evident in genotype 1 infection, demonstrating a genotype-specific effect in the metabolic perturbation in CHC. Further studies are required to confirm that genotype specific effect of HCV on insulin resistance and its link with NASH.

DEDICATION

My thesis is dedicated to my beloved husband, Dave and my parents. Thank you for all your support, encouragement, love and patience. I also dedicate this to my children, Joshua and Aoife, for bringing me so much joy and happiness and for keeping me going when the going gets tough.

Acknowledgements

I would not have embarked on this project without the support and encouragement from Dr Chris Babbs, who was the programme director at North Western Deanery at the time. I am grateful for his encouragement and for the guidance he has shown me during my clinical training.

The work I presented here would not have been possible without the expertise and advise from many people at the University of Birmingham. Professor David Adams and Dr Zania Stamataki are two key individuals who inspired me in my academic career, and they continue to inspire me until today. I would like to express my deepest gratitude to my supervisors, Professor Jane McKeating and Professor Jeremy Tomlinson, who supported and motivated me throughout my PhD. I would also like to thank Professor Mutimer for his words of wisdom and guidance.

The clinical study would not have been possible without the staff at the NIHR clinical research facility. In addition, I would also like to express my gratitude to Nigel Davies and Robert Flintham for their relentless effort in making sure the clinical study was possible. Special thank you to Sally, Catherine, Kathie and Emma for assisting in the recruitment of patients in the clinical study.

I would like to thank my colleagues and friends at NIHR Centre for Liver Research (HCV group) and Centre for Diabetes, Endocrinology and Metabolism, who kept me going throughout the years. Specific mention to Ke, Matt Armstrong, Mick O'Reilly, Garrick Wilson, Laura Gathercole, Maryam Naisiri, Jonathan Hazlehurst and Iwona Bujalska. I have made some fantastic friends and will cherish them forever.

Finally I thank the funders, the Medical Research Council, and NIHR without which this project and the entire experience would not have been possible.

Table of Contents

List of figures

List of tables

Frequently used abbreviations

Akt	Protein kinase B
AMPK	5' AMP-activated protein kinase
CPT1A	Carnitine palmitoyl acyl-CoA transferase 1
CHC	Chronic hepatitis C
ChREBP	Carbohydrate responsive element-binding protein
DNL	*De novo* lipogenesis
FFA	Free fatty acid
FIH	Facotr inhibiting HIF
GSK-3	Glycogen synthase kinase 3
HCV	Hepatitis C virus
Hsp90	Heat shock protein 90
HIFS	Hypoxia inducible factors
HRE	Hypoxia-responsive elements
IL	Interleukin
IR	Insulin receptor
IRS	Insulin receptor substrate
MAPK	Mitogen-activated protein kinase
mTOR	Mammalian target of rapamycin
MTP	Microsomal triglyceride transfer protein
NAFLD	Nonalcoholic fatty liver disease
NASH	Nonalcoholic steatohepatitis
NEFA	Non-essential fatty acid
OSA	Obstructive sleep apnoea
PGC-1α	Proliferator-activated receptor-ϒ coactivator-1α
PHDs	Prolyl hydroxylases
PI3K	Phosphatidyl inositol-4,5-biphosphate-3-kinase
PPARα	Peroxisome proliferators-activated receptor alpha
ROS	Reactive oxygen species
RXRα	Retinoid X receptor alpha
SAT	Subcutaneous abdominal tissue
SREBP-1c	Sterol regulatory element binding protein 1c
SVR	Sustained virological response
TNF	Tumour necrosis factor
VEGF	Vascular endothelial growth factor
VLDL	Very low density lipoprotein

1.0 INTRODUCTION

1.1 General Introduction

1.1.1 Liver zonation and physiological oxygen gradient

The morphology and function of hepatocytes vary with position along the liver sinusoids from the portal triad (composed of the bile duct, portal vein and hepatic artery), to the central vein. They receive their supply of nutrients through the portal vein, and delivers metabolized products to other organs through the central vein. The hepatic artery located adjacent to the portal vein, within the portal triad, supplies the liver with blood enriched in oxygen. The directional flow of mixed oxygenated and deoxygenated blood towards the central vein of the hepatic lobule creates a physiological oxygen gradient from the periportal to the perivenular areas of the parenchyma, with an oxygen pressure of 60-65mmHg (~8%) to 30-35mmHg (~4%) (2, 3). The definition of 'normoxia' and 'hypoxia' depends on the normal oxygen tension to which the hepatocyte is exposed. Despite the variable oxygen tensions in the liver, a hypoxic response is rarely observed in a normal healthy liver (4, 5), but modest changes in oxygen tension that can occur in various liver diseases are enough to promote a hypoxic response that stabilizes HIFs (2, 6-8).

1.1.2 Liver zonation and metabolic functions

In 1996, Jungermann demonstrated that hepatocytes were specialized, and their function differed depending on their position along the porto-central axis of the liver cell plate (9, 10). Blood flow within the liver determines the organization of the anatomical unit of the hepatic parenchyma. The hepatocytes lined up in a sponge-like arrangement between the sinusoids show a remarkable heterogeneity with respect to the biochemical and physiological functions they perform. Hepatic glutamine synthesis (via glutamine synthetase) shows a very peculiar and stable pericentral localization in less than 3 rows of hepatocytes surrounding the central veins (11). This dynamic structural and functional heterogeneity is known as metabolic zonation (12). More recently, Harpern *et al* characterized the zonation profiles of all liver genes with high spatial resolution and found that around 50% of liver genes are significantly zonated. They also challenged the traditional binary classification of liver into periportal and pericentral hepatocytes and revealed multiple roles for the intermediate lobule coordinates (13). These include a spatial order of bile acid biosynthesis enzymes that matches their position in the enzymatic cascade. This structure carries out metabolic functions mostly through specialized hepatocytes, which either act in isolation, or together with non-parenchymal cells (14). The role for β-catenin in establishing metabolic zonation in the liver was based on the complementary distribution patterns of active β-catenin in perivenular hepatocytes seen in murine model (15). The zonal metabolic pathways affected by changes in β-catenin signaling include those mediating ammonia metabolism and glutamine synthesis (15, 16).

Glucose metabolism in the liver is based on the reversible shift between glycogen synthesis and degradation as well as between glycolysis and gluconeogenesis. It is thought that these shifts are not only regulated by blood levels of substrates and products, hormones and the activity of the autonomic nervous system (14, 17); but also by liver zonation. The model of metabolic zonation proposes that gluconeogenesis occurs predominantly in the periportal, and glycolysis in the perivenous hepatocytes; based on studies, which showed zonal distribution of glucogenic and glycolytic enzymes (18-20). It also became apparent that Wnt/b-catenin signaling plays a dominant role in controlling zonation of many aspects of carbohydrate metabolism (15, 21, 22). Findings on the possible zonation for lipid metabolism in the liver are more controversial (9, 23). This may be due to the relatively shallow gradients of pathway activities, and a greater variability in different physiological states. Gene expression study has shown higher expression of apolipoprotein CII, in the periportal region in mouse and this preferential localization was also seen in rats (24). Lipogenesis occurs predominantly in the perivenular region and fatty acid degradation in the periportal regions (9, 25). Cyp7a1-medicated synthesis of bile acids derived from cholesterol, showing clear PV zonation (25, 26), and the metabolism of several amino acids (25).

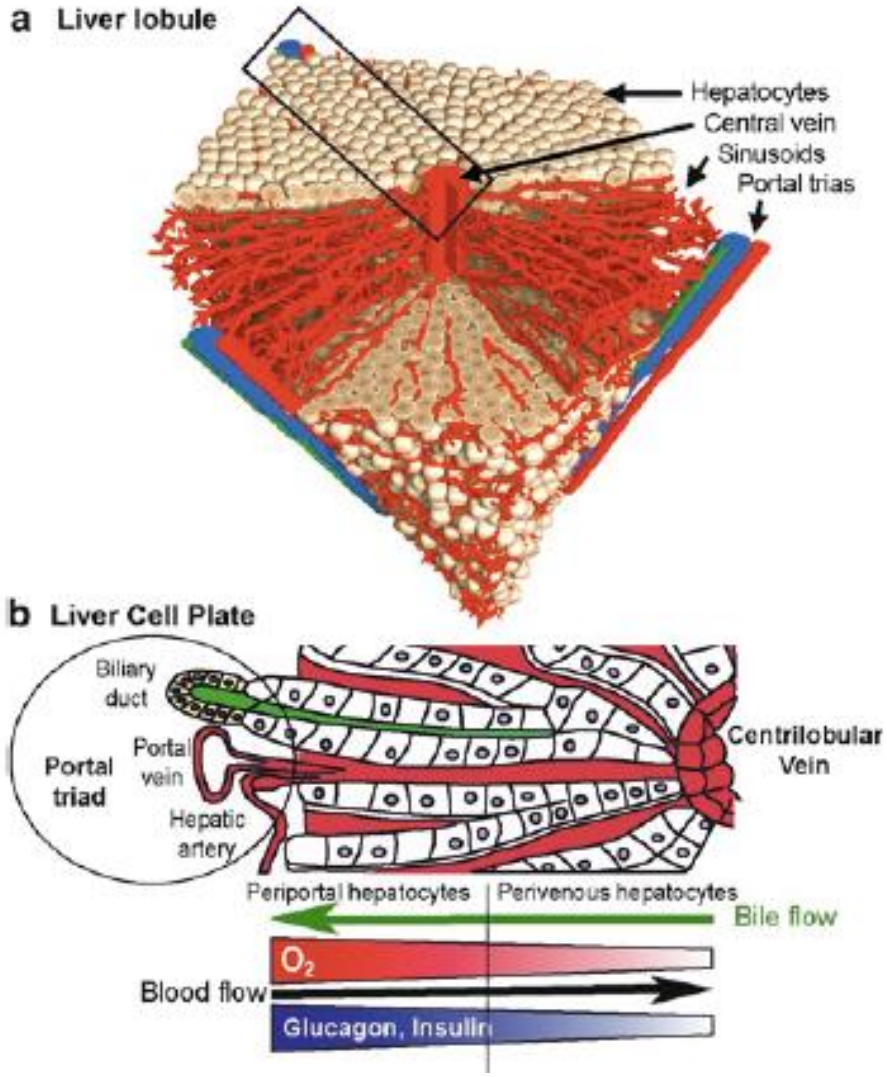

Colnot, S. et al. Molecular Pathology of Liver Diseases

Fig 1-1. Structure of the zonated liver lobule. (a) Three dimensional structure of the liver lobule. The liver lobule is centred around a branch of the centrilobular vein, limited at each end by the portal triad consisting of a branch of the portal vein, the hepatic artery, and a bile duct. (b) The liver cell plate, with blood circulation indicated in red. Bile is shown in green and circulates in the opposite direction to blood. The concentration of oxygen and hormones decreases along a continuous gradient from the periportal to the perivenular area.

1.1.3 Hypoxia-inducible factors (HIFs) and their regulation

Hypoxia-inducible factors (HIFs) are transcription factors that respond to changes in available oxygen in the cellular environment. There are three HIF transcription factors (HIF1, HIF2 and HIF3) that act as heterodimers comprising of alpha and beta subunit.

Oxygen-dependent regulation of HIFs

The alpha subunit is regulated via oxygen-induced proteolytic degradation, whereas the beta subunit is constitutively expressed. Under normoxia, HIF1α is hydroxylated by proline hydroxylases (PHD1, 2 and 3) in the presence of oxygen, Fe2+, 2-oxoglutarate (2-OG) and ascorbate. Hydroxylated HIF1α (OH) is recognised by pVHL (the product of the von Hippel–Lindau tumour suppressor gene), which, together with a multi-subunit ubiquitin ligase complex, tags HIF1α with polyubiquitin; this allows recognition by the proteasome and subsequent degradation [Fig 1-2]. Acetylation of HIF1α also promotes pVHL binding (27). Under hypoxia, PHD activity is reduced and hydroxylation is impaired and HIFα is stabilized, and translocated into the nucleus to form HIF complex, which then binds to hypoxia-responsive elements (HRE) to promote transcription (28). Certain pathological conditions expose the liver to extended periods of low oxygen, resulting in a HIFα dependent feedback loop which increases PHD expression, leading to a reactivation of HIFα hydroxylation and degradation (29). HIF1α expression can represent an acute response to low oxygen pressure,

whereas HIF2α levels may increase over time in hypoxia and play a role during chronic hypoxia (30).

PHDs belong to the family of deoxygenase enzymes that require oxygen, iron and 2-OG for their catalytic activity. They have low affinity to oxygen, which is about 2 to 10 times higher than physiological oxygen concentrations that enable the enzymes to act as oxygen sensors (31). Isoforms PHD1, PHD2 and PHD3 and their substrates are known to be quite diverse and isoform-specific (32). PHD2 is considered critical in regulating the HIF pathway, although its hydroxylase activity is also necessary for regulating other signaling pathways including cofilin phosphorylation and the NDRG3 protein degradation (33, 34). PHD1 and PHD3 have also been shown to regulate HIFs and that, at least for PHD3, the contribution may be as great or greater than that of PHD2 under appropriate conditions (35). Aprelikova *et al* examined the roles of HIF factors on HIF target genes and found that PHD2 was specifically induced by HIF1α, whereas PHD3 was responsive to HIF2α as well as HIF1α (36).

In addition to HIF, factor inhibiting HIF (FIH) also regulates HIF1α expression. FIH hydroxylases an asparaginyl residue in the C-terminal transactivation domain of HIF1α (N803) and inhibits the binding of the heterodimer of HIF1α to its transcriptional coactivator p300 (37). It is thought that PHD inactivation occurs under moderate hypoxia, and both PHD and FIH inactivation occur under severe hypoxia (38).

Oxygen-independent regulation of HIFs.

In addition to the above regulators of HIF activity, other factors such as growth factors, cytokines and signaling molecules can stabilize HIFα subunits in the presence of oxygen – a phenomenon known as 'pseudohypoxia' [Fig 1-3]. Activation of phosphatidyl inositol-4,5-bisphosphate-3-kinase (PI3K) upregulates HIF1α protein translation (39-41). PI3K regulates protein synthesis through its target protein kinase B (Akt) and downstream component mammalian target of rapamycin (mTOR). Certain growth factors activate RAS which in turn stimulates RAS/RAF/MEK/ERK kinase cascade (40). It has also been reported that inhibitors of heat shock protein 90 (Hsp90) could nullify HIF1α levels regardless of the availability of oxygen (42). Hsp90 binds directly to HIF1α to induce conformational changes in its structure, which couples with HIF1β to initiate its transactivation (43). Hsp90 can also stabilize HIF1α against its non-VHL dependent degradation.

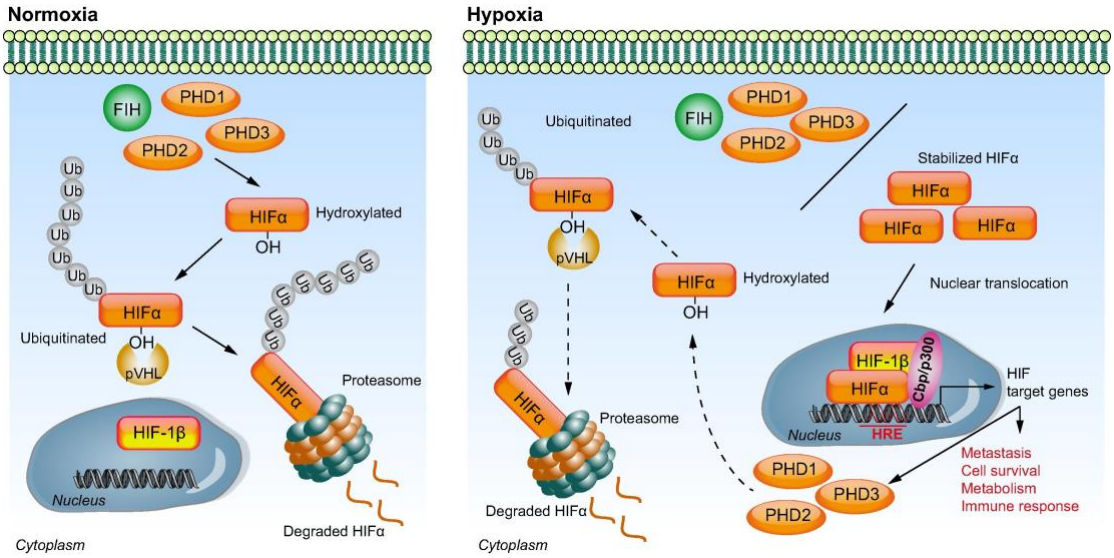

Fig 1-2. Oxygen-dependent HIF signaling. Under normal oxygen tension, the cellular oxygen sensors prolyl hydroxylases (PHD1–3) and factor inhibiting HIF (FIH) hydroxylate specific residues of HIFα subunits (HIF1α and 2α for PHDs and HIF1α for FIH). Hydroxylated HIFα is recognized by the von Hippel-Lindau (pVHL) E3 ubiquitin ligase that polyubiquitinates HIFα resulting in proteasomal degradation. Under low oxygen, PHD and FIH activity is inhibited resulting in stable HIFα expression and nuclear translocation where it dimerizes with its beta subunit. With the help of co-activators, including Cbp/p300, the HIF complex acts a transcription factor by binding to specific DNA sequences defined as hypoxia responsive elements (HREs), activating the transcription of genes involved in an array of signaling events including tumour metastasis, cell survival, metabolism and immune functions. The HIFα signaling pathway is self-regulatory, nuclear HIF-1α promotes PHD expression resulting in a negative feedback loop that ensures the pathway is not constitutively active. *Wilson et al. Journal of Hepatol 2014 (1).*

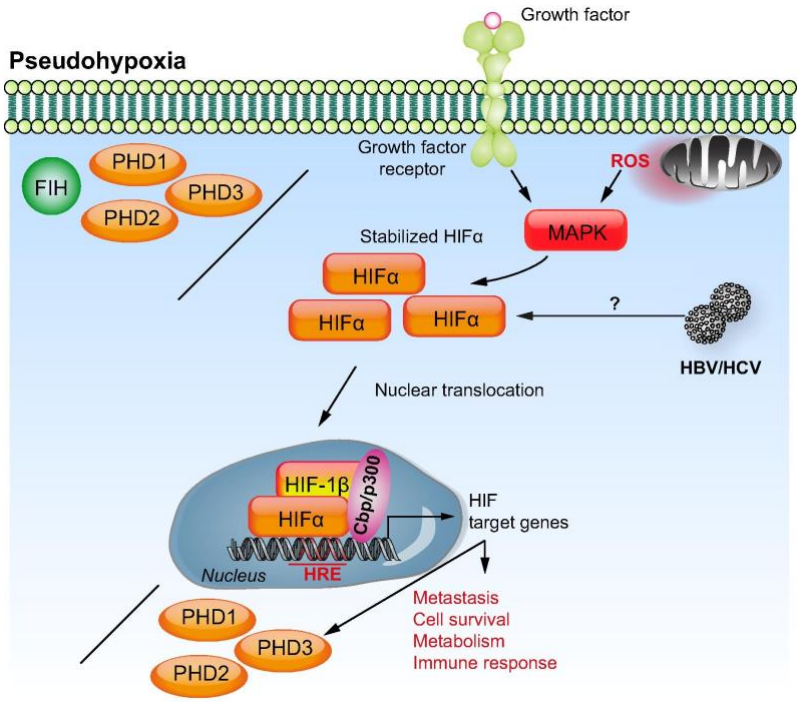

Fig 1-3. Oxygen-independent HIF signaling. HIFα can be constitutively expressed irrespective of oxygen tension due to loss of PHD and FIH function, a state defined as pseudohypoxia. This can occur as a result of virus infection or aberrant kinase signaling. For example, binding of a growth factor to its cognate receptor activates the MAPK pathway that stabilizes HIFα. Similarly mitochondrial dysfunction can promote reactive oxygen species (ROS) production that acts on MAPK to stabilize HIFα. *Wilson et al. Journal of Hepatol 2014 (1).*

1.1.4 Lipid metabolism and insulin resistance

Lipid flux in the liver

Triglycerides are formed from the esterification of three non-esterified fatty acids (NEFA) to a glycerol backbone. Five major pathways determine liver fat volume: (i) the uptake of free fatty acids (FAs) and triglycerides from the diet; (ii) *de novo* lipogenesis (DNL); (iii) FAs oxidation; (iv) the export of triglycerides as very low density lipoprotein (VLDL) into the bloodstream; and (v) the flux of FAs released from adipose tissue through lipolysis. Dietary fats are taken up by the intestine and packaged into chylomicrons for delivery to the systemic circulation. The majority of the triglyceride in the chylomicrons is hydrolysed to release NEFA for peripheral uptake. Approximately 20% is delivered directly to the liver (44) [Fig 1-4].

Lipogenesis is the process by which intramitochondrial acetyl-CoA is converted to fatty acids. Acetyl-CoA can be derived from the degradation of carbohydrates and a number of amino acids. It encompasses both the processes of fatty acid and triglyceride synthesis (where fatty acids are esterified with glycerol to form fats) (45). The products are then secreted from the liver in the form of VLDL. Insulin stimulates sterol regulatory element binding protein-1c (SREBP-1c), whereas glucose stimulates carbohydrate responsive element-binding protein (ChREBP). Both of these transcription factors promote DNL, a highly regulated pathway that converts excess carbohydrate into fatty acids that are then esterified to storage

triacylglycerols. SREBP-1c and ChREBP promote DNL via activation of key rate-limiting enzymes, namely acetyl-CoA carboxylase (ACC) and fatty acid synthase (FAS) (44, 46).

β-oxidation is the catabolic process by which fatty acid molecules are broken down to generate acetyl-CoA (47). Fatty acids primarily enter a cell via fatty acid protein transporters on the cell surface. Once inside, fatty acyl-CoA synthase (FACS) adds a CoA group to the fatty acid. Carnitine palmitoyltransferase 1 (CPT1) then converts the long-chain acyl-CoA to long-chain acylcarnitine. The fatty acid moiety is transported by carnitine translocase (CAT) across the inner mitochondrial membrane. CPT2 then converts the long-chain acylcarnitine back to long-chain acyl-CoA. The long-chain acyl-CoA can then enter the fatty acid β-oxidation pathway, resulting in the production of one acetyl-CoA from each cycle of β-oxidation. This acetyl-CoA then enters the tricarboxylic acid (TCA) cycle. NEFA are released from adipose tissue in the fasting and insulin resistant states via lipolysis. Lipolysis is the hydrolysis of NEFA and glycerol from triglyceride.

Hepatic steatosis occurs when an excess of triglyceride accumulate in hepatocytes, which arises from an imbalance between triglyceride synthesis (uptake) and utilization (export). This can result from an excess in the delivery of NEFA via adipose tissue lipolysis as a consequence of (1) adipose insulin resistance and/or excess dietary consumption, (2) excess in endogenous synthesis via DNL, (3) decrease in FFA breakdown via β-oxidation in the mitochondria, or (4) decreased export via packaging with apolipoprotein (apo-B) into VLDL.

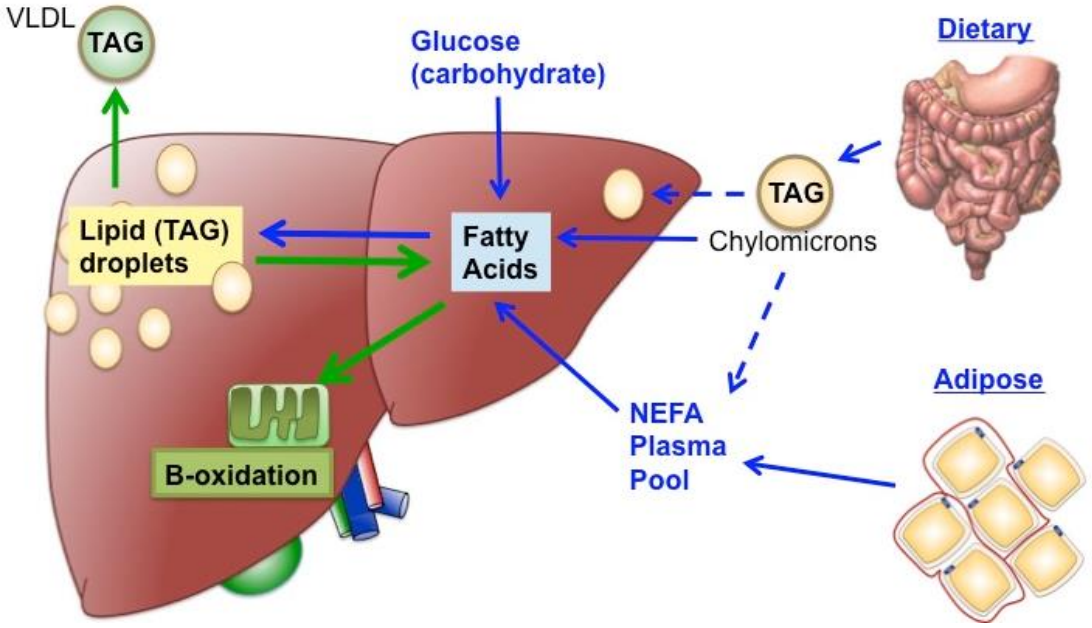

Fig 1-4. Model of lipid flux in the liver. DNL indicates new fat synthesis from dietary carbohydrate; chylomicrons are lipoproteins made in the intestine, which carry dietary fat. TAG=triglyceride, VLDL=very low density lipoprotein, NEFA=non-essential fatty acid.

Insulin receptor signaling pathway and insulin resistance

Insulin is synthesized in the β cells of the pancreatic islets and is the major hormone controlling critical energy functions such as glucose and lipid metabolism. Insulin activates the insulin receptor (IR) tyrosine kinase, which phosphorylates and recruits different substrate adaptors such as the insulin receptor substrate (IRS) family of proteins. Tyrosine phosphorylated IRS then displays binding sites for numerous signaling partners. Among them, phophoinositide 3-kinase (PI3K) has a major role in insulin function, mainly via the activation of the Akt/Protein kinase B (PKB) and the PKCζ cascades. Activated Akt induces the translocation of glucose transporter type 4 (GLUT-4) from intracellular compartments to the cell surface where it is required for glucose uptake (48). Akt also induces glycogen synthesis through inhibition of glycogen synthase kinase 3 (GSK-3); protein synthesis via mammalian target of rapamycin (mTOR) and downstream elements [Fig 1-5]. Akt phosphorylates and directly inhibits FoxO transcription factors, which regulate metabolism and autophagy. Inversely, 5' AMP-activated protein kinase (AMPK) is known to directly regulate FoxO3 and activate transcriptional activity.

There are several mechanisms underlying increased glucose production. These include production of free glucose by increased glycogenolysis in the liver, increased gluconeogenesis, activation of forkhead box transcription factor (FoxO1) and insulin-glucagon hormonal imbalance (49). Several factors contribute to elevated gluconeogenesis in diabetes, namely increased supply of

glucogenic precursors to the liver (glycerol, amino acids, free fatty acids), increased lipid content, increased cytokines and adipokines, and decreased insulin receptor (IR) signaling in hepatocytes (49). Accumulation of ectopic lipid metabolites, activation of the unfolded protein response (UPR) pathway, and innate immune pathways have all been implicated in the pathogenesis of insulin resistance (50). UPR, also known as endoplasmic reticulum stress response is initiated with the accumulation of unfolded proteins with the ER lumen. Activation of the UPR provides cells the ability to adapt to different physiological demands, which can sometimes be overwhelmed in insulin resistant states (51, 52), or be maladaptive (53).

The effects of insulin vary according to the physiological function of the tissues and organs. Tissues defined as insulin dependent, based on intracellular glucose transport, are principally skeletal muscle and adipose tissue. Glucose uptake into skeletal muscle is via GLUT4, and accounts for 60-70% of whole-body insulin mediated uptake (54). In the fed state insulin promotes glycogen synthesis via activation of glycogen synthase. Muscle cells do not rely on glucose for energy during the basal state, when insulin levels are low. Insulin suppresses protein catabolism while insulin deficiency promotes it, releasing amino acids for gluconeogenesis. In insulin resistance, muscle glycogen synthesis is impaired, and this results in reduced intracellular glucose translocation (55).

Glucose uptake into adipocytes in the postprandial state is also via GLUT4, and it is estimated to account for 10% of whole-body insulin-mediated glucose uptake (54). In adipose tissue, insulin stimulates glucose uptake, promotes lipogenesis

and suppresses lipolysis, and promotes free fatty acid flux into the bloodstream. Similar to muscle cells, adipocytes do not rely on glucose in the basal state, and intracellular energy is supplied by fatty acid oxidation in insulin-deficient states. In insulin resistance, there is increased free fatty acid availability and delivery to the liver, promoting hepatic VLDL production (56). Lipoprotein lipase activity is insulin-dependent and suppressed in insulin resistance, and peripheral uptake of triglycerides from VLDL is also diminished. In addition to FFAs, adipose tissue also secrete cytokines which worsen insulin resistance, such as interleukin (IL)-6, tumour necrosis factor (TNF)-6, plasminogen activator inhibitor (PAI)-1, angiotensinogen and leptin (57).

In the liver, glucose uptake is not insulin dependent, and accounts for 30% of whole body insulin-mediated glucose disposal (54). GLUT-2 is highly expressed in the liver, and can efficiently transport glucose (58, 59). Insulin mediates glycogen and protein synthesis and lipoprotein metabolism (60). It also inhibits gluconeogenesis. Alteration in lipoprotein metabolism is a major hepatic component of insulin resistance, resulting in increased FFA delivery, reduced VLDL catabolism by insulin resistant adipocytes, and subsequently increased hepatic triglyceride synthesis (61).

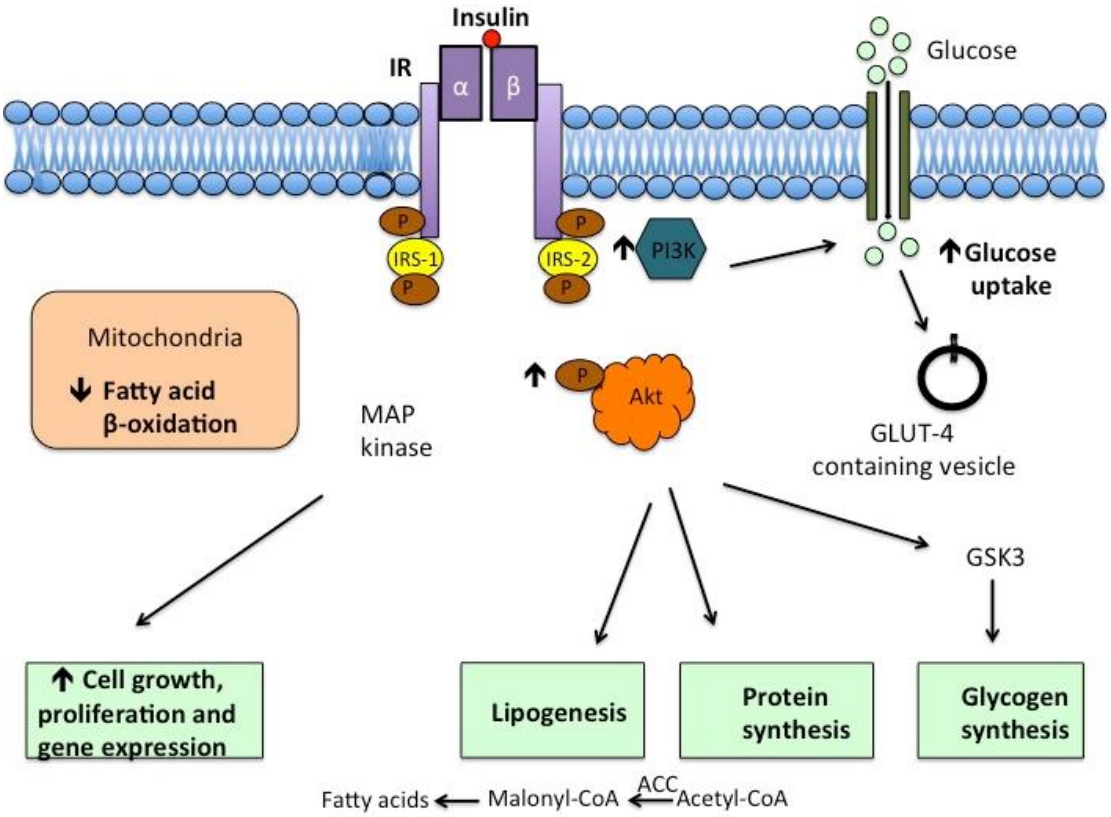

Fig 1-5. Insulin and its mechanism of actions. Insulin binds to α-subunit of the insulin receptor, resulting in a conformational change in the membrane-bound tyrosine kinase domains on each β-subunit. The tyrosine kinase activity causes phosphorylation of the MAP-kinase and PI-3K kinase responsible for expressing the mitogenic and metabolic actions of insulin. MAP=mitogen-activated protein kinase; PI-3K=phosphoinositide 3-kinase; IR= insulin receptor, IRS=insulin receptor substrate; P=phosphate; ACC=acetyl co-A carboxylase; GSK3= glycogen synthase kinase-3

1.2 HIFs and hepatic lipid accumulation

Metabolism under hypoxia is significantly different from that under normoxia. It has been well elucidated that HIFs play a central role in regulating lipid metabolism under hypoxia (2, 62). Increased *DNL* coupled with an increase in FFA uptake has also been shown in perivenular cells in mice (63), supporting a role for low oxygen in the regulation of hepatic lipid metabolism. The role and contribution of HIF1 and HIF2 in steatosis have also been explored. HIF1α promotes LDL and VLDL uptake through the regulation of VLDL receptor gene expression under hypoxia (64). More recently, HIF1α and HIF-2α have been shown to be critically involved in hypoxia-induced lipid accumulation in hepatocytes through the reduction of proliferator-activated receptor-ϒ coactivator-1α (PGC-1α)-medicated fatty acid β-oxidation (65). Activation of HIF1α in ethanol-fed cre-lox mouse model induced hepatocyte steatosis and increase in triglyceride levels, and HIF1α deletion prevented lipid accumulation (5). On the contrary, Nishiyama *et al.* showed that there was an increase in lipid accumulation in hepatocyte specific HIF1α knockout mice fed an ethanol diet (66), whilst Kim *et al.* reported that activating HIF1α or HIF2α had a minimal effect on lipid accumulation (67). Therefore the contribution of HIF1α or HIF2α in promoting hepatic lipid accumulation remains to be elucidated.

Obstructive sleep apnoea (OSA) is a condition defined by recurrent obstruction of the upper airway during sleep leading to apneic-hypopnoeic episodes. The prevalence of metabolic syndrome in severe OSA is as high as 80%. In addition, those with severe OSA are three times more likely to develop metabolic

syndrome, after adjustment for body mass index (BMI) (68). Emerging evidence suggests that OSA may play a role in the progression of hepatic steatosis and NASH and it has been linked to the elevation of liver enzymes and the development of hepatic steatosis, lobular necrosis and fibrosis by liver biopsy, which was associated with increased morbidity and mortality (69-71). Treatment of OSA with continuous positive airway pressure (CPAP) may have beneficial effect on lipid profile (72-74). Results from animal studies unambiguously show that intermittent hypoxia is a direct cause of hyperlipidaemia and that it increases total cholesterol, HDL-C and triglycerides after 5 days, and LDL cholesterol after 4 weeks (75, 76). The level of hyperlipidaemia correlates to the severity of the hypoxic stimulus (76). Others have also linked the severity of nocturnal hypoxia and progression from fatty liver to non-alcoholic steatohepatitis (77, 78). Intermittent hypoxia induces dyslipidaemia via the (1) upregulation of key hepatic transcription factor of lipid biosynthesis SREBP-1c, SREBP-1c-regulated enzyme and sterol coenzyme A desaturase 1 (SCD-1) (75, 76, 79, 80); (2) induction of adipose tissue lipolysis (81) and (3) inhibition of VLDL clearance, by suppressing lipoprotein lipase activity (82).

1.3 CHC, steatosis and insulin resistance

1.3.1 Hepatitis C viral structure and life cycle

Hepatitis C virus (HCV) is a hepatotropic RNA virus of the genus Hepacivirus in the *Flaviviridae* family. HCV is a positive-sense, single-stranded enveloped RNA virus approximately 9600 nucleotides in length. Due to the error prone RNA polymerase, HCV displays remarkable genetic diversity that promotes viral escape from host immune responses and antiviral drugs (83). There are 6 major HCV genotypes (1-6) that vary by over 30% in nucleotide sequence (84). The HCV open reading frame encodes a single polyprotein that is cleaved by host and viral proteases into 10 individual viral proteins with various characteristics (85).

The structural proteins consist of core protein, E1, E2 and ion channel protein p7 [Fig 1-6]. HCV core is the viral nucleocapsid protein with numerous functions including: RNA binding, immune modulation, cell signaling, oncogenic potential and autophagy. The core protein associates with the lipid droplets and directs particle assembly that includes the incorporation of E1 and E2 envelope. The HCV envelope glycoproteins are targets for the humoral immune response and the resulting neutralizing antibodies can exert a selective pressure on viral quasispecies (86-88). The small ion channel protein p7 is required for viral assembly and release. Non-structural proteins consist of NS2, NS3, NS4A, NS4B, NS5A and NS5B and are the minimal viral proteins components required for RNA replication (89, 90). The C-terminal of NS3 is a superfamily 2 helicase that is essential for virus replication (91). NS4A is a transmembrane protein that acts as

a cofactor for NS3 protease, and is important in the regulation of replicase activity (92, 93). NS4B contains multiple transmembrane segments and remodels the endoplasmic reticulum membrane (94), a common feature of many positive-strand RNA viruses (95). NS5A is a multifunctional zinc-binding phosphoprotein, which has become a promising drug target (96). NS5B is the RNA-dependent RNA polymerase with a C-terminal membrane-anchoring segment (97).

The assembly of HCV requires a platform of cellular lipid droplets and interactions between NS5A and the core protein (98) (Fig 5). Thus, most HCV-associated metabolic alterations in hosts involve core (99-104) and NS5A (105-108) proteins. Assembled particles bud into the endoplasmic reticulum (ER) and traffic through the secretory pathway, from which they are exported from the cell in conjunction with lipoprotein secretory pathways (109, 110) [Fig 1-7].

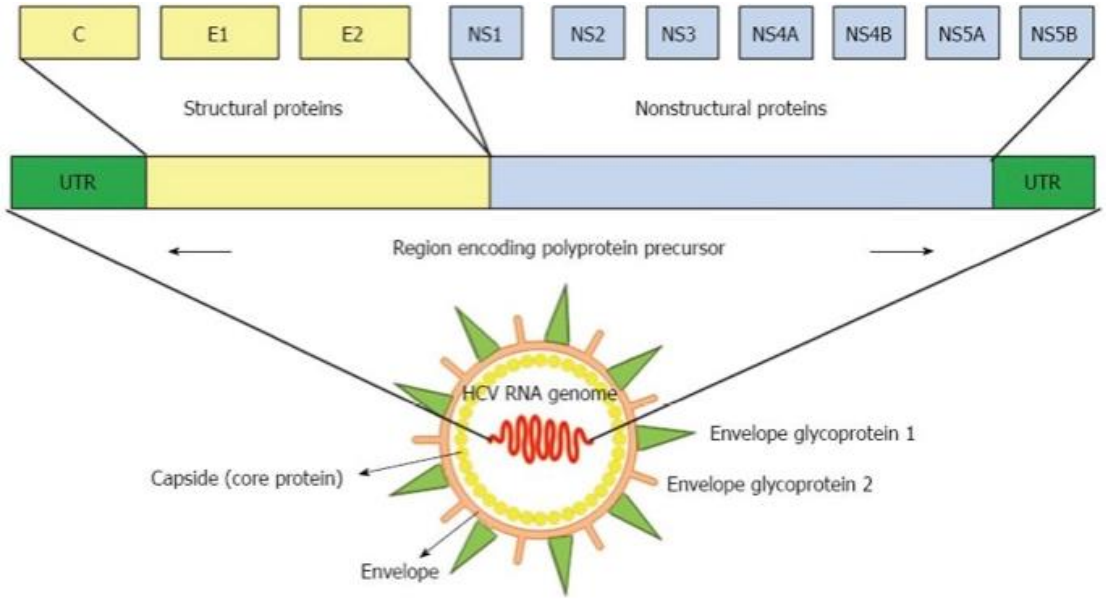

Chang ML World J Gastroenterol 2016

Fig 1-6. Hepatitis C viral genome. Hepatitis C virus is a single-stranded RNA virus, and its genomic organization shows highly conserved 5' and 3' non-structural proteins. UTR=untranslated region, C=core protein, E1 and E2=envelope glycoprotein 1 and 2, NS=non-structural protein.

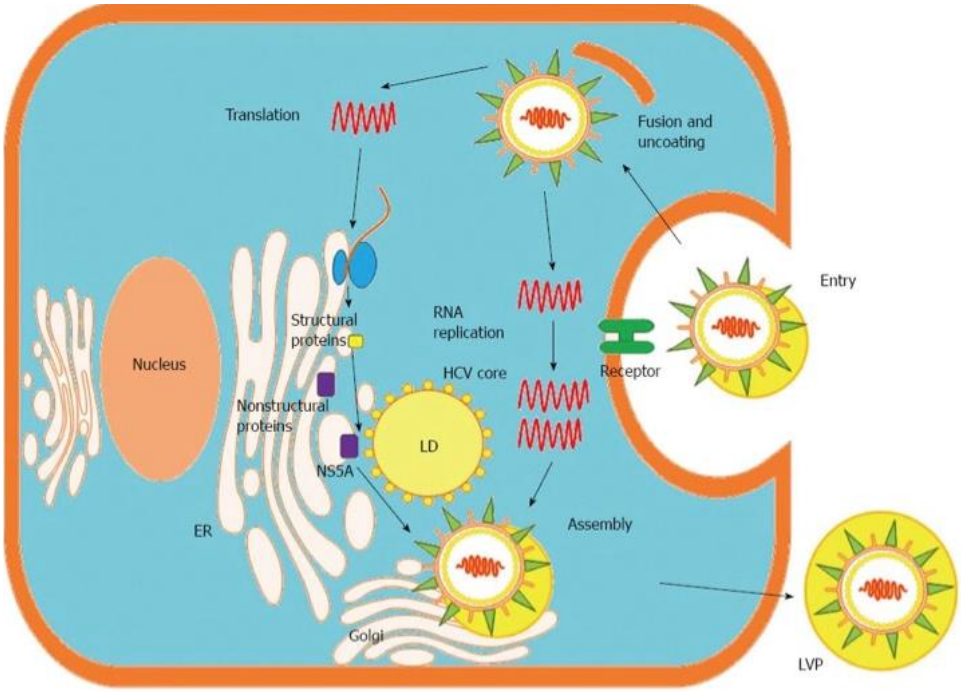

Chang ML World J Gastroenterol 2016

Fig 1-7. Life cycle of hepatitis C virus in the hepatocyte. HCV LVPs enter hepatocytes via receptor-mediated endocytosis. Released viral RNA is translated at the endoplasmic reticulum (ER), producing a single polyprotein precursor that is cleaved by host and viral proteases. The viral NS proteins form RNA replication complexes in lipid rafts, where positive-strand RNA is replicated via a negative-strand intermediate. Newly synthesized positive-strand RNA is encapsidated by the HCV core protein in close proximity to LDs, and envelope glycoproteins are acquired through budding into the ER lumen. LVPs mature in the ER through interactions with lipoproteins and exit the cell via the cellular golgi apparatus. LD=lipid droplet, LVP=lipoviral particle, Golgi=golgi apparatus

1.3.2 Mechanisms of HCV-induced lipid accumulation.

The association of HCV infection and steatosis is shown in studies demonstrating that the virus hijacks the lipid-producing machinery of hepatocytes for its benefit (106, 111). The HCV core protein has been studied at length in both cell culture and in transgenic mice. Intracellular lipid build-up seems to occur when HCV core protein is highly expressed (111). The core protein localizes at the surface of lipid droplets within the cytoplasm in cells transfected with HCV (112). HCV core protein-transgenic mice develop hepatic steatosis due to impaired β-oxidation caused by mitochondrial damage (113). Amongst individuals with CHC, those with genotype 3 CHC have the highest prevalence of hepatic steatosis (114). The proposed mechanisms for this are outlined below.

Increased de novo lipogenesis

In vitro, core protein interacts with the cell machinery involved in lipid metabolism such as apolipoproteins A1 and A2, which are involved in triglyceride accumulation and storage in the hepatocytes (111). HCV core protein also up-regulates sterol regulatory element binding protein 1c (SREBP-1c), a transcriptional factor that mediates several lipogenic genes in lipid metabolism (115-117) as well as binds to DNA-binding domain of retinoid X receptor alpha (RXRα), a nuclear receptor that regulates several genes involved in cellular lipids synthesis, thus promoting DNL (103).

Decreased VLDL secretion

HCV core protein also inhibits microsomal triglyceride transfer protein (MTP) activity. As this is a rate-limiting enzyme playing a key role in the very low density lipoproteins (VLDL) assembly, the direct and likely consequence of its inactivation is accumulation of unsecreted triglycerides, hence steatosis (118). Core protein may also accumulate in mitochondria, impairing electron transport and thus increasing the production of oxygen reactive species (ROS) (119). Oxidative stress leads to peroxidation of lipids and structural proteins, disturbing the cellular traffic apparatus and VLDL secretion (120).

Decreased fatty acid oxidation

Recent studies have demonstrated a diminished PPARα (peroxisome proliferators-activated receptor alpha) expression induced by HCV core protein (121, 122). PPARα regulates the transcription of mitochondrial carnitine palmitoyl acyl-CoA transferase 1 (CPT1A), which is a rate-limiting enzyme in mitochondrial β-oxidation mediating the entry of fatty acids into the mitochondria. Other studies have shown that HCV interact with mitochondria to induce reactive oxygen production (123) and also the α and β-subunits of the mitochondrial trifunctional protein, both thought to decrease β-oxidation. Human studies confirmed these *in vitro* findings by showing that HCV-infected patients had lower total ketone body concentration than their healthy uninfected counterparts (124), indicating that mitochondrial lipid β-oxidation is impaired in

livers of HCV-infected patients, because ketogenesis is a liver-specific metabolism that occurs in mitochondria and is directly coupled to mitochondrial lipid β –oxidation [Fig 1-8].

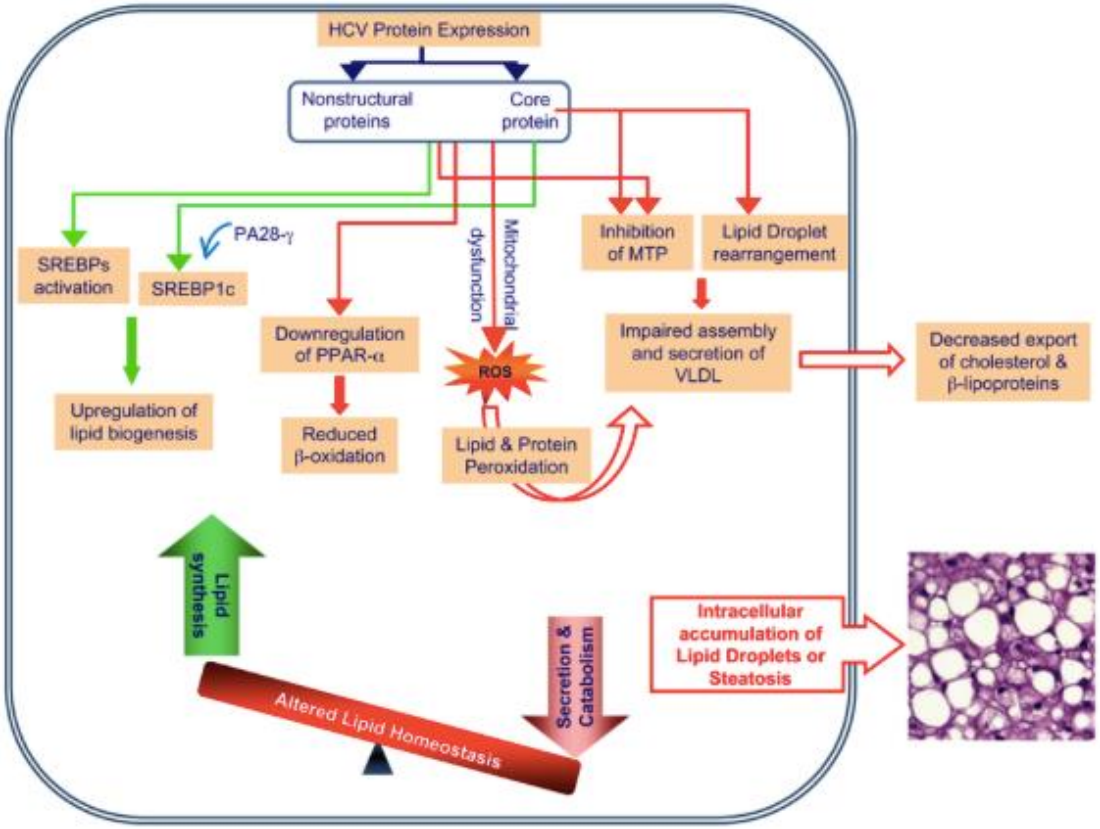

Gulam et al. Trends in Endocrinology and Metabolism. 2009

Fig 1-8. HCV-induced alterations in lipid metabolism and steatosis. SREBP-1c =sterol regulatory element binding protein 1c, PPARα = peroxisome proliferators-activated receptor alpha, MTP = microsomal triglyceride transfer protein, VLDL =very low density lipoproteins.

1.3.3 Mechanisms of HCV-induced insulin resistance

HCV directly perturbs insulin signaling by modulating the insulin receptor and IRS-1 and down-regulating PI3K (125). HCV core protein expression in hepatocytes upregulates Ser312 phosphorylation status of IRS-1 and modulates downstream Akt activity by inhibiting Thr308 phosphorylation (126). Ser312 and Ser1101 phosphorylation of IRS-1 inhibits its association with the insulin receptor, promoting its degradation (127), and subsequently blocking Tyr-phosphorylation of IRS-1 and Thr308 phosphorylation of Akt for the inhibition of glucose uptake. Knockout of the IRS-1 and 2 genes in murine models induces insulin resistance and compensatory hyperinsulinaemia, indicating the importance of IRS-1 and 2 as mediators of insulin action (128, 129). Down-regulation of IRS-1 and IRS-2 was also seen in HCV core-transgenic mice livers (130).

HCV also induces insulin resistance via the up-regulation of suppressor of cytokine signaling-3 (SOCS-3), SOCS-7, TNFα and proteasome-activator 28-gamma (PA28γ), and down-regulation of peroxisome proliferator-activated receptor-gamma (PPARγ) (130-132). HCV core protein of HCV genotype 3a promotes IRS-1 degradation through the downregulation of PPARγ and by upregulating the SOCS7, and the core protein of genotype 1b activates mTOR (131). In addition, HCV activates mTOR/S6K1 signaling pathway in inhibiting IRS-1 function and perturbs glucose metabolism via downregulation of GLUT4 (127). Knobler and Schattner have suggested that CHC patients with more severe liver diseases may have an exaggerated intrahepatic TNFα response, resulting in

insulin resistance and a higher risk of developing diabetes (133). TNFα induces insulin resistance by interfering with the insulin signaling pathway, particularly inhibiting tyrosine phosphorylation of the insulin receptor and IRS-1 in adipocytes (134) and inhibiting the effect on insulin action in the liver (132, 135, 136). This ultimately results in a reduction in glucose uptake in muscle, and an increase in hepatic glucose production.

In human studies, liver biopsy specimens obtained from non-obese, non-diabetic HCV-infected patients demonstrated that HCV inhibited the insulin-stimulated tyrosine phosphorylation of hepatic IRS-1, resulting in inhibition of the PI3K-Akt pathway (125, 130). Other studies proposed that impairment of fatty acid β-oxidation was responsible for the hepatic steatosis associated with CHC (124). There have been reports that HCV genotypes might play an important role in deciding the pathway by which it impairs insulin signaling.

The target tissues of HCV-related metabolic disturbances are thought to be not just the liver [19], but also skeletal muscle (137, 138). Some studies showed that patients with CHC without fibrosis and metabolic syndrome had an endogenous glucose production more than three times the normal and an abnormal muscle uptake of glucose, with a normal suppression of lipolysis (137). The presence of hepatic insulin resistance results in an increase in glucose production, while peripheral insulin resistance results in a reduction in glucose uptake. Vanni *et al*. confirmed the predominant role of muscle in the development of insulin resistance, with an approximate 80% of peripheral contribution, demonstrating a higher glucose disposal during clamp in controls compared to patients with

CHC (137). It is evident that the insulin resistance in CHC is different, but often super-imposed to the host metabolic derangements and that the two conditions influence and enhance each other.

1.3.4 Clinical implications of HCV-induced hepatic steatosis and insulin resistance

Several epidemiological studies report that metabolic disease was more prevalent in patients with CHC than in those without (139). These results were confirmed by several other cross-sectional studies linking CHC with insulin resistance (140-143). The degree of insulin resistance has been shown to correlate with the grade of inflammation in HCV infected patients (144). HCV-induced insulin resistance impacts on treatment response to interferon-based therapy and exacerbates hepatic fibrosis, leading to hepatocellular carcinoma (145).

An association between steatosis and the severity of fibrosis has been observed irrespective of HCV genotype (146-149). Fartoux *et al*. showed that while insulin levels were predictive of fibrosis in their univariate analysis, subsequent multivariate analysis confirmed steatosis, but not insulin levels, to be independently associated with fibrosis (150). Steatosis is associated with increased production of reactive oxygen species which initiate lipid peroxidation, resulting in hepatic stellate cell activation (151). However, in non-CHC aetiology

such as NASH, disease progression is recognised as being slower than that observed in patients with CHC and steatosis. Thus it is likely that the coexistence of HCV and steatosis aggravates and accelerates the injury induced by each alone. In this setting, hepatic inflammation induced by the host response, together with the increased production of several proinflammatory and profibrotic cytokines, provide the substrate for the "second hit" in the steatotic liver. Also, the ability of the virus itself to induce oxidative stress and promote lipid peroxidation may further aggravate the pathogenic process induced by steatosis. It is also plausible that fat may render HCV infected liver more vulnerable to injury. Livers with steatosis are more sensitive to TNFα mediated inflammation and liver injury (152). Moreover, in HCV livers with steatosis, apoptosis activity has been noted to be increased compared with infected livers without steatosis (153).

1.4 HIFs and Chronic hepatitis C

The studies on HIFs in CHC started from models exploring the role of viral oncogenesis (154-158). HIF activity is induced in response to viral infection, but accumulating evidence suggests that the net consequence can favour the pathogen rather than the host. Certain viruses have evolved mechanisms to stabilize HIF1α to exert an anti-apoptotic effect that promotes survival of the infected cell (155, 159-161). Hepatitis C virus stabilizes HIF1α and promotes a pseudohypoxic state (6, 162). HCV-infected Huh-7 cells release angiogenic factors such as vascular endothelial growth factor (VEGF) as a consequence of

HIF1α stabilization (6, 8, 163, 164), and this is mediated by HCV core protein (165). Hypoxia also promotes HCV replication, and inhibition of HIF1α activity reduced viral replication, suggesting a key role for HIF-regulated genes in potentiating the HCV lifecycle (8, 166).

Recent development of high-troughput metabolomics has provided new insights into how viruses disrupt metabolic homeostasis (167, 168). Metabolic profiling of HCV infected cells revealed a shift from a catabolic to an anabolic state, promoting the survival of infected cells (169). Ripoli *et al.* demonstrated that HCV protein expression activated HIF1α, and as a consequence, upregulated the expression of HIF-controlled genes, including those coding for glycolytic enzymes (162). Given the role of HIF1α in regulating lipid and glucose metabolism (170, 171) and that the liver microenvironment is affected by hypoxia (2, 9, 172), HCV stabilization of HIF1α may have a positive effect on viral replication via the induction of a transformed metabolic phenotype.

1.5 Non-alcoholic fatty liver disease (NAFLD)

Non-alcoholic fatty liver disease is defined as an accumulation of lipids in hepatocytes that exceed 5% of the weight of the liver, after excluding hepatitis B and C virus infection and ethanol intake of more than 20g per day. It encompasses a spectrum ranging from steatosis to steatohepatitis and fibrosis (173). NAFLD is often associated with insulin resistance, obesity, diabetes

mellitus, hyperlipidaemia, visceral adiposity and other cardiometabolic alterations (174-178). Most patients with NAFLD develop metabolic syndrome, so it is thought that NAFLD is a hepatic manifestation of metabolic syndrome (179, 180).

1.5.1 Prevalence and pathophysiology of NAFLD

The growing epidemic of obesity and type 2 diabetes has seen an unprecedented rise in the prevalence of NAFLD (181), which is estimated to be 20-30% in the general population in the Western counties (182-185) and 15% in Asian countries (186-188). In Europe, 40-60% of liver fibrosis is caused by NAFLD [3], and is one of the leading indications for liver transplantation (189).

Fat accumulates in the liver mainly in the form of triglycerides, although several other lipid species are present. Similar to HCV-induced steatosis, accumulation of triglycerides in NAFLD is the result of the expansion of the intrahepatic pool of FFAs. FFA influx is dependent on the dietary fat via chylomicron metabolism, *DNL* and the amount of FFA released by adipose tissue due to insulin resistance and excessive lipolysis (as described earlier in the chapter). More than half of the FFA pool is derived from excess adipose tissue lipolysis (190). Although NASH occurs in the context of a fatty liver, it is debatable whether steatosis *per se* is a predictor of the presence of NASH. Experimental studies have shown that interference with triglyceride accumulation and effective decrease of steatosis

was not only ineffective in ameliorating NASH, but could even worsen the condition (191, 192).

The "two-hit hypothesis" in NAFLD pathogenesis was first described in 1998 (193). The first hit, hepatic steatosis, makes the liver more susceptible to injury mediated by the second hits, such as inflammatory cytokines/adipokines. These in turn, activate lipid peroxidation which are key mediators of necroinflammation and fibrosis in NASH (194). This theory has been questioned in recent years due to the availability of data to suggest that circulating NEFA and their metabolic by-products (diacylglycerol/triacylglycerol) induce direct lipotoxic injury to key metabolic organs, such as the pancreas, skeletal muscle and liver (195-198). As the majority of NEFA originates from the adipose tissue in NAFLD, it is now the current belief that the initial insult occurs in the adipose tissue.

1.5.2 NAFLD and insulin resistance

Systemic insulin resistance is recognized as one of the main features of NASH (199, 200). Several studies have also identified the liver (200, 201) as well as the skeletal muscle (200-202) as the sites of insulin resistance in patients with NAFLD. In fact, Kato *et al.* suggested that hepatic steatosis *per se*, is a central pathological surrogate indicative of skeletal muscle insulin resistance in NAFLD, and this cross-talk between the organs maintains whole body metabolic homeostasis (202). More recently, adipose tissue insulin resistance has been

implicated in the metabolic disarray observed in NAFLD (203). Adipose tissue is recognized as an important source of fatty acids for the liver, in driving lipid synthesis (190). In an insulin-sensitive state, insulin promotes lipid storage, through fatty acid uptake, re-esterification and de novo lipogenesis, and inhibits triglyceride lipolysis, the process whereby triglycerides are hydrolysed to release NEFAs. In patients with NASH, circulating serum NEFAs are elevated in both fasting and insulinaemic states (203-206). This lipotoxicity can in turn, induce both hepatic and skeletal muscle insulin resistance [14]. Traditionally, visceral adipose tissue was thought to be the major contributor of insulin resistance seen in NASH, due to its close proximity to the portal vein and abundance of pro-inflamamtory mediators [16 17]. More recently, Armstrong *et al.* showed that patients with NASH had profound abdominal subcutaneous adipose tissue dysfunction by measuring their interstitial glycerol release assessed using microdialysis, (201).

1.6 HYPOTHESIS AND AIMS

Hypotheses: *(1) Hypoxia-inducible factors (HIFs) regulate hepatocellular lipid metabolism and play a role in chronic hepatitis C-induced hepatocellular lipid accumulation. (2) Adipose tissue insulin resistance is the cardinal feature of the metabolic abnormalities associated with chronic hepatitis C and this improves following viral eradication. The relative contribution of tissue specific insulin resistance to the metabolic syndrome differs in patients with CHC and NASH.*

Aims:

1. To elucidate the metabolic impacts of hypoxia on human hepatocyte models, and to explore novel mechanistic pathways at the transcriptional and functional level

2. To define the mechanisms by which HCV affects hepatic lipid homeostasis *in vitro*

3. To define global and tissue specific changes in insulin sensitivity in chronic hepatitis C before and after viral eradication by measuring changes in systemic, liver and adipose tissue insulin sensitivity

4. To compare global and tissue specific changes in insulin sensitivity between healthy subjects, CHC and NASH patients

2.0 MATERIALS AND METHODS

2.1 Tissue culture

Huh 7 (American Type Culture Collection, VA, USA) and HepG2 (Charles Rice, The Rockefeller University, New York, NY) hepatoma cells were maintained in Dulbecco's modified Eagle's medium (DMEM) (Gibco, USA), supplemented with 10% foetal bovine serum (FBS), 1% L-Glutamine, 1% non-essential amino acids (NEAA) and 50 units/ml penicillin/streptomycin (Gibco) in a humidified atmosphere at 37°C, in 20% oxygen and 5% carbon dioxide. When the cells were 70-80% confluent, they were incubated under 1% oxygen and 5% carbon dioxide or treated with drugs (detailed in Table 4) for a further 24 hours before RNA, protein and lipid extraction.

Freezing cells

Stored cells were preserved in liquid nitrogen. After pelleting the cells as above cells were resuspended in freezing media (95% FBS, 5% DMSO [Sigma-Aldrich]) and transferred into cryovials for freezing. Cryovials were placed in Mr Frosty freezing container (Wessington Cryogenics) and transferred to an -80°C freezer. After overnight storage the cryovials were transferred to liquid nitrogen.

When cells were required for experiments, cryovials were removed from liquid nitrogen, thawed, washed in PBS and centrifuged to remove cellular debris. Cells were then counted and viability assessed using trypan blue exclusion. Cells were resuspended in appropriate culture media and plated on (coated) tissue culture plastic.

2.2 Antibodies and treatment

The antibodies and treatments used in this study are listed in the following tables.

Table 2-1: PRIMARY ANTIBODIES

Antibody name	Antigen	Type	Specificity	Species	Source
Anti-CD81 (2s131)	Human CD81	Purified IgG	Monoclonal	Mouse	In house
9E10	HCV NS5A	Hybridoma supernatant	Monoclonal	Mouse	Charles Rice, Rockefeller University, NY
NS5A S38	HCV NS5A	Purified	Polyclonal	Mouse	In house
Anti-HIF-1α (Clone 67)	Human HIF-1α	Purified	Monoclonal	Mouse	Novus Biologicals, Europe
Anti-HIF-2 α	Human HIF-2α	Unpurified	Monoclonal	Mouse	Peter Radcliffe, University of Oxford
Phospho-Akt (Thr308)	Human phospho-Akt	Purified	Polyclonal	Rabbit	Cell Signaling Technology, UK
Akt	Human Akt	Purified	Polyclonal	Rabbit	Cell Signaling Technology, UK
Anti-β-actin	Human β-actin	Purified	Monoclonal	Mouse	Sigma Aldrich, MO, USA

Table 2-2: SECONDARY ANTIBODIES

Antibody name	Antigen	Type	Specificity	Species	Source
Rabbit Alexa Fluor 488	Rabbit IgG	Purified IgG (H+L)	Polyclonal	Goat	Molecular Probes, Invitrogen, CA
Mouse Alexa Fluor 488	Mouse IgG	Purified IgG (H+L)	Polyclonal	Goat	Molecular Probes, Invitrogen, CA
Rat Alexa Fluor 488	Rat IgG	Purified IgG (H+L)	Polyclonal	Goat	Molecular Probes, Invitrogen, CA
Anti-Rabbit HRP	Rabbit IgG	Purified IgG	Polyclonal	Donkey	GE Healthcare, PA
Anti-Mouse HRP	Mouse IgG	Purified IgG	Polyclonal	Sheep	GE Healthcare, PA

Table 2-3: ANTIBODIES CONCENTRATION

Antibodies	Application	Working concentration (μg/ml)
Anti-CD81 (2s131)	IF, WB	1
9E10	IF	2
NS5A S38	IF	1
Anti-HIF-1α (Clone 67)	IF, WB	0.25
Anti-HIF-2α	IF, WB	1
Anti-β-actin	WB	0.5
Alexa Fluor 488	IF	1/500
Anti-Rabbit HRP	WB	1/1000
Anti-Mouse HRP	WB	1/1000

IF=Immunofluorescence; WB=Western blotting

Table 2-4: DRUGS USED IN THIS STUDY

Name	Source	Working concentration	Median toxicity
NSC0134754, HIF-pathway inhibitor	Margaret Ashcroft, University College London	0.02uM	2uM
VX-950 - target	LKT laboratories, United States	5ug/mL	N/A
FG4592, PHD inhibitor	Cayman Chemicals, UK	10uM	N/A
CCT6-84	Peter Radcliffe, University of Oxford, UK	10uM	N/A
Insulin Soluble Human	Sigma, Aldrich, MO, USA	10 or 100nM	N/A
Sodium acetate	Sigma, Aldrich, MO, USA	10uM	N/A

HIF=hypoxia-inducible factor, PHD=prolyl hydroxylases

2.3 Virus genesis, infection and transfection

Table 2-5: PLASMIDS

Name	Source
HCVcc J6/JFH-1	Charles Rice, Rockefeller University, NY
HCVcc SA13/JFH-1	Jens Bukh, Copenhagen Hospital, Denmark
HIF-1α	Daniel Tenant, School of Cancer Sciences, Birmingham
HIF-2α	Daniel Tenant, School of Cancer Sciences, Birmingham
HRE-luciferase reporter	Margaret Ashcroft, Royal Free and University College, London

2.3.1 Generation of cell culture HCV (HCVcc)

HCVcc viruses are based on the non-structural (replicase) proteins of HCV JFH-1 strain, a unique isolate that is able to produce infectious particles in Huh-7 cells. All subsequent HCVcc strains incorporate JFH-1 non-structural proteins and differ only by the structural proteins.

RNA synthesis

RNA transcripts of HCV genomes J6/JFH and SA13/JFH were produced using the T7RNA Polymerase Kit (Promega, UK) according to the manufacturer's instructions. In brief, 5ug of plasmid containing a cDNA clone of the HCV genome was linearized by restriction digest using the XbaI enzyme (New England Biolabs, UK). 1ug of the linearized plasmid was used as template for RNA transcription; this was achieved by incubating the reaction mix (t7 RNA polymerase mix from the manufacturer's kit) at 37°C for 4 hours. Thereafter, the RNA was purified using the RNAeasy MiniElute Kit (Qiagen, Netherlands) according to the manufacturer's instructions. RNA quality was assessed by gel electrophoresis on a 1% agarose gel (Bioline, UK). RNA yields were quantified using a spectrophotometer (Amersham, UK) with typical yields between 100-1500ng/µl.

Electroporation

Early passage (passage 1-35) Huh 7 cells were grown in T175 tissue culture flasks until 80-90% confluent. Cells were trypsinized and resuspended in DMEM. Thereafter, cells were washed with ice-cold PBS and pelleted by centrifugation at 25000rpm for 5mins at 1°C; this process was repeated and pellets were resuspended in ice-cold PBS at $1.5x10^7$cells/ml. 400ul of the cell suspension was mixed with 5ug of HCV genomic RNA and transferred to electroporation cuvettes (Sigma). Electroporation was carried out at 600 volts in an Electro Square Porator (Harvard Apparatus, USA). Electroporated cells were allowed to stand for 5 minutes at room temperature to rest before transferring them into 10mls of pre-warmed Iscove's Modified Dubelcco Medium (IMDM) + 10% human serum, 1% L-glutamine and penicillin/streptomycin.

8mls of the cell suspension was transferred to a T75 tissue culture flask and the remainder placed into wells of a 24 well tissue culture plate for the monitoring of HCV protein expression. Cells were incubated at 37°C in a category 3 containment laboratory and the media was replaced with DMEM+3% FBS the following day. At 72 hours post electroporation, viral replication was quantified by staining the cells seeded in 24 well plates with mouse S38 anti-NS5A monoclonal antibody (mAb) for NS5A using immunofluorescence. Providing 60-80% of cells expressed NS5A, HCVcc particles were harvested from the T75 flasks between 4 and 14 days post electroporation after which cells were discarded. Cells were methanol fixed and NS5A positive cells were determined

by immunofluorescence with S38 antibody as described in section 2.4.5. Viral infectivity was enumerated by counting NS5A foci or individual infected cells using a fluorescence microscope.

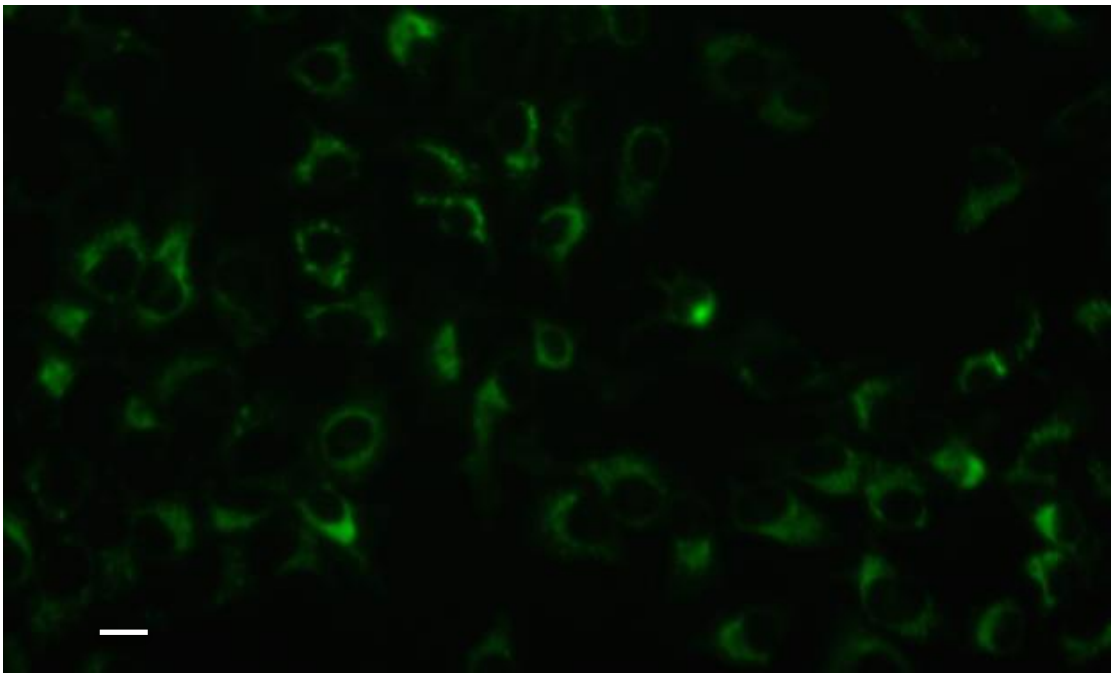

Fig 2-1. HCV NS5A positive foci Huh7 cells were infected with HCVcc SA13/JFH-1, at 48 hours post infection cells were fixed with methanol and stained for HCV NS5A (green) using S38 monoclonal antibody and an Alexa Flour 488 secondary antibody. Scale bar represents 10um.

2.3.2 Virus (HCVcc) infection assay

Harvested virus from electroporation was used to infect target hepatoma cells seeded at 4 x 10^4 cells/ml on a 48 well tissue culture plate 24 hours before infection. To infect cells, the media was removed and replaced with 100ul of

HCVcc virus diluted in DMEM with 3% FBS, L-glutamine and penicillin/streptomycin.

Cells were incubated for 8 hours at 37°C, the HCVcc inoculum was removed and cells washed with PBS to remove any unbound virus. The cells were cultured in 4 mls serum free DMEM with L-glutamine and penicillin/streptomycin and media containing secreted virions harvested at 4-hour intervals and pooled. Harvested virus was clarified by centrifugation at 3000rpm for 5 minutes and stored at -80°C. infection allowed to proceed for 48-72 hours at 37°C.

2.3.3 Plasmid luciferase assay

A full-length human HIF-1a and HIF-2a expression constructs (pCMVβ-HA-HIFα) was provided by Dr. Daniel Tennant (Department of Cancer Sciences, University of Birmingham, UK). The pGL-HRE luciferase reporter construct contains a triple repeat of the iNOS HRE binding sequence and was kindly provided by Dr. Margaret Ashcroft (University College London). The pGL3-basic and control vectors were obtained from Promega (Southampton, United Kingdom).

Cells were seeded at $1.5X10^5$ cells/ml in p6 wells. Once settled, cells were transfected with 2 μg of pGL3/HRE-Luc, and/or 8 μg of pHIF-1a or pHIF-2a per well using FuGENE™ 2000. At 24 h after transfection, cells were trypsinised and reseeded onto smaller wells for lipogenesis and FFA uptake (sections 2.5.1 and

2.5.2), protein/RNA analysis (sections 2.4.1 and 2.4.2) and luciferase measurement. Luciferase activity was measured using the luciferase assay system (Promega, Madison, WI, USA) with a luminometer according to the manufacturer's instructions.

2.4 Other techniques

2.4.1 Protein extraction and Western blotting

Cell lysates were prepared from adherent cells seeded at 4 x 10^4 cells/ml in 24 well plates and maintained in culture for 24 or 48 hours. Cells were incubated under normoxia or hypoxia (1% oxygen) in the presence or absence of insulin (10nM), NSC (0.02uM) or FG4592 (50uM). Culture media was removed and cells washed in PBS. RIPA or Urea/SDS lysis buffer supplemented with protease and phosphate inhibitors (Roche, UK) was added and cells incubated on ice for 30 minutes. The lysate was centrifuged at 15000rpm for 20 minutes at 4˚C to separate nuclei and insolubilized cell membranes from protein. The supernatant was collected and stored at -20˚C. Protein concentration was determined using the BCA Protein Assay Kit (Thermo Scientific, USA) according to the manufacturer's instructions. Briefly, 100µl of each sample or BSA standard were mixed with 200µl of BCA Working Reagent in a 96 well plate in triplicates and incubated at 37˚C for 30 minutes. The plate was allowed to cool at room temperature and the absorbance read at 490nm using a Multiskan Ascent plate reader (Thermo Electron Corporation). Protein concentration of each sample was determined using a standard curve.

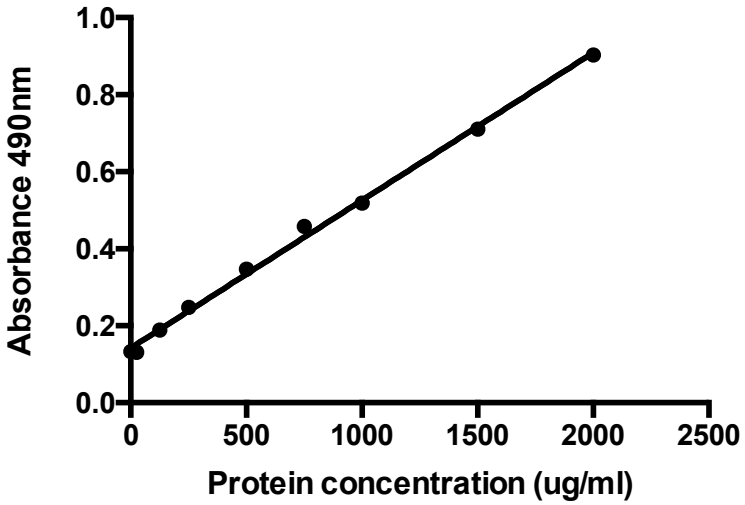

Samples were prepared by adding defined amounts of protein to 3x Laemmli loading dye (H_2O, 30% v/v Glycerol, 6% w/v SDS, 0.2% v/v Bromophenol Blue and 0.2M Tris-HCV; pH 6.8), with 10% 2-β-mercaptoethanol. The total volume was adjusted to 25ul with H_2O and samples were denatured by heating at 95˚C for 5 minutes followed by cooling at room temperature before loading.

Proteins were separated by gel electrophoresis using the Mini Protean 3 System (Bio-Rad laboratories, USA) according to the manufacturer's instructions. Briefly, 20ug of protein lysates were loaded onto 8% sodium dodecyl sulphate-polyacrylamide gels (SDS-PAGE) and gels run at 200 volts constant for 30 minutes. Proteins were then transferred to polyvinylidene membranes (Millipore, USA) using a Mini Trans-Blot Electrophoresis Transfer System (Bio-Rad). Briefly, polyvinulidene membranes were cut to appropriate sizes to match the diameter of the gel and pre-treated with methanol for 2 minutes, rinsed with

H_2O and incubated in transfer buffer (25mM Trizma Base, 0.2M Glycine, 200ml methanol and 10% SDS) at room temperature for 5 minutes. Gels were equilibrated in transfer buffer to prevent shrinking and transfer was carried out at 350mA for 90 minutes at room temperature.

Immuno-blotting and chemiluminescent detection of proteins.

Following successful transfer, membranes were placed in 50ml falcon tubes; to block non-specific antibody binding, membranes were incubated in antibody buffer (10mM Trizma base, 0.1M Sodium Chloride, 10% v/v Tween-20 and 5% Marvel dry milk) for 45 minutes at room temperature. The antibody blocking buffer was removed and the membranes were incubated in primary antibodies (table 2.1) diluted with antibody buffer overnight in 50ml falcon tubes and gentle agitation on a tube roller (Barloworld Scientific, UK) at 4˚C.

The following day, membranes were washed 4 times for 5 minutes each with washing buffer (10mM Trizma base, 0.1M Sodium Chloride and 10% v/v Tween; pH 7.5). Incubation with HRP-conjugated secondary antibodies was carried out for 1.5 hours at 4˚C followed by excess washing. Chemiluminescent detection of HRP-conjugated antibodies was achieved with an ECL Western Blotting Detection System (Amersham, UK). Briefly, membranes were incubated in ECL detection reagent for 1 minutes, wrapped in plastic and exposed to CL-Xposure X-Ray Films (Thermo Scientific) or using the PXi machine for 5-30 minutes (depending on the proteins).

2.4.2 Trypan blue assay

The Trypan blue assay is a dye exclusion staining assay, which is based on uptake of trypan blue dye by dead cells due to loss of membrane integrity, so the dead cells appear darker than viable cells. The assay was measured by previously described method (207). In brief, one to three days after cell plating under normoxia and hypoxia, cells were detached by trypsinization and the number of viable cells were counted using a Trypan blue stain reagent and hematocytometer.

2.4.3 RNA extraction and quantitative RT-PCR

HCV genome copy number was measured by qRT-PCR, using a Cells Direct Kit (Invitrogen) according to the manufacturer's instructions. Quantitative PCR was carried out using Applied Biosystems reagents and expression assays (Qiagen). PCRs for genes of interest and for housekeeping gene GAPDH were carried out in singleplex (i.e. reactions carried out in separate wells). For the gene of interest in a single reaction (100wells) the following components were added: 750µl of 2X PCR Mix, 25µl GAPDH, 30µl RT-Tag enzyme mix and 400µl nuclease free water. 2 ul of RNA sample was added into each well. Samples were run using 7500 real-time PCR system (Applied Biosystems, Warrington, UK). Data were expressed as ct values (ct=cycle number at which logarithmic PCR plots cross a calculated threshold line) and used to determine Δct values [Δct = (ct of the target gene) –

(ct of the housekeeping gene)], lower Δct values reflecting higher mRNA expression. Fold changes were calculated using transformation [fold increase = 2-difference in ΔCT].

2.4.4 RNA interference studies

Huh7 hepatoma cells were seeded at $4x10^4$ cells/ml and transfected with 5uM of scrambled RNA/control, 5uM of HIF-1α or HIF-2α small interfering RNA (siRNA) oligonucleotides using the FuGENE™ (Promega) and Dharmafect 4 (Dharmacon) transfection reagents according to the manufacturer's protocols. 24 hours after transfection, cells were exposed to serum starvation for 8 hours and then incubated under normoxia or hypoxia for a further 24 hours. 16 hours into incubation, media was replaced with fresh media containing 1-[^{14}C]-acetic acid [0.12 μCi/L] with unlabeled sodium acetate [10 μM] and cells were lysed for lipid or protein analysis. The following siRNA oligonucleotides were purchased through Qiagen's prevalidated siRNA database: ARNT siRNA target sequence, GAAGUCAGAUGGUUUAUUU; HIF-1 HP validated siRNA, catalog no. SI02664053; HIF-2 HP validated siRNA, catalog no. SI02663038. Control siRNAs were purchased from Dharmacon siGENOME nontargeting siRNA pool 2 (D0012061405).

2.4.5 In-direct immunofluorescence

Fluorescent microscopy

Cells were seeded at 4 x 10^4 cells/ml in 24 well plates (Becton Dickinson) and fixed prior to staining by incubation with ice-cold methanol (Fisher Scientific, UK) or 4% PFA (TAAB, UK) for 5 minutes and 20 minutes, respectively. Cells were blocked for 20 minutes with PBS + 0.5% BSA and permeabilized with PBS + 0.5% BSA + 0.01% of permeabilization detergent (saponin or Triton X-100). Primary antibody staining was performed by incubation (1 hour) at room temperature with antibody or control isotype diluted in the appropriate buffer. The antibody concentrations used in this study are listed in tables 1-3.

The antibody diluents were removed by aspiration after an hour, and washed with PBS. This process was repeated twice. Secondary antibody staining was achieved with a fluorescent conjugated antibody diluted in the appropriate buffer and incubation in the dark at room temperature for 1 hour. Cells were washed in PBS as described, the nuclei were counterstained by incubation in 4',6-diamidino-2-phenylindole [DAPI] 10ug/ml (Sigma, UK) for 1 minute at room temperature. Stained cells were visualized using a fluorescent microscope (Nikon TE200, Japan) and images were taken using a digital camera (Hammatsu, Japan).

2.5 Lipid flux assay

2.5.1 *De novo* lipogenesis (DNL): Acetyl-CoA carboxylase (ACC) assay

Principle

DNL is a key component of lipid accumulation within the liver and adipocytes. DNL encompasses fatty acid synthesis and subsequent triglyceride (TG) synthesis (when fatty acids are esterified with glycerol to form fats). A key step of fatty acid synthesis is the conversion of acetyl Coenzyme A (CoA) to malonyl CoA in the cytoplasm of the cells, and its subsequent conversion to fatty acid. This key reaction is catalysed by the enzyme acetyl-CoA carboxylase 1 (ACC1), which itself is de-phosphorylated and activated by insulin. This assay measures the incorporation of a 1-[^{14}C]-labeled acetic acid tracer combined with unlabeled ('cold') sodium acetate in cells (Jamdar SC, Biochem J 1978). After incubation cellular lipids are extracted and the retained ^{14}C radioactivity measured by scintillation counting.

Method

DNL was measured by the amount of uptake of 1-[^{14}C]-acetate into the lipid component of cells, as described previously (208). After culture in serum-free media, cells were incubated for a further 8 hours with media containing 1-[^{14}C]-

acetic acid [0.12 µCi/L] with unlabeled sodium acetate [10 µM]. After incubation at 37 ^{0}C, cells were washed three times with ice cold PBS, scraped into 250 µl PBS, and transferred into glass tubes. To extract the lipid fraction, 5 mls Folch solvent (chloroform: methanol 2:1) was added to the cells and vortexed vigorously for 20 seconds, after which 1ml distilled water was added and vortexed for a further 1 minute. The glass tubes were then centrifuged at 300x g for 5 minutes to separate the sample into two distinct phases - aqueous (upper layer) and solvent (lower layer) - with protein collecting at the interface. The aqueous layer was aspirated off and the solvent was transferred to a scintillation tube to evaporate until dryness using a sample dryer in a fume cupboard overnight. Once dry, 5 mls of cold scintillation cocktail was added to each tube and the 14C radioactivity retained in the cellular lipid was determined by scintillation counting, using the liquid scintillation analyzer 2500 RT/AB (Packard, A Canberra Company, Oxfordshire, UK). The ^{14}C radioactivity retained in the cellular lipid was expressed as disintegrations per minute (dpm)/per well.

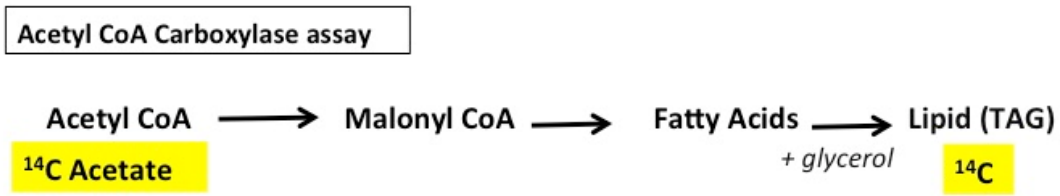

2.5.2 Non-essential fatty acid (NEFA) uptake and β-oxidation

Principles

NEFA that are required for energy homeostasis and triglyceride synthesis in the liver are available from the adipose-derived NEFA plasma pool and hepatic fatty acid synthesis (190). The plasma NEFA concentration is derived from lipolysis in adipocytes, which occurs mainly in the fasting state and is repressed by insulin (209, 210). NEFA are taken up by hepatocytes in a facilitated fashion by specific binding/transport membrane proteins (i.e. fatty acid binding protein, fatty acid transport protein), and not by a passive process. This assay measures the intracellular (cytosolic) accumulation of 9,10-[^{3}H]-labelled palmitate tracer. After incubation intracellular lipids are extracted and the retained ^{3}H radioactivity is measured by scintillation counting.

β-oxidation is the pathway by which fatty acids are sequentially broken down in the mitochondria, generating acyl-CoA molecules which enter the TCA cycle ultimately leading to increased ATP production. It is a rapid and effective metabolic pathway for the allocation of energy within the liver (especially in the fasted state). Prior to β-oxidation, NEFA are activated by acyl-CoA-synthase to fatty acid acyl-CoA substrates in the cytosol to facilitate uptake into mitochondria. Long-chain NEFA, such as palmitate, are transported across the mitochondrial membrane via CPT1 (211). In the mitochondria, acyl-CoA dehydrogenase catalyses the breakdown of long-chain NEFA acyl-CoA into acetyl CoA molecules. This assay measures β-oxidation by quantification of [^{3}H]-labelled H_2O generated and released by the cells into the media and measured by

scintillation counting (212).

Method

Hepatoma cells were cultured and treated in 24-well plates and incubated with 500ul of serum free media containing 0.1 mmol/L palmitate (9,10-[^{3}H] palmitic acid (5uCi/ml) (GE Healthcare, Bucks, UK) with cold palmitate to a final concentration of 10uM palmitate, 2% BSA and treatments for 24 hour. After incubation, cells were washed with cold PBS three times before 250ul of 1% Triton was added. Cells were scraped and transferred to plastic scintillation vials with scintillation cocktail to measure NEFA uptake.

The rate of β-oxidation was measured by the conversion of 9,10-[^{3}H] palmitate (Perkin Elmer) to [^{3}H] labeled- H_2O, using a modification of the method described by Gathercole et al (213). After incubation for 24 hours, the 250ul of media was retained and precipitated twice with equal volumes of 10% trichloroacetic acid to remove excess labelled palmitate. The supernatants (0.5ml) were extracted by addition of methanol:chloroform (2:1) and 1ml of 2mol/L KCl:HCl, followed by centrifugation at 3000 g for 5 minutes. Aqueous phase (0.5mL) was added to scintillation cocktail (PerkinElmer, Bucks, UK), Aqueous samples were counted using a Wallac 1414 Liquid Scintillation Counter (PerkinElmer, Bucks, UK) to measure the rate of β-oxidation.

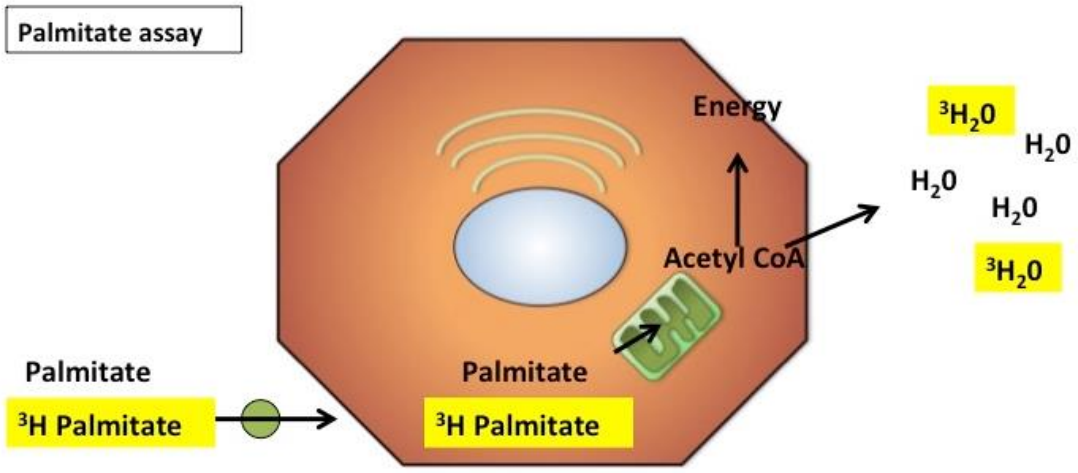

Fig 2-2. NEFA uptake and β-oxidation. This assay measures the intracellular (cytosolic) accumulation of 9,10-[^{3}H]-labelled palmitate tracer and the conversion of 9,10-[^{3}H] palmitate) to [^{3}H] labeled- H_2O, After incubation intracellular lipids are extracted and the retained ^{3}H radioactivity is measured by scintillation counting.

2.6 Statistical analysis

Results are shown as the mean ± standard deviation unless otherwise stated. Data compared using non-parametric statistics since normality of small samples cannot be readily established. For comparisons of two groups the Mann-Whitney U test was used. For experiments containing multiple comparisons data were compared with the Kruskal-Wallis test using Dunn's correction for multiple comparisons. Linear regression analyses were used as indicated to explore relationships between continuous variables, and to calculate protein and RNA concentrations from standard curves. All statistical analyses were done with Prism 5.0 (GraphPad).

3.0 EFFECTS OF LOW OXYGEN ON HEPATIC LIPID ACCUMULATION

3.1 INTRODUCTION

Blood flow to the liver is unique in that it receives both oxygenated and (partially) deoxygenated blood. Blood flows from branches of the hepatic artery and mixes in the sinusoids to supply the hepatocytes with oxygen. This mixture percolates through the sinusoids and collects in a central vein which drains into the hepatic vein. This directional blood flow towards the central vein of the lobule creates a physiological oxygen gradient, resulting in a higher oxygen tension in the periportal area to a lower oxygen tension in the perivenous area of the liver parenchyma (2, 3). This is associated with liver zonation, a phenomenon where hepatocytes show distinct functional and structural heterogeneity across the parenchyma (9, 25, 214). Hypoxia-inducible factors I, II and III are transcription factors that enable a cell to respond to changes in available oxygen in its local environment. Under physiological oxygen concentration, HIFs are constantly degraded following hydroxylation. However, modest changes in oxygen tension that can occur in various liver pathologies such as viral hepatitis, alcoholic and non-alcoholic fatty liver disease, or carcinogenesis, promote a hypoxic response that stabilizes HIFs (2, 6-8).

It is widely published in the literature that low oxygen induces changes in intracellular lipid content and triglyceride levels in hepatocytes *in vitro* and *in*

vivo (5, 215-217). Studies in humans and rodents have revealed several regulators which perturb lipid metabolism in liver diseases, namely, sterol response element binding protein (SREBP); a transcription factor that controls DNL and peroxisome proliferator-activated receptors (PPARs) which regulate fatty acid metabolism (218, 219). Carbohydrate response element binding protein (ChREBP) and X-box binding protein (XBP)-1 are also thought to regulate hepatic lipid metabolism (220, 221). Although these studies have elucidated various signaling pathways that regulate lipid metabolism in fatty liver diseases, little is known regarding upstream stimuli. Clinical studies have linked obstructive sleep apnoea (OSA), a condition defined by the presence of apneic-hypopnoeic episodes, to elevation of liver enzymes, derangement of lipid profile, development of hepatic steatosis, lobular necrosis, fibrosis and increased morbidity and mortality (68-71). The prevalence of metabolic syndrome in severe OSA is as high as 80%. In addition, those with severe OSA are three times more likely to develop metabolic syndrome, after adjustment for body mass index (BMI) (68). One study suggests that acute hypoxia suppresses lipoprotein lipase activity in patients with OSA, leading to lipid accumulation, although this was not seen in healthy subjects exposed to acute hypoxia (82). Others have linked the severity of nocturnal hypoxia and progression from fatty liver to non-alcoholic steatohepatitis (77, 78).

The role for hypoxia in the pathogenesis of both alcoholic and non-alcoholic fatty liver diseases has been studied extensively (222-224). Rats fed a continuous ethanol diet showed liver hypoxia (4, 223, 225), although the direct contribution of HIFα to alcoholic liver injury remains controversial. Other murine studies

show that increased *de novo* lipogenesis and esterification of exogenous fatty acids and very low density lipoprotein lipids occur in the perivenular cells with lower oxygen tension (63), supporting a role for low oxygen in regulating hepatic lipid metabolism. The relevance of hypoxia in chronic ethanol ingestion has also been substantiated in human studies (226, 227). Multiple lines of evidence suggest that HIFs play a central role in the regulation of hepatic lipid metabolism. Hepatocyte specific deletion of the von Hippel-Lindau (VHL) gene is accompanied by a phenotype of hypervascularity and steatosis (69). Simultaneous expression of degradation-resistant HIF1α and HIF2α resulted in a similar phenotype of hepatic lipid accumulation in murine models (4). However the relative role of HIF1 and/or HIF2 in regulating hepatic lipid metabolism is unclear. Whilst some studies suggest that HIF1α play a more dominant role (5, 67, 228), others propose that HIF2α is more steatogenic (7, 229). This is supported by a recent study that reported an accumulation of lipids in a murine model of liver-specific HIF2 activation whereby HIF2α up-regulated lipid biosynthetic pathways, suppressed fatty acid β-oxidation, and increased lipid droplet surface protein ADFP (229).

3.2 HYPOTHESIS AND AIMS

Hypothesis: *Hypoxia-inducible factors regulate hepatocellular lipid metabolism*

Aims:

In this chapter, we aim to elucidate the metabolic impact of hypoxia on human hepatocyte models and explore novel mechanistic pathways at the transcriptional and functional level.

3.3 RESULTS

3.3.1 Low oxygen results in HIF stabilization

We evaluated HIF transcriptional activity using a synthetic reporter by exposing Huh-7 hepatoma cells to different oxygen tension. Physiological oxygen gradient in a healthy liver ranges from 4 to 8%. Therefore to study the effect of low oxygen, and its dose-dependency, we incubated cells under two different levels of hypoxia, 3 and 1%. After 24 hours, cells were lysed for protein extraction. The induction of both HIF1 and HIF2 proteins under lower oxygen was dependent on oxygen tension, detected by western blot [Fig 3-1A].

In a similar experimental design, *Frampton et al* (unpublished) assessed the kinetics of hypoxia-driven transcriptional activity using a hypoxic response element (HRE) reporter system, which consisted of a vector containing luciferase reporter gene downstream to a minimal promoter with a HRE whose activity is HIF-dependent. Huh-7 hepatoma cells were transfected to express the HRE luciferase reporter and incubated under 21%, 3% or 1% oxygen for up to 24 hours. HRE activity peaked at 16 hours following low oxygen treatment, and there was a higher HRE activity noted in cells incubated under 1% compared to 3% oxygen concentration after 24 hours [Fig 3-1B]. Taken together, these results suggest that exposure to lower oxygen tension stabilizes HIF expression and activity.

1A.

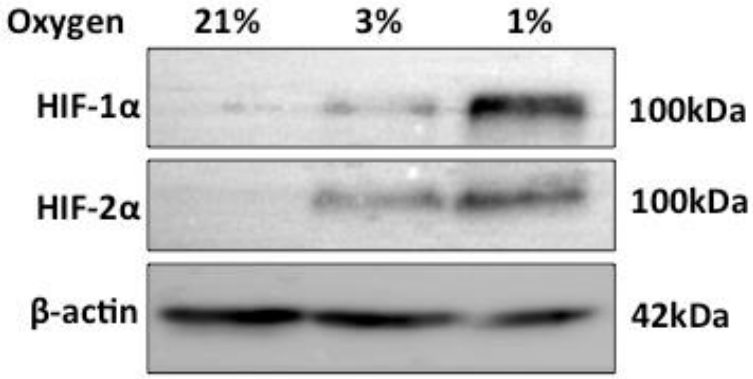

1B.

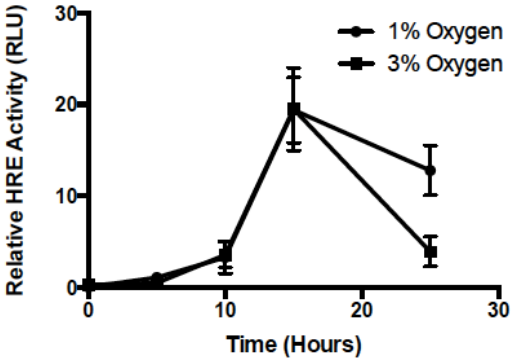

Frampton, N

Fig 3-1. Comparison of HIF kinetics in Huh-7 cells exposed to two different hypoxic oxygen concentrations. Western blot detection of HIF-1α and HIF-2α from lysate of Huh-7 cells incubated at different oxygen tension (21, 3 or 1% oxygen) for 24 hours. A representative image is shown for each protein. β-actin was used as a loading control [A]. HRE luciferase assay was measured in Huh-7 cells transfected with an HRE luciferase reporter gene and exposed to 21%, 3% or 1% oxygen for up to 24 hours. The data is plotted as relative fold change in activity between hypoxic and normoxic conditions [B]. Data are presented as mean±SE. Experiments were performed in triplicates and repeated thrice.

3.3.2 Oxygen tension regulates hepatic lipid accumulation

DNL, FFA and β-oxidation were measured in hepatoma cells exposed to 21, 3 or 1 % oxygen for 24 hours using isotope-labelled tracers measured by mass spectrometry. DNL was measured by 1-[^{14}C]-acetate incorporation into lipid, whereas FFA uptake was defined by the amount of ^{3}H-palmitate taken up by cells after 12 hours incubation with ^{3}H-labelled and unlabelled palmitate in serum-free media. β-oxidation was measured by the amount of ^{3}H-water released by cells into the culture media. We showed that exposure to low oxygen significantly increased both DNL [Fig 3-2A] and FFA uptake [Fig 3-2B], demonstrating that differential oxygen tensions influences hepatocellular DNL and FFA uptake and yet has a minimal effect on β-oxidation [Fig 3-2C].

To validate the above findings, we measured *de novo* lipogenesis, free fatty acid uptake and β-oxidation in two other hepatoma cells lines, Huh-7.5 and HepG2 alongside Huh-7. Low oxygen (1%) treatment for 24 hours increased DNL 4-fold in Huh-7 cells, 1.5 fold in Huh-7.5 and 2-fold in HepG2 cells compared to cells propagated under 21% oxygen [Fig 3-3A]. Hypoxia also increased FFA uptake, albeit to a lesser degree, compared to normoxia [Fig 3-3B] and had no effect on β-oxidation in all cell lines [Fig 3-3C].

2A.

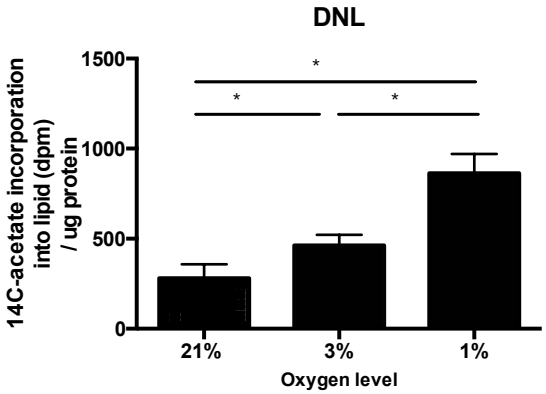

2B.

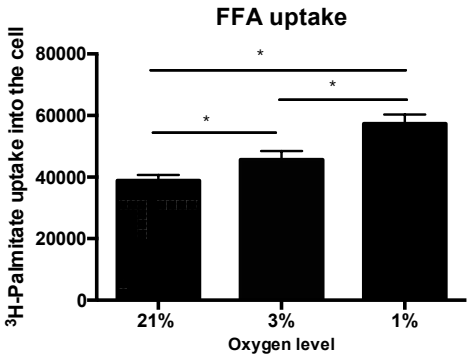

2C.

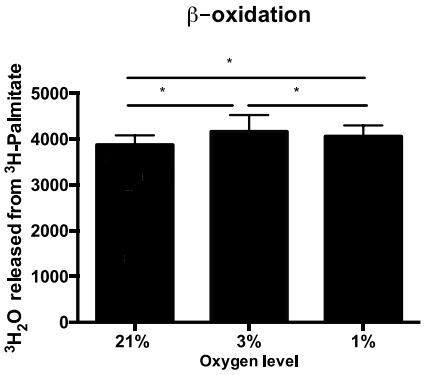

Fig 3-2. Differential oxygen tension influences hepatic lipid accumulation. [A] DNL is determined by measuring 1-[^{14}C]-acetate incorporation into lipid in Huh-7, Huh-7.5 and HepG2 hepatoma cells incubated with ^{14}C-acetate incubated under 21% oxygen (normoxia), 3% or 1% oxygen (hypoxia) for 24 hours. [B] FFA uptake was defined by the amount of ^{3}H-palmitate taken up by cells after 12 hours incubation with ^{3}H-palmitate in serum-free media. [C] β-oxidation was measured by the amount of ^{3}H-water released by cells into the culture media. Cells were incubated under these conditions for 24 hours. Data are presented as mean±SE. Experiments were performed in quadruplicates and repeated thrice. *$p<0.05$. Unpaired student's t test

3A.

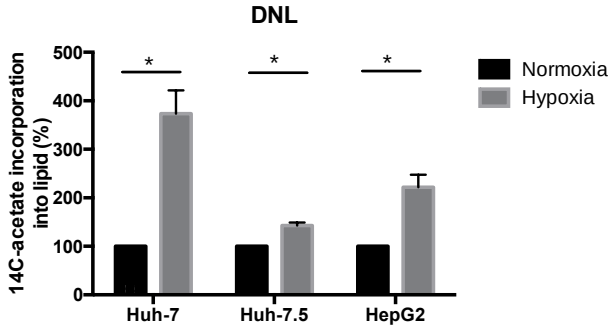

3B.

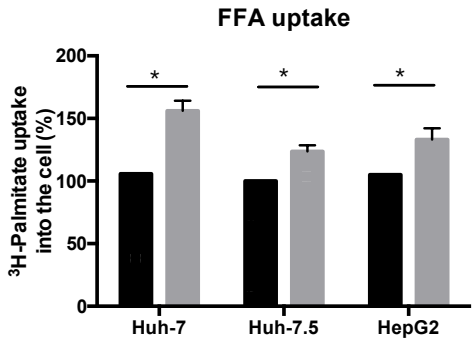

3C.

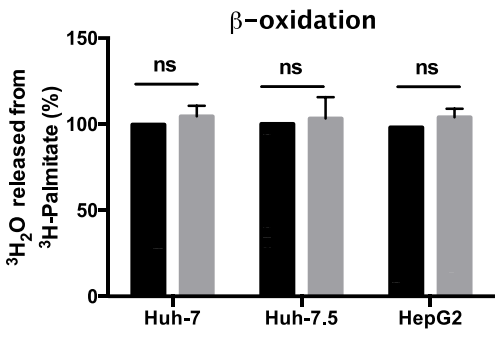

Fig 3-3. Hypoxia increases DNL and FFA uptake across hepatoma cell lines. DNL [A], FFA uptake [B] and β-oxidation [C] were measured at 21 or 1% oxygen tension. Data are presented as mean±SE. Experiments were performed in quadruplicates and repeated thrice. *$p<0.05$, ns=non-significant. Unpaired student's t test.

3.3.3 Hypoxia-driven increase in *de novo* lipogenesis and free fatty acid uptake is dependent on the HIF-signaling pathway.

In recent years, Ashcroft *et al* identified a compound, NSC 134754 that targets the HIF signaling pathway, which prevents HIF stabilization under low oxygen (230, 231). To ascertain whether HIF regulates the low oxygen potentiation of DNL and FFA uptake we observed in hepatoma cells, cells were treated with the HIF inhibitor, exposed to normoxia and hypoxia for 24h and DNL assessed. NSC at 0.02μM abrogated hypoxia-driven increase in DNL in Huh-7 [Fig 3-4A]. In a parallel experiment, the optimal dose of NSC required to fully reverse the effect of hypoxia driven lipogenesis in our cell culture system was obtained by measuring 14^{C}-uptake into cells cultured under hypoxic conditions treated with varying doses of NSC [Fig 3-4B]. Dose at 0.02μM was adequate to fully reverse the effect of hypoxia-induced increase in DNL and cell viability showed that doses higher than 0.1μM were toxic to cells. *Wilson et al* demonstrated that NSC inhibited HIF1α expression in HepG2 cells as shown by confocal imaging and western blot detection (8).

Prolyl hydroxylase domain inhibitors (PHDi) have been tested *in vitro* and in murine models to target HIF pathways in various medical conditions such as haematological, pulmonary, and renal diseases (232-235). Four discovered compounds are currently in phase 3 human clinical trials (236). We used one of the inhibitors, FG4592 (Cayman Chemical, Michigan, USA) in our experiments. In the first instance, we evaluated the molecule in stabilizing HIFs in HepG2 hepatoma cells over time. Cells were lysed and HIF protein assessed by Western

Blot [Frampton, N. unpulished data]. We found that a single dose of FG4592 stabilized both HIF1α and HIF2α at 24, 48 and 72 hours (Fig 3-5A). We then measured ^{14C}-acetate uptake into Huh-7 hepatoma cells treated with FG4592 under normoxia for 24 hours. As seen in cells incubated under hypoxia, DNL was increased in PHDi-treated cells [Fig 3-5B & 5C], strengthening our hypotheses that hypoxia-driven hepatic lipid accumulation is HIF-dependent. No effect on β-oxidation was seen [Fig 3-5D].

4A. **4B.**

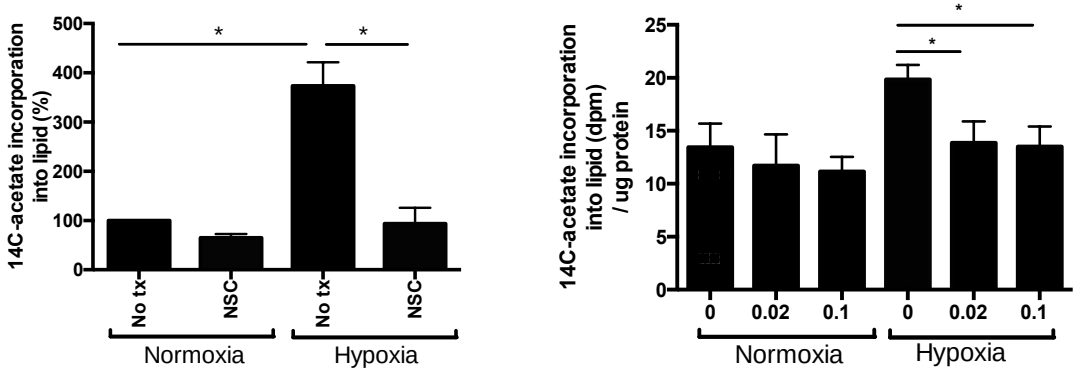

Fig.3-4 Hypoxia-driven increase in *de novo* lipogenesis (DNL) is dependent on HIF-signaling pathway. Huh-7 hepatoma cells were incubated under normoxia (21%) or hypoxia (1% oxygen) with or without NSC, for 24 hours. [A] Hypoxia increases lipogenesis and this effect is completely reversed with 0.02uM of NSC. [B] Dose response of NSC was measured against ^{14}C-acetate uptake into cells which were treated with 0.02uM or 0.1uM of NSC under 21 or 1% oxygen. A dose of 0.02uM adequately reversed the effect of hypoxia on DNL. Data are presented as mean±SE. Experiments were performed in quadruplicates and repeated thrice. *p<0.05. Unpaired student's t test.

5A.

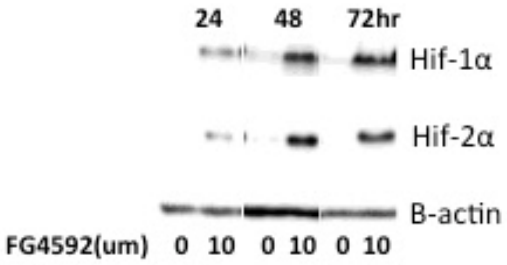

Frampton, N

5B.

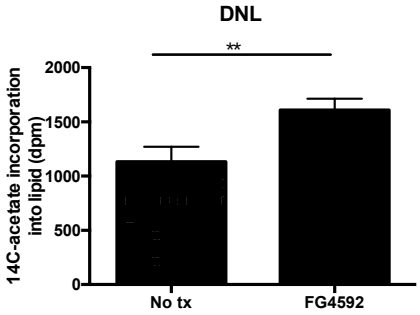

5C.

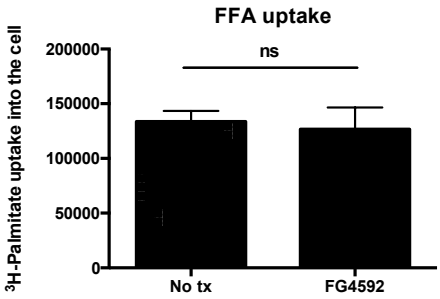

5D.

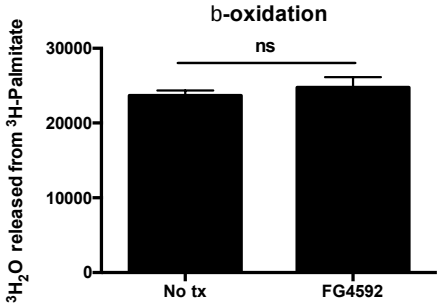

Fig 3-5. Hypoxia-induced increase in DNL is HIF-dependent. [A] HepG2 cells were treated with FG4592 (10um) for 24, 48 or 72 hours before lysis. Lysates were measured for HIF-1α and HIF-2α proteins by Western blot. β-actin was used as loading control (*Frampton, N*). In a different set of experiments, cells were treated with 10uM of FG4592 and incubated under normoxia (21%) for 24 hours. DNL [B], FFA uptake [C] and β-oxidation [D] were measured. Data are presented as mean±SE. Experiments were performed in quadruplicates and repeated thrice. **p<0.01, ns=non-significant. Unpaired student's t test.

3.3.4 Both HIF1α and HIF2α play a role in hepatic lipid accumulation

To confirm a role for HIF1α or HIF2α in regulating hypoxia-induced lipogenesis, RNA interference (RNAi) technique was used to transiently silence HIF expression in Huh-7 hepatoma cells. In brief, siRNAs targeting HIF1α or HIF2α along with a scrambled control were transfected into Huh-7 cells and incubated for 24 hours under normoxia. Cells were then incubated for a further 24 hours in 21 or 1% oxygen. Silencing efficiency was analysed by measuring HIF expression by western blotting. HIF1α band was not seen in the siHIF1α knockdown cells but a faint HIF2α protein band was still visible in the HIF2α knockdown cells, suggesting lower silencing efficiency of the HIF2α transfection [Fig 3-6A]. HIF1α knockdown reduced the effect of hypoxia driven increase in lipogenesis by 40% compared to control cells, however, there was no effect of HIF2α silencing on lipogenesis [Fig 3-6B]. From this, we conclude that HIF1α played a role in hepatic lipid accumulation in hypoxia. However, HIF2α transfection was suboptimal and did not seem to alter lipogenesis in these experiments.

The role of HIFs on lipogenesis was analyzed by over-expressing HIFs in hepatoma cells. The cells were transfected with plasmids encoding for HIF1α or HIF2α with HRE-Luc reporter and incubated under normoxic conditions for 36 hours. Transfection efficiency was also confirmed by HIF protein expression by western blot [Fig 3-7A]. To determine the localization of HIFs in hepatoma cells, we performed immunofluorescence analysis for HIF1α and HIF2α expression in

the transfected cells. Following transfection, cells were probed with anti-mouse HIF1α (NOVUS Biologicals) or anti-mouse HIF2α (ABCAM) antibodies and examined by confocal microscopy. HIF1α could be readily detected in the nuclei of HIF1α transfected and desferoxamine or DMOG-treated cells, that were used as positive controls for the experiments. Localization of HIF2α was less clearly defined in these cells due to a high background staining observed with the antibody [Fig 3-7B]. HIF function in the over-expressing cells was also confirmed by measuring the transcript levels of known HIF-target genes, VEGF and EPO, by RT-PCR. VEGF and EPO were upregulated by 2 and 4 fold in the HIF1α transfected cells and by 2 and 6 fold in the HIF2α transfected cells, compared to control [Fig 3-7C]. Overexpression of either HIF1α or HIF2α significantly increased DNL and FFA uptake in Huh-7 hepatoma cells [Fig 3-7D & 7E].

We had utilized several techniques to confirm transfection efficiency for overexpressing HIF in our cell culture system. We showed that overexpression of either HIF1α or HIF2α significantly increased hepatic steatosis. Taken together, we are convinced that both HIFs, at least in part, play a role in hepatic lipid accumulation.

6A.

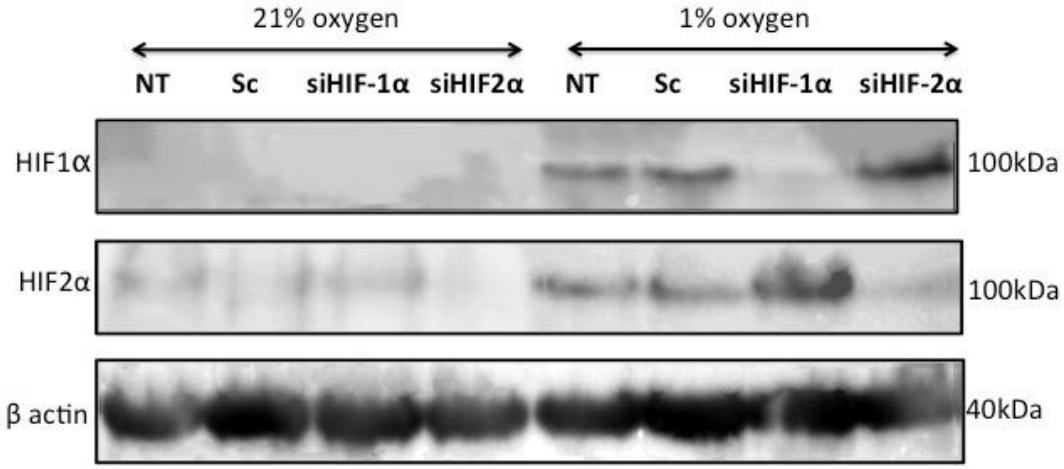

6B.

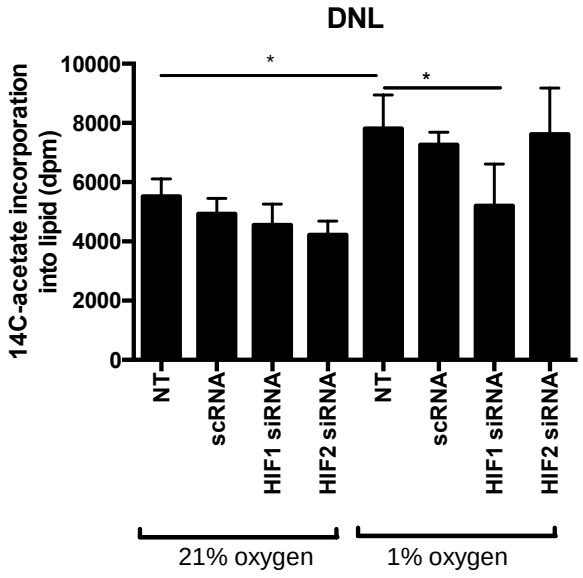

Fig 3-6. Effect(s) of HIF1α- and HIF2α-knockdown on lipogenesis. [A] Huh-7 hepatoma cells were transfected with siRNA-mediated scrambled RNA (scRNA), HIF1 or HIF-2α for 24 hours. Cells were incubated at 21% or 1% oxygen for a further 24 hours. Following this, HIF protein expression was determined by Western blotting from lysate. [B] Following transfection, 1-[^{14}C]-acetate incorporation into lipid was measured in these cells. Data are presented as mean±SE. Experiments were performed in quadruplicates and repeated thrice. *$p<0.05$, ns=non-significant. Unpaired Student's t test

7A.

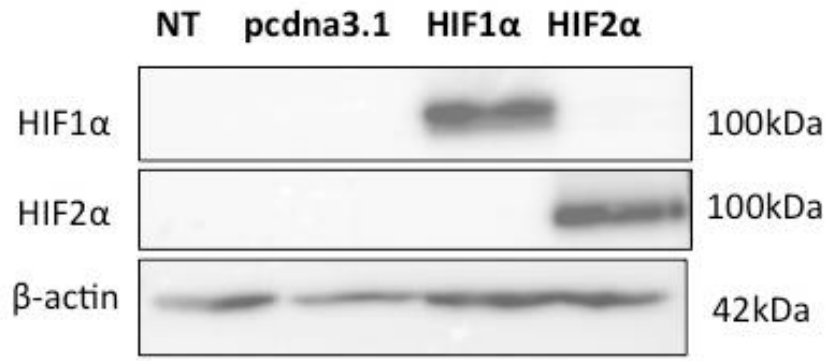
NT
pcdna3.1
HIF1α
HIF2α
HIF1α
100kDa
HIF2α
100kDa
β-actin
42kDa

7B.

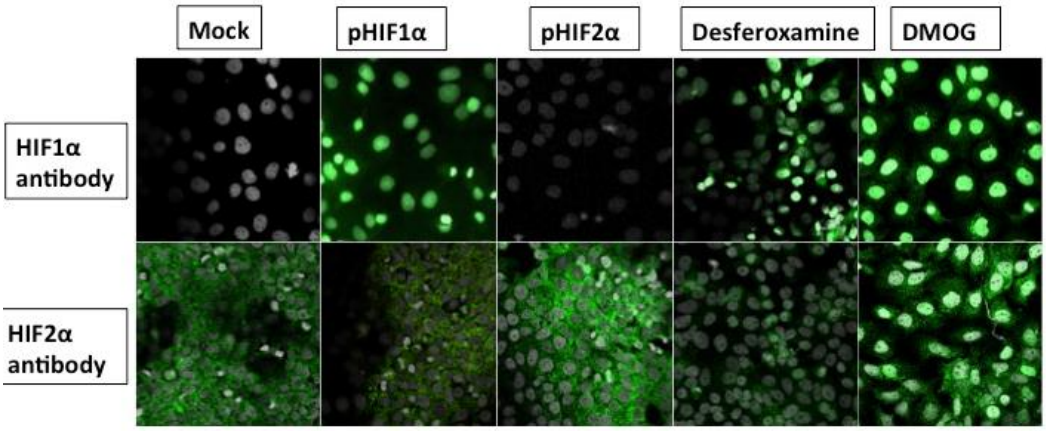
Mock
pHIF1α
pHIF2α
Desferoxamine
DMOG
HIF1α antibody
HIF2α antibody

7C.

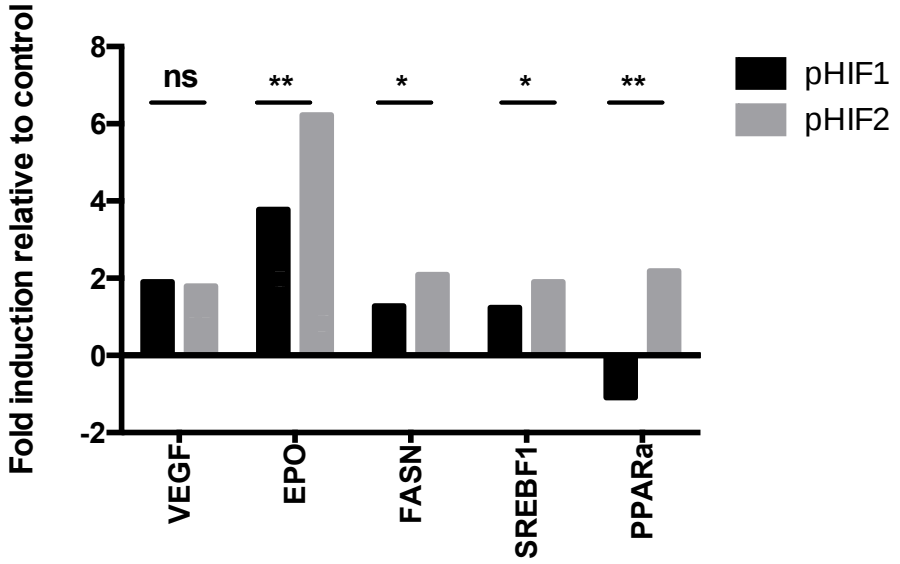

7D.

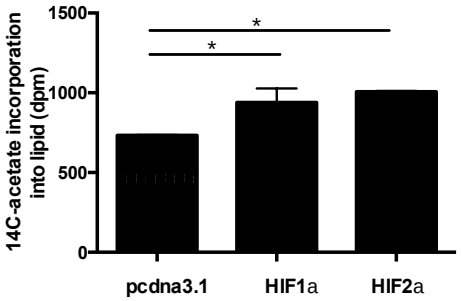

7E.

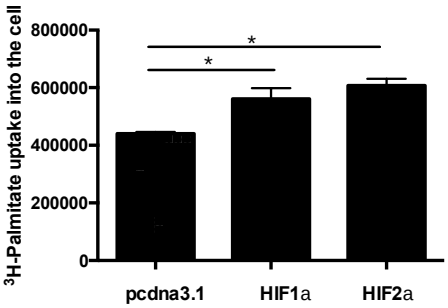

Fig 3-7. Hypoxia-driven lipogenesis is HIF-1α and HIF-2α-dependent. Mock (pcDNA), HIF1α or HIF2α plasmid was transfected into Huh-7 hepatoma cells and incubated under 21% oxygen for 36 hours. Transfection was confirmed by nuclear staining of HIF using confocal microscopy [A], HIF protein expressions by western blotting [B] and selected transcripts (VEGR and EPO) [C]. mRNA expression of lipid genes (FASN, SREBF1 and PPARα) was quantified by RT-PCR [C] and 1-[^{14}C]-acetate incorporation into lipid [D], and FFA uptake [E] were measured in these cells. Data are presented as mean±SE. Experiments were performed in quadruplicates and repeated thrice. *p<0.05, **p<0.01, ns=non-significant. Unpaired student's t test

3.3.5 Low oxygen and HIF modulated genes involved in hepatic lipid accumulation

We assessed the effect of low oxygen and FG4592 (Roxadustat) on HIF-target gene expression in Huh-7 hepatoma cells. Under normoxic conditions, HIF-specific prolyl hydroxylases initiate the degradation of oxygen-sensitive HIF isoforms. As 2-oxyglutarate (2-OG) is a required co-factor for HIF prolyl hydroxylases activity, analogs of 2-OG such as FG-4592 that inhibit prolyl hydroxylases and catalyzes the post-translational formation of 4-hydroxyproline in HIF alpha proteins, prevent HIF degradation (237).

The effect of low oxygen on lipid metabolism in Huh-7 hepatocyte derived cells was studied by performing a PCR microarray on a selected panel of known HIF-regulated genes (n=84). This revealed an induction of many known hypoxia-responsive genes including those encoding mitochondrial and lipid/glycolytic enzymes. A heatmap of the identified genes (Huh-7/control, Huh-7/hypoxia and Huh-7/FG4592) is shown in Figure 3-8A {Frampton *et al*, unpublished), where the colour of each section is proportional to the significance of change of genes (red, upregulated; green, downregulated).

Pyruvate dehydrogenase kinase-1 (PDK-1), 6-phosphofructokinase liver type (PFKL) and hexokinase-2 (HK2) were identified as genes involved in cell lipid or carbohydrate metabolism [Figure 3-8B]. We found that low oxygen, but not FG4592, down-regulated PDK-1 25-fold. PDK-1 regulates pyruvate dehydrogenase (PDH) by a phosphorylation/ dephosphorylation cycle.

Phosphorylation of PDH by pyruvate dehydrogenase kinase (PDK) results in inactivation. A low PDK1 activity keeps PDH in a dephosphorylated and active state, thus maintaining high carbohydrate fuel for lipid synthesis. Low oxygen and FG4592, increased PFKL and HK2, that are involved in key steps in glycolysis.

In line with the above findings, the mRNA levels of sterol regulatory element-binding protein 1 (SREBF1), fatty acid synthase (FASN) and peroxisome proliferator-activated receptor alpha (PPARα), were measured in Huh-7 hepatoma cells [Fig 3-9]. SREBF1 regulates cholesterol biosynthesis and uptake, and fatty acid biosynthesis. FASN catalyzes the synthesis of palmitate (a long chain saturated fatty acid) from acetyl-CoA and malonyl-CoA. Activation of PPARα promotes uptake, utilization and catabolism of fatty acids including mitochondrial fatty acid β-oxidation. When compared to normoxia, hypoxia increased these genes by approximately 2 fold. [Fig 3-9], confirming the lipogenic effect of low oxygen in hepatoma cells.

8A.

8B.

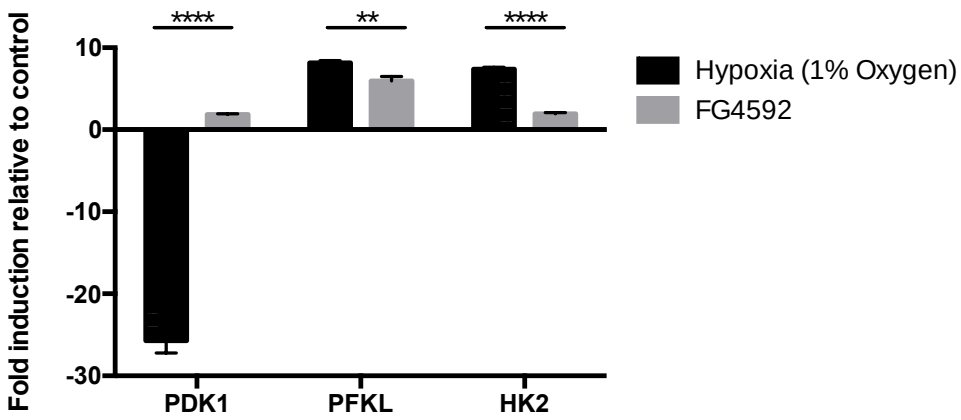

Fig 3-8. Hypoxia and FG4592 regulate pyruvate dehydrogenease kinase-1 (PDK-1), 6-phosphofructokinase liver type (6-PFKL) and hexokinase-2 (HK2) gene transcripts in Huh-7 hepatoma cells. Heatmap of Huh-7 hepatoma cells incubated under 21% oxygen, 1% oxygen or treated with 10um FG4592 (under 21% oxygen) for 24 hours. Rows: samples, Columns: genes. The colour of each sample is proportional to the significance of change of genes (red, upregulated; green, downregulated) [A]**.** Fold induction of metabolic genes from the PCR microarray [B]. Data from 3 independent experiments in quadruplicates are presented as mean ± se fold induction compared to untreated cells and quantified relative to GAPDH. **p<0.005, ****p<0.0001. Unpaired Student's t-test

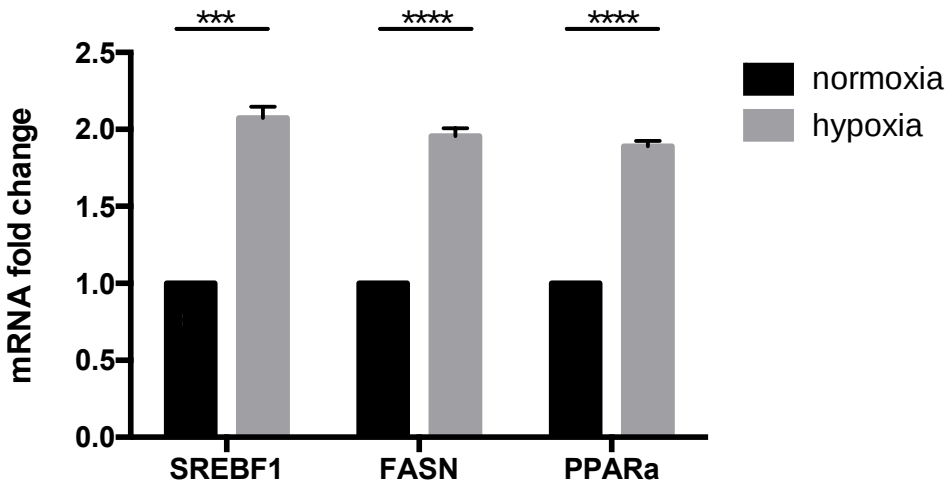

Fig 3-9. Hypoxia regulates sterol regulatory element-binding protein 1 (SREBF1), fatty acid synthase (FASN) peroxisome and proliferator-activated receptor alpha (PPARα) RNA transcript levels in Huh-7 cells. mRNA levels measured by RT-PCR in Huh-7 hepatoma cells seeded at $4x10^4$ cells/ml and incubated under 1% or 21% oxygen for 24 hours. Data from 3 independent experiments in quadruplicates are presented as mean ± se fold induction compared to untreated cells and quantified relative to GAPDH. ***p<0.001, ****p<0.0001. Unpaired Student's t-test

3.3.6 Low oxygen does not alter the proliferative capacity of Huh-7 hepatoma cell lines

Hypoxia has been shown to alter the proliferative capacity of non-hepatoma (238, 239) and hepatoma (240, 241) derived cell lines. To investigate this, Huh-7 cells were cultured under normoxia or hypoxia for up to 72 hours. Following 24, 48 or 72 hours of incubation, cells were detached by trypsinization and the number of viable cells counted using a Trypan blue stain reagent and a hematocytometer. Comparison was made between cells incubated under normoxic and hypoxic conditions at each time point. No significant difference in cell numbers was detected between these 3 time points [Fig 3-10]. It was concluded that the increment in DNL and FFA uptake in Huh-7 cells under hypoxia was not due to increased cell numbers.

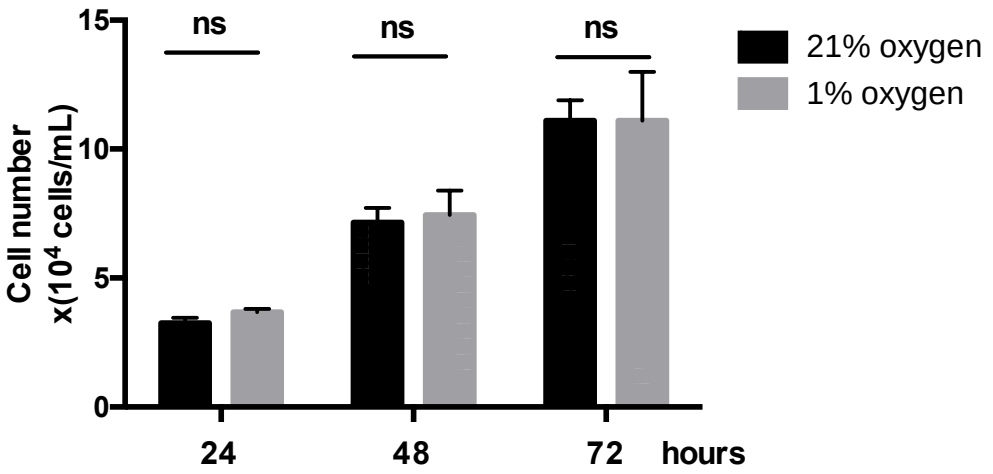

Fig 3-10. Hypoxia does not alter the proliferative capacity of Huh-7 hepatoma cells. Huh-7 cells were seeded at 4x10^4 cells/ml and incubated under normoxia (21% oxygen) or hypoxia (1% oxygen). At 24, 48 or 72 hours, cells were trypsinised (approximate cell confluence 60%, 90% and 100% respectively), and were treated with Trypan blue and counted using hematocytometer. Data are presented as mean±SE. Experiments were performed in quadruplicates and repeated thrice. ns=non-significant. Unpaired Student's t-test

3.4 DISCUSSION

Low oxygen has been shown to induce changes in intracellular lipid content and triglyceride levels both *in vitro* and *in vivo* (5, 215-217). The data described in this chapter showed that hypoxia-induced lipid accumulation is predominantly driven by *de novo* lipogenesis and fatty acid uptake. This is supported by our observation that hypoxia also upregulated the mRNA expression of SREBF-1, FASN and PPARα. In addition, even though hypoxia activated the PPARα RNA levels, it did not result in a change in β–oxidation. These findings differ from the study by Liu *et al*. which showed that hypoxia induced lipid accumulation by suppressing genes involved in lipid clearance and β-oxidation, as well as lipogenic genes SREBF1 and FASN (242). The discrepancy in the role of β-oxidation and lipid accumulation between our study and that of Liu *et al*. can be explained by the different hepatoma cell lines used and the fact that not all activated genes translate into function at the cellular level. The duration of exposure to hypoxia also differs between the studies and this may have different impact on the intricate process in which hypoxia induces liver steatosis.

This study suggested that the increase in hepatic lipid accumulation in hypoxia required the activation of both HIF1α and HIF2α. Reports regarding the roles of HIF1α and HIF2α on hepatic lipid accumulation are conflicting. Deletion of the VHL tumour suppressor gene, that mediates HIF1α and HIF2α proteasome degradation, results in hepatic steatosis almost exclusively by constitutive activation of HIF2α, suggesting a dominant role for HIF2α in regulating hepatocellular lipid metabolism (229, 242). This is further supported by a study

showing the development of severe fatty liver in PHD2/3 double-knockout mice occurring in a HIF2-dependent manner (243). However, much controversy remains regarding the roles of HIF2 as a pro-lipogenic factor, as HIF2-deficient mice also exhibit hepatic steatosis (244) and forced expression of HIF1α, but not HIF2α in the liver stimulates hepatic steatosis in mice (67). HIF1α is also reported to induce neutral lipid formation, under hypoxia (245). This raises important issues in the understanding of the functions of HIFs in regulating liver metabolism, and demonstrates their complexity. Even though our present data suggests that both HIFs regulate lipid metabolism *in vitro*, it is possible that either HIF could have a more dominant role in regulating a specific mechanism of lipid accumulation in the liver. As hepatocytes have distinct metabolic properties depending on their locations in the liver acinus, that is, lipogenesis occurring perivenously and fatty acid degradation periportally (9, 25), different HIF could also act on different region of the liver, thus activating different metabolic pathways.

There are important limitations to the study. Some of the Western blot images for HIF proteins, in particular HIF2α, were suboptimal. This is due to technical difficulties as well as time constraint. It is widely accepted in the field that HIF-2α protein is difficult to image and we believe there are much lower levels of HIF-2α than HIF-1α in hepatocytes or hepatoma cell lines. Therefore, these results require further validation before robust conclusions can be made.

This study has mainly focused on “acute hypoxia” due to the practicality of our cell culture system. Studies have reported that acute sustained hypoxia induces

hypertriglyceridaemia in humans (246, 247) and animals (248). However, the mechanisms by which acute hypoxia induces hyperlipidaemia are less well studied. Jun *et al.* (249) showed that there are differences in the mechanisms by which chronic and acute hypoxia affect lipid accumulation. Whilst acute hypoxia decreased hepatic triglyceride secretion and decreased clearance of plasma triglyceride, chronic hypoxia in mice resulted in the opposite. They also showed that the mean FiO2 dictated the degree of triglyceride elevation, not the duration of exposure to hypoxia. Perhaps the chronicity of hypoxia or intervening periods of normoxic recovery provides an opportunity for transcriptional upregulation of genes involved in lipid synthesis and secretion (76), and thus, could explain some of the differences seen in the literature.

Our study explored the lipogenic effect of hypoxia and suggested that this was partly via the inhibition of PHD activity, as the increase in steatosis by PHD inhibition was modest compared to that of low oxygen. This suggests that hypoxia-induced hepatic steatosis can also be activated via other oxygen-dependent mechanisms, such as FIH inhibition; or via other non-oxygen dependent mechanisms. Animal studies have shown that FIH enzyme has a higher affinity for oxygen than that of the PHD enzymes (250, 251). This may indicate that different enzyme could act at different oxygen concentration and further investigation is required to unveil a functional relationship between the two.

The data described so far suggest that HIF activation results in lipid accumulation. However, some studies have reported the contrary. Chronic intake

of excess alcohol is known to drive lipid accumulation in the liver and cause liver hypoxia concomitantly with increased oxygen consumption. Nishiyama Y *et al* showed in a murine model that HIF1α deletion in the hepatocytes worsened hyperlipidaemia and hepatic lipid accumulation in response to alcohol (66). Furthermore, the PHD inhibitor dimethyloxalylglycine (DMOG), which stabilizes and activates HIFα, reduced alcohol-induced lipid accumulation in control, but not in HIF1α-deficient mice, confirming the anti-lipogenic role of HIFα in alcoholic fatty liver (66). This is perhaps not surprising as intervening episodes of normoxic recovery may exert different metabolic effects in the liver. As DMOG is likely to have many cellular off-target effects, these observations should be interpreted with care.

3.5 CONCLUSION

Much information is now available on the cellular pathways regulating HIF expression and transcriptional activity that increases our understanding of these transcription factors in hypoxic adaptation. Although HIF-1 and HIF-2 can be activated simultaneously or separately by hypoxia in one cell, the consequences on cellular and tissue metabolism appear to differ markedly in a cell type- and context-dependent manner. Further investigation of the roles of HIFs in different cells and conditions is needed to gain a better understanding of the bigger picture and their physiological and pathophysiological roles. These data suggest that that targeting this pathway could provide a unique mechanism for manipulation of metabolism.

4.0 EFFECTS OF HEPATITIS C VIRUS (HCV) ON HEPATIC LIPID ACCUMULATION

4.1 INTRODUCTION

HCV belong to the Flaviviridae family, and possesses a linear, positive-stranded RNA genome of 9600 nucleotides (252). Genomic RNA contains a single open reading frame encoding a polyprotein (~3000 amino acids), which is processed into 10 mature proteins by both cellular and viral proteases. The mature proteins consist of three structural proteins (core, E1 and E2), p7 and the nonstructural (NS) proteins NS2, NS3, NS4A, NS4B, NS5A and NS5B (253).

Chronic hepatitis C (CHC) infection is a global health problem affecting 170 million people and is a leading cause of liver transplantation. Hepatic steatosis in CHC is associated with an increased risk of progressive liver diseases such as cirrhosis and hepatocellular carcinoma (254-256). There are distinct patterns of lipid alterations between patients with different genotypes of CHC after viral clearance (257) with hepatic steatosis being more prevalent in patients with genotype 3 CHC (258). Its presence in CHC associates with viral load and response to antivirals agents. However, our understanding of viral–induced hepatic steatosis largely derives from *in vitro* studies with infectious molecular clones based on the genotype 2 viral isolate, JFH-1 (259, 260). A direct comparison between different genotypes has rarely been performed using the same model and experimental conditions. Hepatic steatosis is one of the

histologic features of CHC and the occurrence and severity of steatosis associates with viral load and response to antiviral agents.

Hepatic steatosis can be caused by an increase in *de novo* lipogenesis, fatty acid uptake and synthesis, a decrease in fatty acid β-oxidation, or reduced levels of very-low density lipoprotein secretion (46, 190, 261). HCV hijacks the lipid-producing machinery of hepatocytes for its benefit (106, 111). It is believed that HCV core protein causes intracellular lipid accumulation by altering lipogenic gene expression and protein activity, alongside effects on mitochondrial oxidative function (113, 262-265). HCV is reported to activate sterol regulatory element binding proteins (SREBPs) (266, 267), essential transcriptional regulators of cholesterol and fatty acid metabolism (268, 269). The importance of genes such as peroxisome proliferator-activated receptor-alpha (PPARα) and the proteasome activator (PA28)-gamma in HCV-mediated steatosis has been elucidated from studies in genetically altered mice (270). PPARα is a known to regulate oxidative enzymes and fatty acid import into mitochondria via induction of the carnitine palmitoyl acyl-CoA transferase 1 (CPT1A) gene (121, 271). PA28γ is required for the up-regulation of sterol regulatory element-binding protein 1c (SREBF-1c) transcription by the HCV core protein and induction of liver steatosis (270, 272). However, the mechanistic basis of these functional effects remains unclear.

We have shown in the previous chapter that HIFs play a role in hypoxia-induced lipid accumulation. Since several studies have reported that HCV infection stabilizes HIF (6, 165), we hypothesize that there could be a role for HIF in HCV-

induced hepatocellular lipid regulation. HCV has been shown to induce hepatic lipid accumulation in human hepatoma cell lines (269, 273-275). Hence, in this chapter, we aim to study the link between HCV and hepatocellular lipid metabolism and to explore the underlying mechanism by which HCV induces hepatocellular lipid metabolism including relative contributions of DNL, FFA and β–oxidation.

4.2 HYPOTHESIS AND AIMS

Hypothesis:

Host factor such as hypoxia inducible factor play a role in HCV-induced hepatocellular lipid alteration.

Aims:

To define the mechanisms by which HCV affects hepatic lipid homeostasis *in vitro.*

4.3 RESULTS

4.3.1 HCV stabilizes hypoxia inducible factors (HIFs)-1α and 2α

Huh-7 hepatoma cells were infected with mock or SA13/JFH, for 24 or 48 hours. We demonstrated HIF stabilisation by HCV by quantifying HIF1α and HIF2α proteins (western blot). This showed a time dependent increase in the expresion of both HIF isoforms following HCV infection [Fig 4-1A to C]. HIF stabilisation by HCV was functionally active with increased mRNA levels of validated HIF-target genes in the infected cells. mRNA expression of VEGF [4-1D] and was upregulated by 5 and 10 fold in Huh-7 hepatoma cells infected with HCV for 24 and 48 hour respectively; and mRNA expression of EPO [4-1E] was upregulated by 2 or 4 fold respectively.

HCV replication may be inhibited by cell confluence due to a decline in the nucleoside pool (276). To ensure cell viability following HCV infection, cells were detached by trypsinization after 48 hours of incubation. The number of viable cells stained with Trypan blue reagent was counted using a hemocytometer. No difference in cell numbers was detected at different multiplicity of infection (MOI) of HCV [Fig 4-1F].

1A.

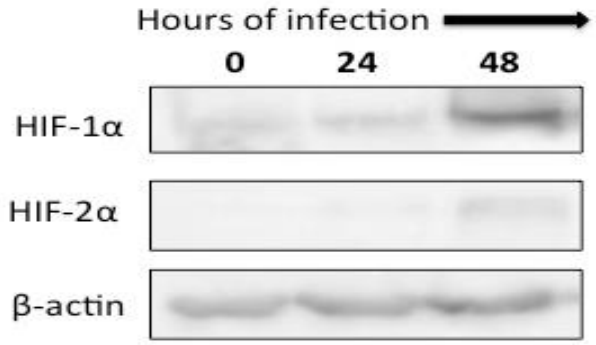
Hours of infection
0
24
48
HIF-1α
HIF-2α
β-actin

1B.

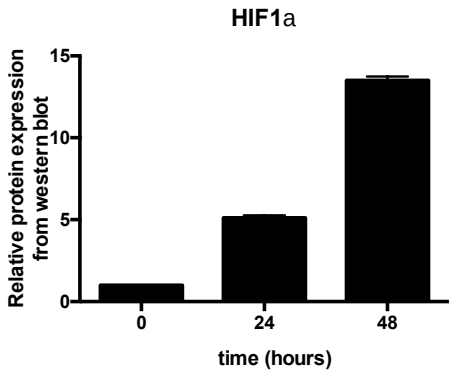
HIF1a
Relative protein expression from western blot
15
10
5
0
0
24
48
time (hours)

1C.

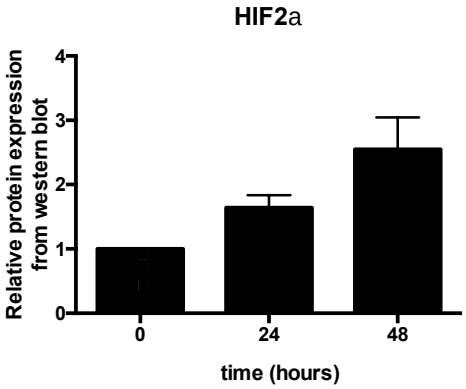
HIF2a
Relative protein expression from western blot
4
3
2
1
0
0
24
48
time (hours)

1D.

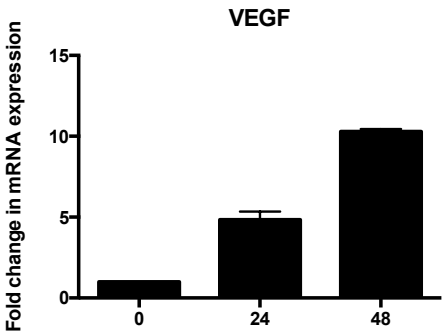
VEGF
Fold change in mRNA expression
15
10
5
0
0
24
48

1E.

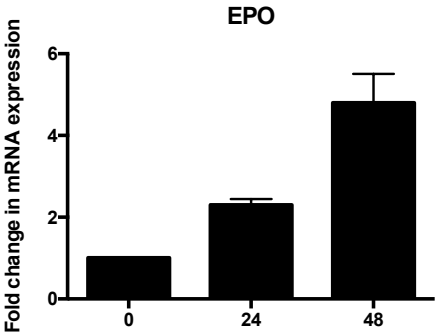
EPO
Fold change in mRNA expression
6
4
2
0
0
24
48

1F.

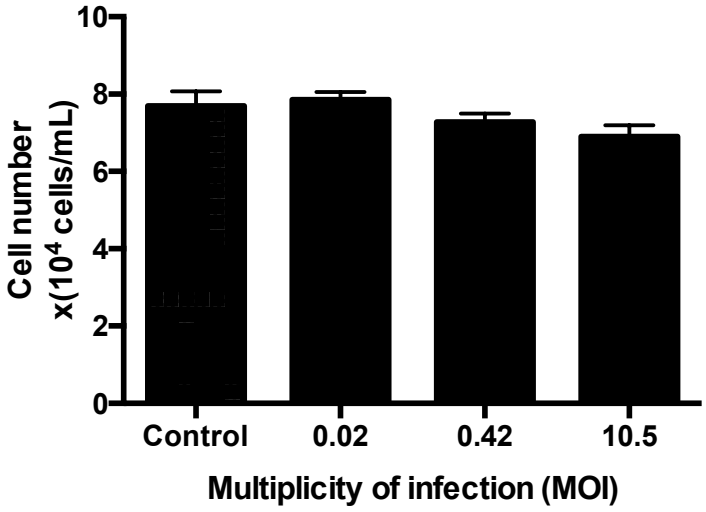

Fig 4-1. HCV infection stabilizes HIF-1α and 2α. Western blot of HIF1α and HIF2α proteins in mock and HCV-infected Huh-7 cells. 25ug of total protein was loaded per lane. A representative image is shown for each protein. β-actin was used as a loading control [A]. Relative quantification of respective HIF1α [B] and 2α [C] proteins from western blot, adjusted to loading control. mRNA expression of known hypoxia-induced transcripts:- vascular endothelial growth factor (VEGF) and erythropoietin (EPO) in mock and HCV-infected Huh-7 cells [D & E]. At the end of the experiment (48 hour), the viability of cells infected with mock or SA13/JFH was determined by Trypan blue and counted using hemocytometer (F). Huh-7 hepatoma cells were seeded at $4x10^4$ cells/ml and infected with SA13/JFH at MOI 0.42 FFU/cell for 24 or 48 hours. Data are presented as the mean fold change+SD performed in triplicate wells and quantified relative to GAPDH. Experiments were repeated thrice. Unpaired Student's t-test

4.3.2 HCV infection regulates hepatic *de novo* lipogenesis and free fatty acid uptake

Current literature showed that HCV core protein is steatogenic and patients with CHC demonstrate hepatic steatosis to varying degrees (269, 277, 278). We have shown that SA13/JFH infection increased SREBF1 and FASN mRNA levels by two fold [Fig 4-2]. To examine the functional effect of HCV infection on hepatic lipid accumulation, we measured DNL, FFA uptake and β-oxidation in mock and HCV infected Huh-7 hepatoma cells using isotope-labelled tracers as described in the previous chapter. Surprisingly, HCV infection decreased DNL [Fig 4-3A] and FFA uptake [Fig 4-3B] and had no detectable effect on β-oxidation [Fig 4-3C]. This observation was dependent on the multiplicity of infection (MOI) of HCV infection. A higher MOI (10.5) was associated with the lowest DNL and FFA uptake in infected cells and conversely, a lower MOI (0.02) was associated with the highest level of DNL, which was comparable to that of control. This suggests that the effect of HCV on DNL and FFA uptake may be dose dependent. HCV infection was confirmed by NS5A immunofluorescence analysis [Fig 4-3D].

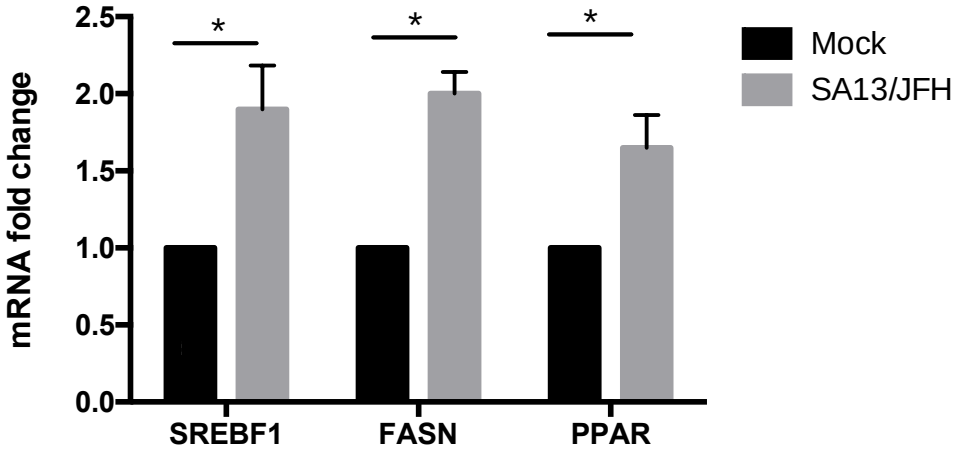

Fig 4-2. HCV regulates sterol regulatory element-binding protein 1 (SREBF1), fatty acid synthase (FASN) and peroxisome and proliferator-activated receptor alpha (PPARα) RNA transcript levels in Huh-7 cells. mRNA levels measured by RT-PCR in Huh-7 hepatoma cells seeded at $4x10^4$ cells/ml and infected with mock or SA13/JFH HCVcc for 48 hours. Data are presented as the mean fold change (+SD) of experiments performed in triplicate wells and repeated twice and quantified relative to GAPDH. *p<0.05. Unpaired Student's t-test

3A.

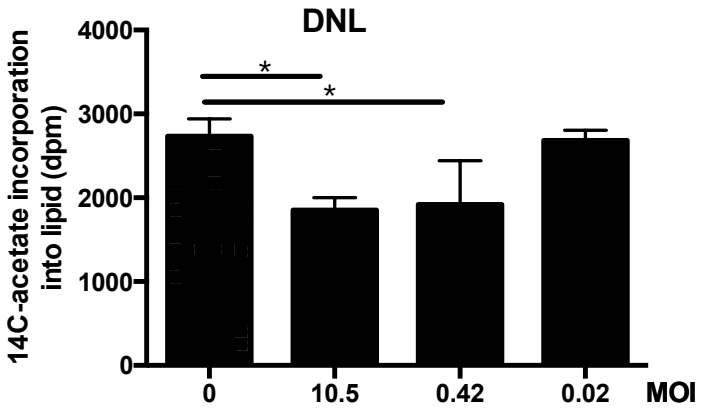
DNL
14C-acetate incorporation into lipid (dpm)
4000
3000
2000
1000
0
*
*
0
10.5
0.42
0.02
MOI

3B.

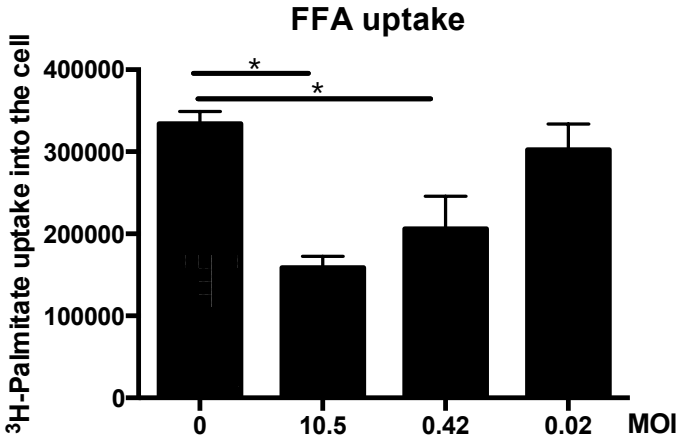
FFA uptake
3H-Palmitate uptake into the cell
400000
300000
200000
100000
0
*
*
0
10.5
0.42
0.02
MOI

3C.

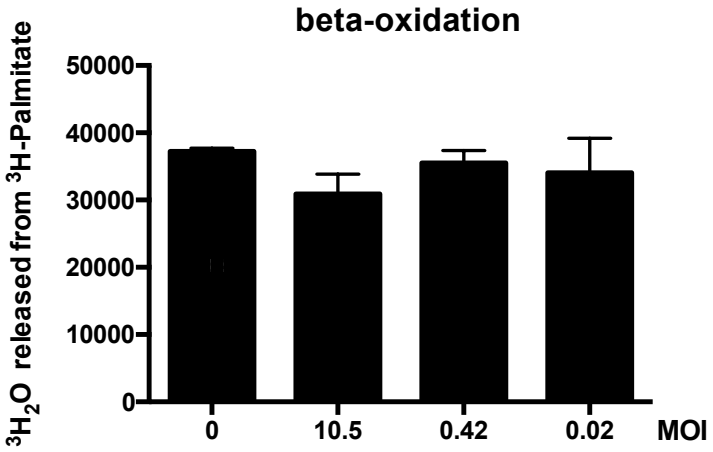
beta-oxidation
3H2O released from 3H-Palmitate
50000
40000
30000
20000
10000
0
0
10.5
0.42
0.02
MOI

3D.

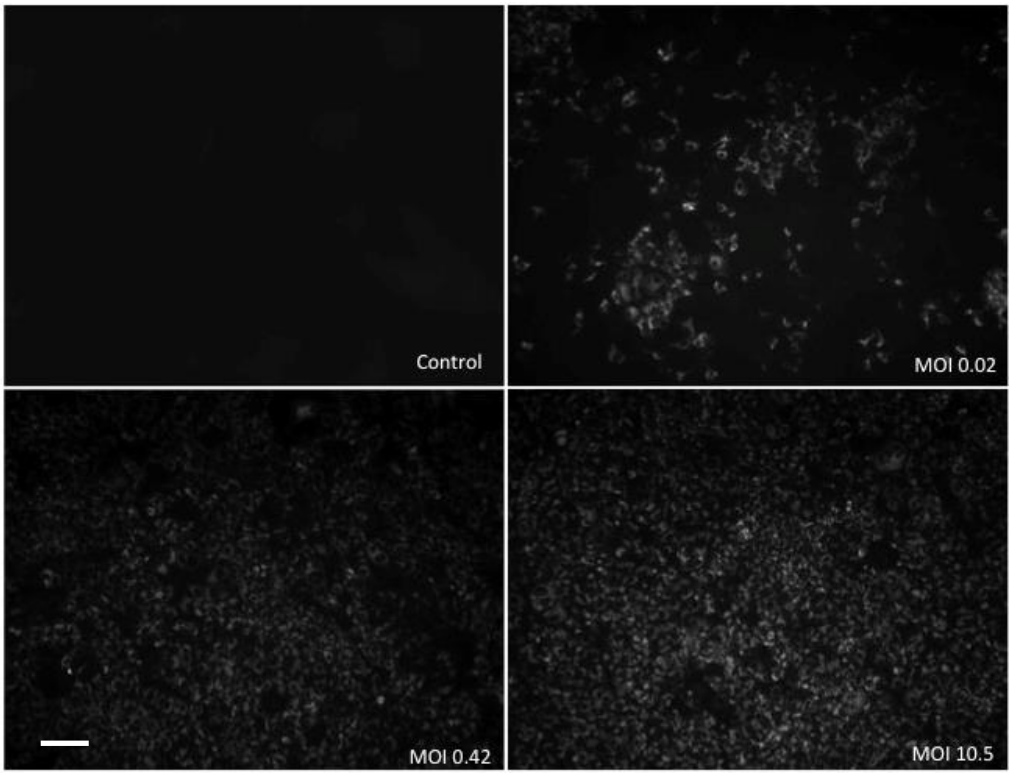

Fig 4-3. HCV infection decreases *de novo* lipogenesis (DNL) and free fatty acid (FFA) uptake in a dose-dependent manner, but does not impact β-oxidation. Huh-7 hepatoma cells were seeded at $4x10^4$ cells/ml and infected with mock or SA13/JFH at an MOI of 0, 0.02, 0.42 or 10.5 FFU/cell and incubated for 48 hours before lysis and lipid extraction. DNL was measured by 1-[^{14}C]-acetate incorporation into cell [A], FFA uptake was measured by ^{3}H-palmitate uptake [B] into lipid in cells and β-oxidation was measured by the amount of ^{3}H-water released by cells into the culture media [C]. Image shows foci formation in infected cells at different MOI. Foci were detected by staining for HCV NS5A protein (grey). Scale bar represent 40um [D]. Experiments were in performed in quadruplicates and repeated thrice. *$p<0.05$. Unpaired Student's t test

4.3.3 HCV perturbation of host cell lipid accumulation is dependent on viral replication

Unpurified HCVcc was used to infect the Huh-7 hepatoma cell lines in our study. To determine whether the effect of HCV on host cell lipid accumulation was viral specific or dependent on viral-induced cytokines or growth factors, we measured DNL and fatty acid uptake in the presence or absence of a neutralizing mAb that targets the cellular receptor CD81, which inhibits viral entry or NS3 protease inhibitor VX-950 (5 ug/ml), which inhibits viral replication.

We showed that incubation with either anti-CD81 antibodies or VX-950 successfully inhibited HCVcc infection, as confirmed by marked reduction of HCV NS5A staining on immunofluorescense [Fig 4-4A]. SA13/JFH-infected cells showed a reduction in DNL [Fig 4-4B] and FFA uptake [Fig 4-4C] compared to mock-infected cells. These effects were reversed with anti-CD81 monoclonal antibodies and VX-950. No effect was seen with β–oxidation [Fig 4-4D]. This data suggests that HCV inhibition of hepatocellular lipid accumulation is dependent on HCV entry and replication. Interestingly, there was a significant reduction in FFA uptake in non-infected cells incubated with either agents, when compared to untreated non-infected cells. A similar trend was also observed with DNL but this did not reach statistical significance.

4A.

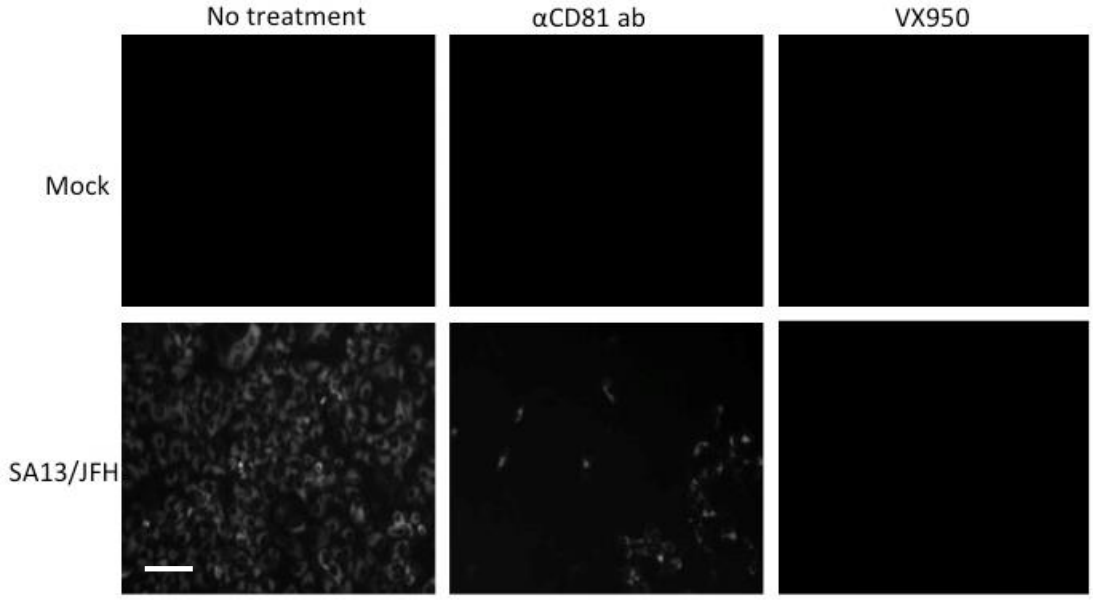
No treatment
αCD81 ab
VX950
Mock
SA13/JFH

4B.

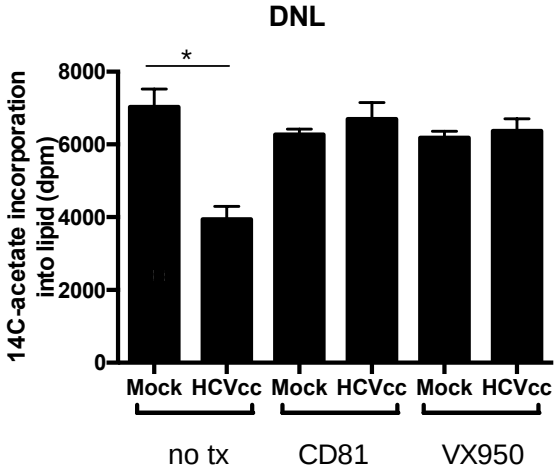
DNL
*
14C-acetate incorporation into lipid (dpm)
8000
6000
4000
2000
0
Mock HCVcc Mock HCVcc Mock HCVcc
no tx
CD81
VX950

4C.

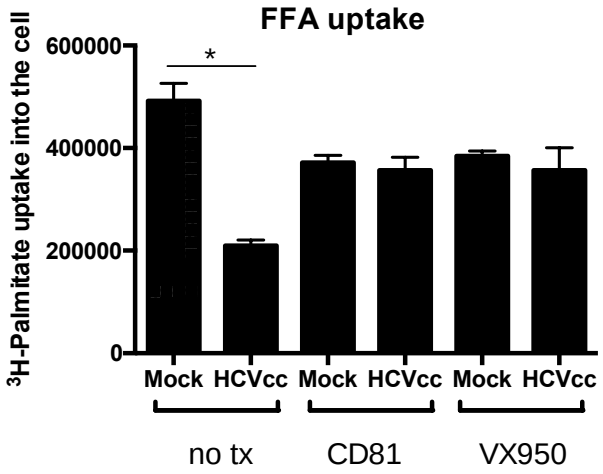

4D.

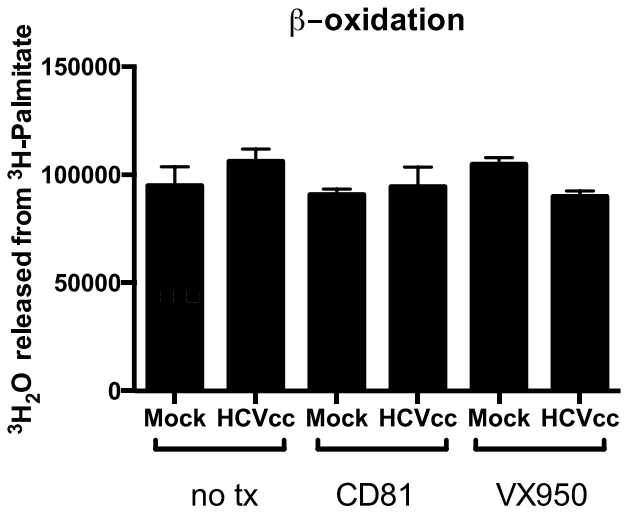

Fig 4-4. HCV inhibition of DNL and FFA uptake in Huh-7 hepatoma cells is dependent on viral entry and replication. Huh-7 cells were seeded at $4x10^4$ cells/ml and when 60-70% confluent, were treated with or without 1ug/ml of αCD81 antibody for 1 hour. Cells were then inoculated with HCVcc SA13/JFH at MOI 10.5 with or without 5ug/ml of VX950 (a protease inhibitor) and incubated for a further 48 hours. DNL [A], FFA uptake [B] and β-oxidation [C] in cells were measured using methods described previously. Experiments were performed twice and in quadruplicates. [D] Image shows foci formation detected by staining for HCV NS5A protein (grey). Scale bar represent 20um. *$p<0.05$. Unpaired Student's t test

4.3.4 HCV inhibition of hepatocellular DNL is viral strain-dependent

HCVcc isolates are grouped into seven genotypes, whereby the junction between the chimera is at the structural (S) – non structural (NS) protein. Accumulating evidence indicates that viral determinants in the core to NS2 proteins modulate host metabolism. To clarify this, two HCVcc isolates were used to infect two types of hepatoma cell lines. Chimeric HCV genotype 2a J6/JFH and genotype 5 SA13/JFH were used as both produced high infectivity in Huh-7 and Huh-7.5 hepatoma cells in our culture systems.

Both cell lines were infected with either viral strains for 48 hours. NS5A staining of the infected cells showed comparable frequency of antigen expressing cells in J6 or SA13 infected cells with increased infection observed in the more permissive Huh-7.5 cells (Fig. 4-5A) (279). HCVcc SA13/JFH infection significantly reduced DNL [Fig 4-5B] and FFA uptake [Fig 4-5C] in both Huh-7 and Huh-7.5 cell lines, with minimal effect on β–oxidation {Fig 4-5D]. However, HCVcc J6/JFH-infection had no effect on DNL, FFA uptake or β–oxidation [Fig 4-5B to D], suggesting strain-dependent effects.

5A.

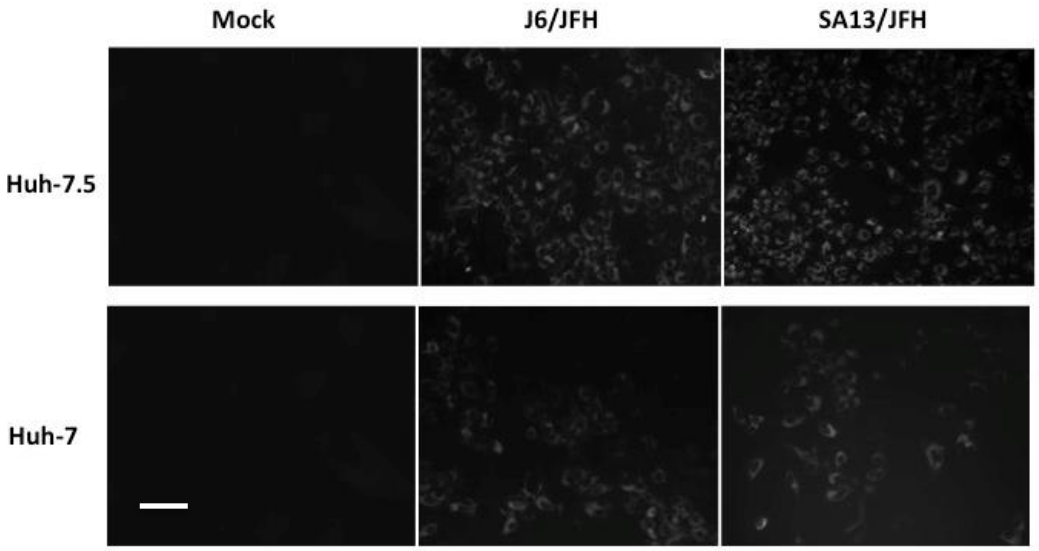
Mock
J6/JFH
SA13/JFH
Huh-7.5
Huh-7

5B.

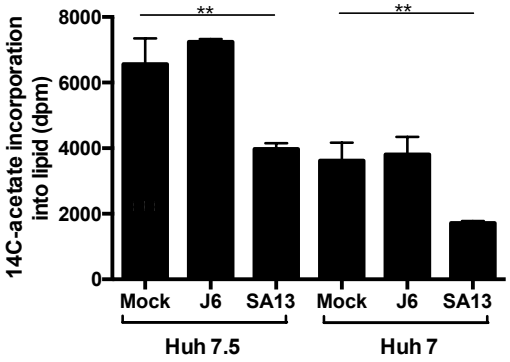
14C-acetate incorporation into lipid (dpm)
8000
6000
4000
2000
0
**
**
Mock
J6
SA13
Mock
J6
SA13
Huh 7.5
Huh 7

5C.

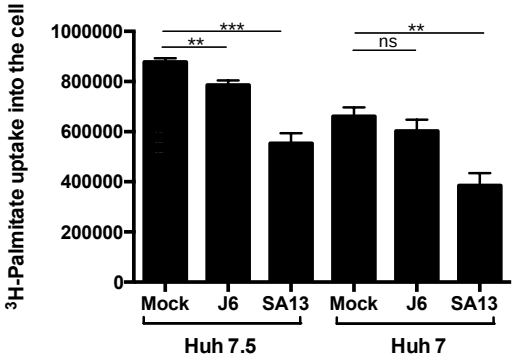
3H-Palmitate uptake into the cell
1000000
800000
600000
400000
200000
0
***
**
**
ns
Mock
J6
SA13
Mock
J6
SA13
Huh 7.5
Huh 7

5D.

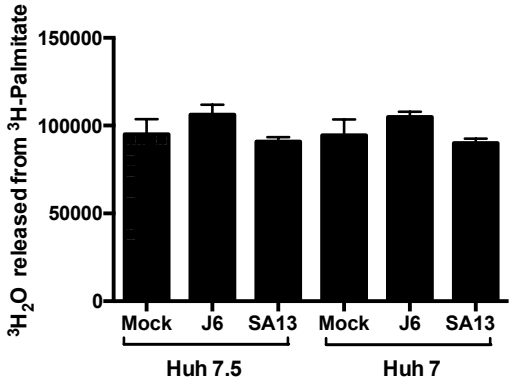

Fig 4-5. HCV inhibition of DNL is specific to viral strain. Huh-7.5 and Huh-7 cells were seeded at $5x10^4$ cell/mL and inoculated with either HCVcc J6/JFH or SA13/JFH at MOI 0.79 and 0.35 respectively, for 48 hours. Image shows foci formation detected by staining for HCV NS5A protein (grey). Scale bar represent 20um [A]. DNL [B], FFA uptake [C] and β-oxidation [D] in Huh-7 and Huh-7.5 hepatoma cells were quantified using methods described previously. Experiments were performed twice in quadruplicates. *p<0.05. **p<0.01, ***p<0.001. Two-way ANOVA

4.3.5 HCV infection decreases DNL under both normoxic and hypoxic conditions

Physiological oxygen gradients that exists in the liver and changes to oxygen tension that can occur in various liver pathologies such as viral hepatitis infection mean that the liver microenviroment can be more "hypoxic" than the environment hepatoma cells are cultured *in vitro*. To delineate the effects of HCV on lipid flux under more physiological conditions, we inoculated Huh-7 hepatoma cells with SA13/JFH and incubated them under 21% and 1% oxygen for 48 hours. NS5A staining between SA13/JFH-infected cells incubated under 21% or 1% oxygen were comparable under both conditions [Fig 4-6A]. HCV infection stabilized HIF1α expression in cells incubated under both atmospheric conditions. Higher intensity HIF1α protein band was seen in infected cells incubated under hypoxia, suggesting additive effects of HCV infection and low oxygen signals in stabilising HIF1α. A faint HIF2α protein band was seen in infected cells cultured under normoxia but not in cells cultured under hypoxia. [4-6B]. The latter observation is likely a result of under-optimisation of the primary antibody targeted against HIF2α. These observations correlated with the relative quantification of HIF proteins showed in Fig 4-6C.

We also showed that HCV infection reduced DNL under normoxic or hypoxic conditions. Even though hypoxia alone would increase DNL, the net effect of HCV infection and hypoxia was a reduction in DNL in Huh-7 hepatoma cells [Fig 4-6D].

6A.

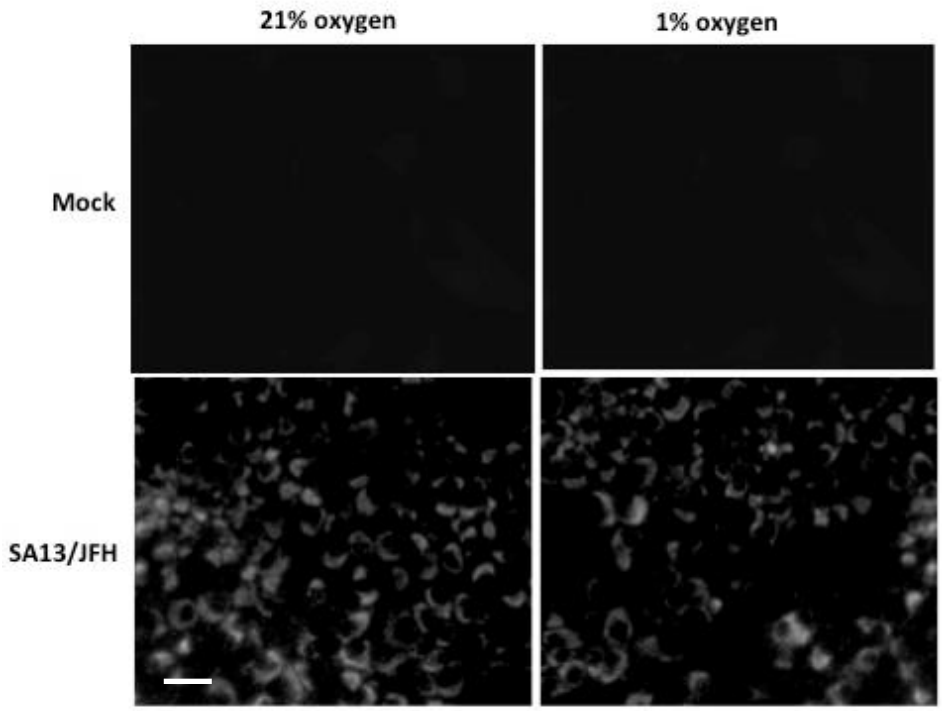
21% oxygen
1% oxygen
Mock
SA13/JFH

6B.

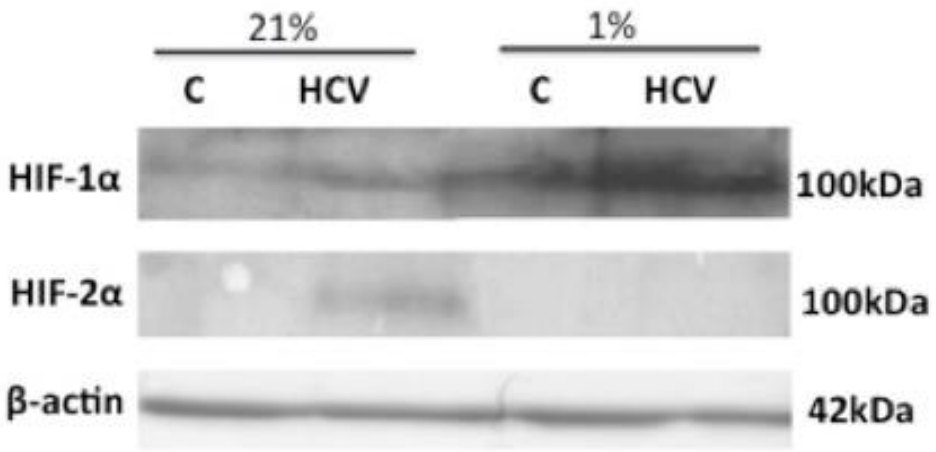
21%
1%
C
HCV
C
HCV
HIF-1α
100kDa
HIF-2α
100kDa
β-actin
42kDa

6C.

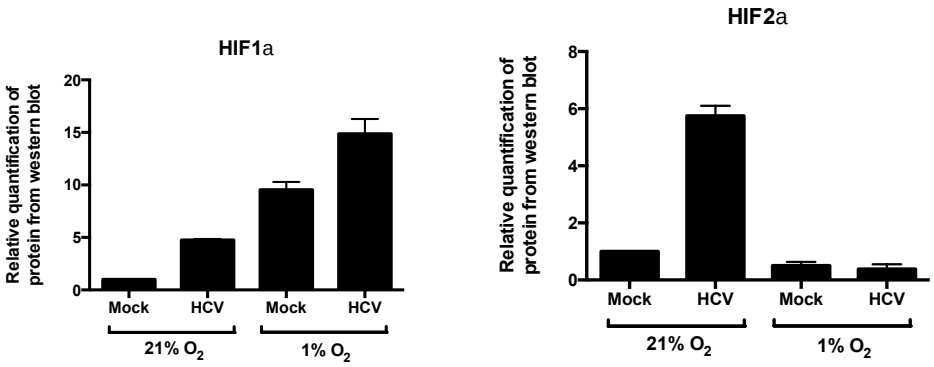

6D.

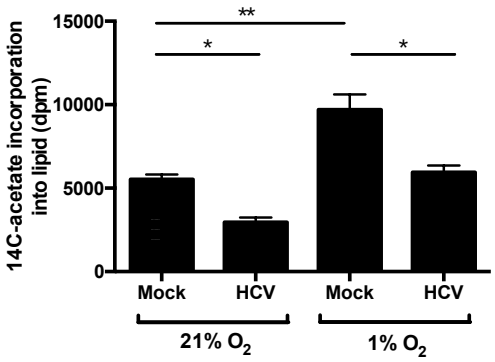

Fig 4-6. HCV infection reduces DNL under normoxic (21%) and hypoxic (1% oxygen) conditions. Huh-7 hepatoma cells were infected with mock or SA13/JFH at MOI 8.5 and immediately placed under 21% oxygen or 1% oxygen. NS5A positive (infected) Huh-7 hepatoma cells are shown in grey. Scale bar represents 10um [A]. HIF protein expressions were measured by western blot [B] and the density of each protein band was quantified against loading control [C]. Cells were lysed after 48 hours and measured for DNL by 1-[^{14}C]-acetate incorporation into lipid in cells [D]. Experiments were performed twice in quadruplicates (n=2). *$p<0.05$, **$p<0.001$. Unpaired Student's t-test

4.4 DISCUSSION

HCV is dependent on host lipid metabolism to complete its life cycle and this is largely mediated via the viral encoded core protein. We demonstrated that HCV infection increased the mRNA expression of lipid genes SREBF1, FASN and PPARα. Other studies aimed at interrogating the molecular mechanisms of HCV-induced lipid accumulation have also linked these genes to hepatic steatosis *in vitro* (124, 269, 277, 278, 280). Even though HCV activated lipogenic gene, post-transcriptionally, this did not translate into function at cellular level, as HCV reduced *de novo* lipogenesis and FFA uptake. As far as we know, few studies have utilised radio-isotopes to measure lipid flux in the setting of HCV infection *in vitro*. *Amako et al.* measured ^{3}H-palmitate incorporation by Huh-7.5 cell lines and found that HCV JFH-1 infection reduced ^{3}H-palmitate uptake, suggesting an attenuation of mitochondrial lipid β-oxidation (281). However, we did not observe any changes in β-oxidation between mock and HCV-infected cells in our model system. These discrepancies between our study and that of Amako Y *et al*. may be explained by the different hepatoma cell lines or viral strains used. As described in the previous chapter, HIF-2a protein can sometimes be difficult to image via Western blotting and therefore, further validation is required before robust conclusion can be drawn.

Apart form DNL, FFA uptake and β-oxidation, liver fat volume is also determined by the export of TG as VLDL into the bloodstream, and the flux of fatty acids released from adipose tissue through lipolysis. The latter two were not measured in this study. Douglas *et al* showed that reactive oxygen species, which are

induced by HCV infection, attenuate lipid synthesis and enhanced β-oxidation in HCV infected Huh-7.5 cells, yet cellular lipids still accumulated during infection. He concluded that as serum polyunsaturated fatty acids were elevated in the infected cells, altered lipid import/export pathways in the cells were responsible for the observed increase in lipid accumulation (275). In addition, different lipogenic pathways are activated in different liver diseases (190, 261) and in the case of CHC, DNL and FFA uptake may not be the main pathways by which HCV affect hepatic lipid metabolism.

Contrary to our findings, CHC has been shown to induce hepatocellular lipid accumulation *in vitro* (277, 281, 282). However, it is unclear whether these effects were virus-dependent or a consequence of host inflammatory responses. Even though we observed a reduction in DNL and FFA uptake following HCV SA13/JFH infection, that was not observed in J6/JFH infected cells suggesting that HCV-induced hepatocellular lipid alteration may be dependent on the viral strain, and specifically the viral encoded structural protein.

HCV alters the host lipid metabolism to favour its own replication and virion production, these pathophysiological changes are shared by all viral genotypes clinically while steatosis is more frequent and severe in genotype 3 infections (283), suggesting an involvement of additional mechanisms in case of an infection with this genotype. Unfortunately, the differential efficiency, shown by the various viral genotypes, in leading to the appearance of large fat droplets has been poorly studied (284). To date, much of our understanding of viral–induced hepatic steatosis derives from *in vitro* studies with infectious molecular clones

based on the genotype 2 isolate, JFH-1, (259, 260) as is with our study. Moreover, a direct comparison between different genotypes has been rarely performed, using the same model and experimental conditions. Therefore, the viral strain specificity observed in this study should be interpreted cautiously.

To date, as far as we are aware of, HCV-induced dyslipidaemia has been studied exclusively under atmospheric oxygen tension (21%). In the contrary, the role of hypoxia, in particular, hypoxia inducible factors (HIFs) , in the pathogenesis of alcoholic and non-alcoholic fatty liver diseases has been studied extensively (222-224). On their own, low oxygen induces hepatic lipid accumulation whilst HCV inhibits lipid accumulation. It is perhaps slightly surprising that the combined effect of low oxygen and HCV still reduced hepatocellular DNL and FFA uptake. This raises important questions as to the roles of HCV and other yet to be identified host factor(s), which regulate liver metabolism in CHC.

4.5 CONCLUSION

We are beginning to dissect the mechanisms by which HCV alters hepatocellular lipid metabolism. Further investigations comparing the different pathways by which different HCV strains alter liver fat volume is needed. With the advent of directly acting antivirals, genotype three CHC is now the most difficult and urgent to treat and understanding the link between hepatic steatosis and CHC is becoming even more important.

5.0 METABOLIC PHENOTYPE IN CONTROL, CHC AND NASH

5.1 INTRODUCTION

In the past, hepatic steatosis was a histological diagnosis associated with type 2 diabetes mellitus and obesity. The liver was essentially regarded as a target organ affected by either concurrent or pre-existent metabolic disorder such as insulin resistance and type 2 diabetes mellitus (285, 286). Several studies have now shown that hepatic steatosis precedes the development of metabolic disorder in a large proportion of cases (287-289). Non-alcoholic fatty liver disease (NAFLD) and chronic hepatitis C (CHC) are increasingly identified as diseases which are conducive to metabolic disorders (290). With the high prevalence rates of NAFLD and CHC, it is expected that these two diseases will occur together in a certain proportion of patients. Whilst the mechanism for the development of steatosis and insulin resistance in the setting of NAFLD is well understood, the mechanisms for these in CHC are less well defined.

Hepatic steatosis and insulin resistance occur more frequently in patients with HCV infection than in the general population in the Western world (140-143, 291-293). Type 2 diabetes mellitus (DM) is also more prevalent in patients with HCV-associated cirrhosis compared to other causes of cirrhosis (139). The macrovesicular steatosis present in patients with HCV is distributed in the periportal areas rather than the centrilobular region, which is more commonly seen in non-alcoholic fatty liver disease (294), indicating that HCV may be

directly inducing steatosis rather than being an unrelated finding. HCV-induced insulin resistance has been reported to impact on treatment response to interferon-based therapy and exacerbates hepatic fibrosis, leading to hepatocellular carcinoma (145, 295) (141, 143, 293, 296). Over the decades, clinicians have tried to characterize the metabolic syndrome seen in patients with CHC. The interaction of host and viral factors is thought to play a major role in hepatic steatosis and insulin resistance in CHC (106, 111, 116, 120-122, 126, 130, 131). The main sites of insulin resistance in CHC are also thought to be both intra- (137) and extra-hepatic (138). The contribution of obesity to steatosis appears to be greater in patients with genotype 1 CHC (148).

NAFLD comprises of hepatic steatosis, necro-inflammation of varying stages of fibrosis known as non-alcoholic steatohepatitis (NASH) and cirrhosis. It is prevalent and affects 30% of the general population and 70-90% of individuals with type 2 diabetes and/or obesity (297). Type 2 diabetes and obesity are independent risk factor for cirrhosis and carcinogenesis in NAFLD (298-301). Several pathophysiological mechanisms have been proposed for NAFLD (44, 194, 302, 303) but despite these, it still remains unclear why some individuals develope steatohepatitis, cirrhosis and liver failure, whilst others do not. A "multi-hit" hypothesis, which incorporates the interplay of insulin resistance, oxidative stress, and an inflammatory cascade, has been proposed (193, 194). Experts believe that a complex interplay between genetic susceptibility and multiple environmental factors contribute to progressive disease [Day 2002], and it is likely that insulin resistance plays a critical role in the pathogenesis in NAFLD. Using hyperinsulinaemic eyglycaemic clamp techniques coupled with

stable isotopes, several studies have identified the liver and muscle as the key sites of increased insulin resistance in patients with NASH (200, 203-205, 304). More recently, adipose tissue has also been identified as the source of fatty acids which drive lipid synthesis in the liver of patients with NASH (190). The predominant functions of adipose tissue are either to store or mobilize lipids. The degree to which each of these functions is performed depends on the expression of cytokines, which depends on the genetic composition of the individual, the site of adipose tissue, the type and degree of nutrients consumed, humoral factors and the sites of inflammation. Armstrong *et al* demonstrated that patients with NASH have marked adipose tissue dysfunction and increased hepatic and skeletal insulin resistance. In particular, they also found profound levels of insulin resistance and lipolysis in abdominal subcutaneous adipose tissue, which appeared disproportionate to whole-body adipose (201).

To date, no studies have compared the relative contribution of hepatic and peripheral tissue to the metabolic abnormalities associated with CHC vs. NASH. Adopting an integrative physiological approach with functional measures of lipid and carbohydrate flux, we aim to compare the relative contribution of tissue-specific insulin sensitivity in patients with CHC, NASH and healthy controls. All three groups of patients were recruited from a single centre, but at different time points. A standardized protocol was used in all studies.

5.2 HYPOTHESIS AND AIMS

Hypothesis: *The relative contribution of tissue specific insulin resistance to the metabolic syndrome differs in patients with CHC and NASH.*

Aim:

To compare global and tissue specific changes in insulin sensitivity in healthy subjects, CHC and NASH by measuring:-

1. Change in systemic insulin sensitivity
2. Change in liver fat and insulin sensitivity
3. Change in adipose tissue insulin sensitivity

5.3 METHODS

5.3.1 Study subjects

Baseline phenotype of patients with CHC was compared to that of healthy volunteers from the FindIT study conducted by Hazlehurst *et al.* (305) and of patients diagnosed with NASH from LEAN study conducted by Armstrong *et al.* (306). All cohorts of patients were recruited from a single centre and underwent standardized physiological assessments as described below.

Hepatitis C virus (HCV) cohort

Between 1st October 2012 to 30th September 2014, 89 patients were screened and 13 patients were recruited into the study. Patients were naïve to anti-viral treatment, and were non-cirrhotic. Nine patients were infected with genotype 1 and four with genotype 3 HCV.

Inclusion criteria

1. 18-70 years old
2. BMI 18-34 kg/m^2
3. Eligible for antiviral treatment within 6 months of recruitment
4. Successful viral eradication following treatment, measured by undetectable HCV PCR 3 months following end of antiviral treatment
4. Good understanding of English

Exclusion criteria

1. Refusal or lacks capacity to give informed consent to participate in study
2. Evidence of liver cirrhosis shown on transient elastography or liver biopsy
3. Liver diseases of other aetiologies (drug-induced, viral hepatitis, autoimmune hepatitis, primary biliary cirrhosis, primary schlerosing cholangitis, haemochromatosis, alpha-1 antitripsin deficiency, Wilsons disease).
4. Current or previous insulin or oral hyperglycaemic therapy, or HbA1c >9.0%
5. Pregnancy or breastfeeding
6. Average alcohol consumption per week male >21, female >14 units
7. >5% weight loss within the last 6 months
8. ALT or AST > 10x upper limit of normal

<u>Non-alcoholic steatohepatitis (NASH) patients (LEAN study)</u>

Patients with definite diagnosis of non-alcoholic steatohepatitis (NASH) confirmed by biopsy by two independent histopathologists were recruited between 2007-2009. All participants were between 18-70 years of age and have a body mass index (BMI) of >25kg/m2 at screening. Patients with type 2 diabetes had to have stable glycaemic control (HbA1c < 9.0%) and be managed by either diet and/or a stable dose of metformin/sulphonylurea. Patients with history or current significant alcohol consumption, poor glycaemic control (HbA1c > 9.0%), Child's Pugh B or C cirrhosis or another liver disease aetiology were excluded

from the study. Those on concomitant use of drugs reported to be inducers of (methotrexate, amiodarone, steroids) or potential therapies for NASH (TZDs, vitamin E) or other known hepatotoxins were also excluded. Physiological assessments in these patients were performed by by Dr M.J. Amrstrong.

Healthy volunteers (FindIT study)

Twelve healthy male volunteers were recruited from local advertisement between 2006-2009 and provided written informed consent. All were non-diabetic, were normotensive, aged 18–65 years, and had a BMI between 20 and 35 kg/m2. All were non-diabetic, had not been on glucocorticoid or any medications known to impact on glucocorticoid metabolism, within the previous 6 months. Physiological assessments on all the volunteers were performed by Dr J Hazlehurst.

5.3.2 Study design

All patients were invited to visit the Welcome Trust Clinical Research Unit at different time points. In all 3 studies, patient demographics, clinical and biochemical measures were recorded. These included anthropometry (including bioimpedance), fasting haematological and biochemical bloods, liver biochemistry and plasma glucose, which were measured using standard laboratory methods (Roche Modular system, Roche Ltd, Lewes, UK). Serum insulin and NEFA were measured using standard laboratory methods. Patients also underwent 2-step hyperinsulinaemic euglycaemic clamp, $^{2}H_{5}$-glycerol infusion (except LEAN), adipose tissue microdialysis, magnetic resonance spectroscopy of the liver and dual energy absorptiometry (DXA) scans during each visit as part of the metabolic study. A schematic of the metabolic study is shown in Fig 1.

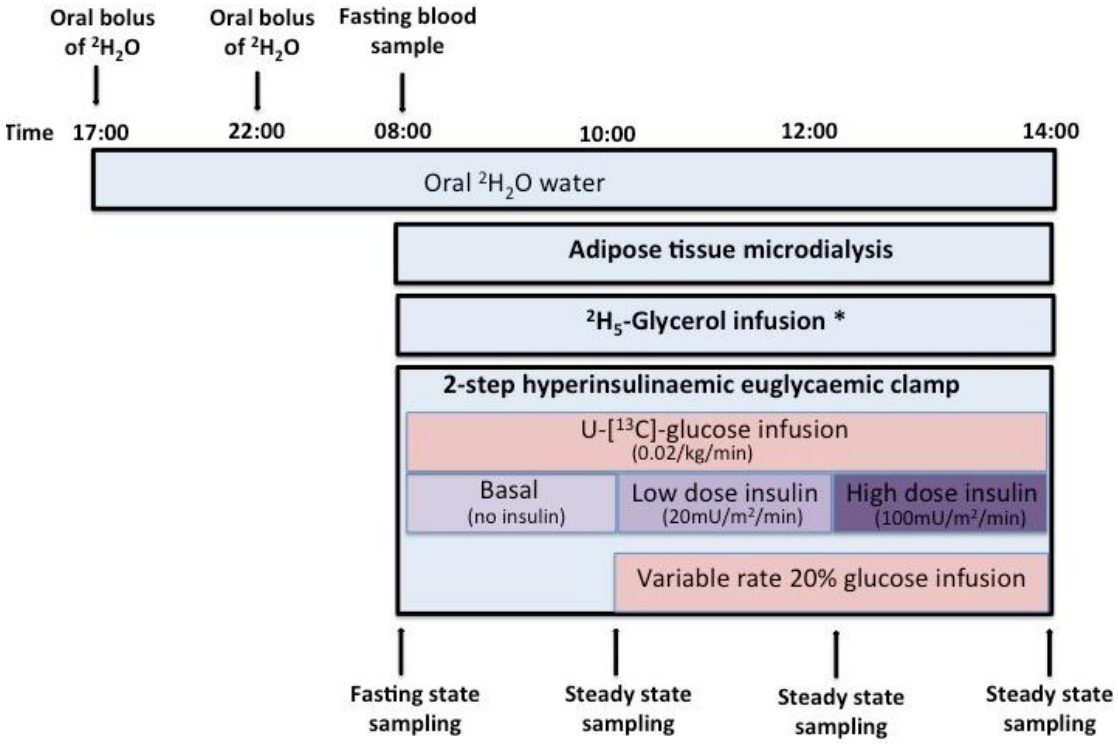

Fig 5-1. Schematics of metabolic study. Participants from all three studies underwent a 2-step hyperinsulinaemic euglycaemic clamp with stable isotope tracers (^{13}C-glucose; $^2H_5$-glycerol; $2H_2O$ deuterated water) and adipose microdialysis. *Patients from FindIT did not have $^2H_5$-glycerol infusion as part of the study protocol.

Hepatic DNL

The evening prior to the clinical study, subjects visited the research facility for blood sampling [measuring free fatty acid (FFA), Very Low Density Lipoprotein (VLDL), triglycerides (TG) and insulin. They were then given a standardized evening meal (carbohydrates 45g, protein 23g, and fat 20g). To determine the rates of *de novo* lipogenesis, they were given oral $^{2}H_2O$ (3g/kg deuterated water in 2 divided doses) at 5pm and 10 pm, followed by drinking water enriched to 0.4%. They then returned to the research facility the next morning in the fasting state (08.00). A blood sample was taken to measure;

- VLDL and TG concentrations
- Enrichment with ^{2}H, and plasma water enrichment from which *de novo* lipogenesis was calculated.

The percentage contribution of hepatic DNL to endogenous palmitate synthesis was determined by the incorporation of $^{2}H_2O$ in the palmitate present in the plasma total triglyceride pool, as previously described (208). This percentage was calculated from the increase in the $^{2}H/^{1}H$ ratio in the palmitate methylester of the total triglyceride fraction and in the water of plasma samples taken before (1700 hours, the evening before) and 14 hours after the initial ingestion of the $^{2}H_2O$ tracer (0800 hours, before the start of the hyperinsulinaemic euglycaemic clamp). The following formula was used: % hepatic DNL contributes to endogenous palmitate synthesis = [delta $^{2}H/^{1}H$ ratio in palmitate methylester]/[delta $^{2}H/^{1}H$ ratio in waterpool] X (34/22) X 100%. In the

equation, 34 is the total number of H-atoms in palmitate methylester and 22 is the number of water molecules incorporated into palmitate via DNL as observed in previous rodent studies (Diraison et al., 1996) and currently used in human studies (Diraison et al., 1997).

2-step hyperinsulinaemic euglycaemic clamp

The 2-step hyperinsulinaemic euglycaemic clamp is the gold standard used to measure hepatic insulin sensitivity (endogenous glucose production) and peripheral, mainly skeletal muscle insulin sensitivity (glucose disposal) *in vivo* [Fig 2]. A bolus of ^{13}C-glucose (CK Gas Ltd, Hook, UK) was administered (2mg/kg) over 1 minute followed by constant rate infusion of ^{13}C-glucose (20 μg/kg/min). Basal steady state samples were taken at 3 time points during the final 30 minutes of the 2 hours before insulin and glucose infusions. At 10am a soluble insulin infusion (Actrapid; Novo Nordisk, Copenhagen, Denmark) was commenced (20mU/m^2/min), together with an infusion of 20% glucose enriched with ^{13}C-glucose to 4%, beginning at 2 mg/kg/min through the same line.

Arterialized blood samples were taken at 5-minute intervals and the glucose infusion rate changed to maintain fasting glycaemic levels. Steady state samples were taken at 3 time points in the final 30 minutes, 2 hours after starting the insulin infusion. The insulin infusion rate was then increased to 100mU/m^2/kg) for 2 hours with sampling as described above.

The M value is defined as the average glucose infusion rate over a period of 120 minutes from the start of the insulin infusion. The M/I ratio is the ratio of the M value to the average plasma insulin concentration during the same period. When a two-step clamp is performed the ΔM/ΔI ratio is defined as the increment of M produced by raising the insulin infusion rate over the corresponding increment of I. The use of these indices, however, makes two fundamental assumptions: first, that at the end of 120' of insulin infusion the experimental subject is at steady state with regard to glucose uptake rate; and second, that the glucose uptake rate increases linearly with increasing insulinaemia, either throughout the insulin concentration range (when using the M/I index for characterizing the subject's response) or between successive insulin concentrations reached in the two-step clamp (when using the ΔM/ΔI index).

Rates of glucose production (Ra glucose) and glucose disposal were calculated using modified versions of the Steel equations (307, 308). In brief, the steady state glucose rate of appearance (Glu Ra) adjusted for insulin concentration (M/I) was indicative of hepatic glucose production; and the steady state glucose rate of disposal (Glu Rd) adjusted for insulin concentration (M/I) was indicative of insulin-mediated glucose uptake.

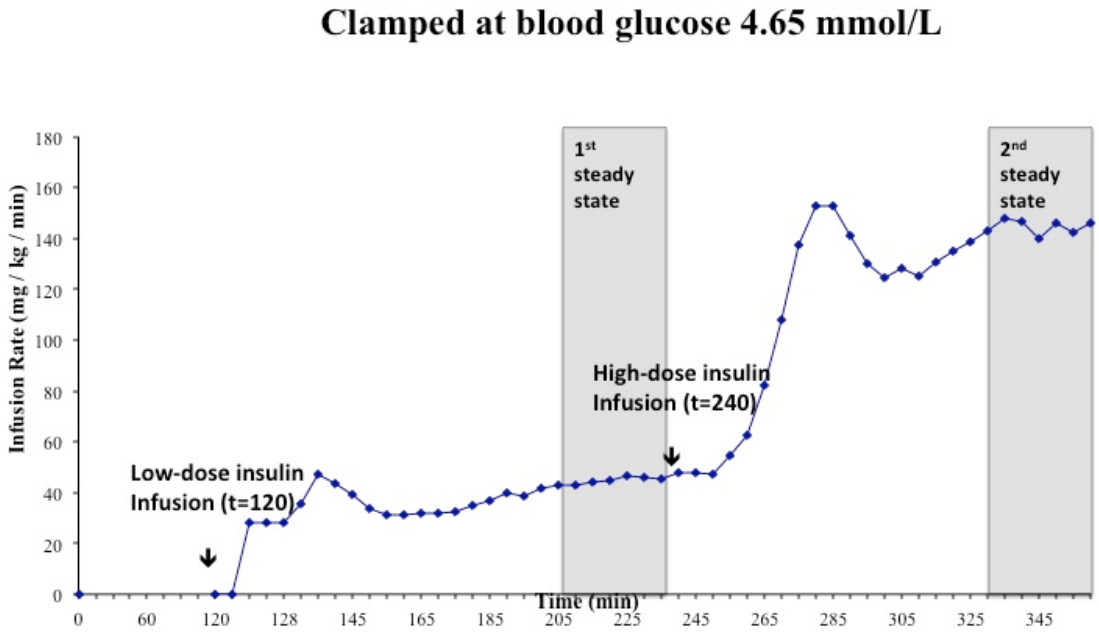

Figure 5-2. A two-step hyperinsulinaemic euglycaemic clamp from the study. The infusion rate of 20% glucose (+4% ^{13}C-glucose isotope) was adapted every 5 minutes to maintain euglycaemia (4.65 mmol/L in current case) throughout 2 hours low-dose insulin (20mU/m^2/min) and 2 hours high-dose insulin (100mU/m^2/min) infusions. Steady-state samples were collected between 210-240 minutes (1st step, representing hepatic insulin sensitivity) and 330-360 minutes (2nd step, representing peripheral insulin sensitivity).

Measuring glucose using near-patient YSI machine

Serum glucose was measured using the 2300 STAT PLUS Analyser (YSI Incorporated, Life Sciences, Ohio, USA).

Required equipment:

- 2 ml plastic tubes to present to the sipper
- Rinsing buffer

• Calibrators

After calibration, the YSI machine was placed in 'RUN' mode. Serum samples were automatically aspirated and glucose result displayed on screen in 15-30 seconds. The YSI automatically self-calibrates every 15 minutes when in RUN mode.

$^{2}H_5$-glycerol infusion (insulin suppressed lipolysis)

Principle: Measurement of glycerol appearance is useful since fatty acid flux underestimates the rate of lipolysis because of re-esterification. Fatty acids can become re-esterified within adipocytes, which prevent release of fatty acids into the bloodstream despite active lipolysis. However, glycerol cannot be reincorporated into triglycerides because glycerol kinase is absent within adipocytes.

Whole body lipolysis was assessed, by measuring glycerol rate of appearance (Gly Ra) using a stable isotope method. Stable levels of $^{2}H_5$-glycerol (0.1umol/kg/min) (CK Gas Ltd, Hook, UK) were infused alongside the 2-step hyperinsulinaemic euglycaemic clamp described above. The decrease in Gly Ra, from basal to steady-state low and high-insulin is an index of the suppression of lipolysis by insulin. Multiple low dose insulin steps are used to construct decay curves to assess the insulin concentration needed to half-maximally suppress Gly Ra (EC_{50}).

Stable Isotope Mass Spectrometry Analysis

The enrichment of U-[13C]-glucose in plasma was determined by gas chromatography-mass spectrometry (model 5973; Agilent technologies, Cheshire, UK). Deuterium enrichment of the body water pool was measured using H2/H2O equilibration device, coupled on-line to a ThermoFinnigan Deltaplus XP Isotope Ratio Mass Spectrometer (IRMS; ThermoFinnigan MAT GmbH, Bremen, Germany). The full methods have been previously described in detail (208). In brief, after adding 200µl of plasma sample and inserting platinum catalyst to a borosilicate sample vial, the vial is capped and automatically flushed with 2% H2 in He equilibration gas. After an equilibration time of 40 minutes, the 2H/1H enrichment of the head space gas is sampled and analysed automatically (mean of 10-fold measurement) on the IRMS using 2% H2 in He as reference gas. The in house coefficient of variation of this assay is <2% for naturally enriched samples and <0.5% for samples with a 2H/1H ratio 0.001 > natural background.

Deuterium enrichment in the palmitate fraction of total plasma triglycerides was measured on an automated GC/TC/IRMS system (Thermo Finnigan Delta Pus XP; Thermo Electron Cooperation, Bremen, Germany) (www.thermo.com). In brief, the lipid fraction was extracted from 1.5 ml of plasma as described by Folch et al (309) and the triglyceride fraction isolated by solid phase extraction Bond Elut NH2-Aminopropyl columns). After transmethylation of the triglyceride fraction (310), the $^{2}H/^{2}H$ ratio in palmitate methylester was measured via a GC separation of the methylated fatty acids followed by pyrolytic conversion of the palmitate methylester into CO and H_2, followed by online continuous flow

measurement of the $^{2}H/^{2}H$ ratio in the separated H_2 peak by the ThermoFinningan Deltaplus XP IRMS (Bremen, Germany). The in house coefficient of variation of this assay is <5% over the sample range observed in this study ($^{2}H/^{2}H$ ratio 0.00000-0.0004 > natural background). The $^{2}H/^{2}H$ ratio of both the body water pool and of the palmitate fraction of total plasma triglyceride was corrected against enrichment curves.

Subcutaneous adipose tissue (SAT) microdialysis

Principle: The contribution of the adipose tissue in the pathophysiology of IR is partly based on its lipolytic activity, resulting in mobilization of free fatty acids and glycerol. Increased levels of free fatty acids are deleterious for glucose utilization and insulin action. In order to determine the impact of HCV on global metabolic phenotype (the absolute rate of exchange of glucose, glycerol and lactate), we performed adipose tissue microdialysis, which allowed the sampling of adipose interstitial fluid. Measurement of pyruvate and glycerol within the fluid can provide an assessment of insulin stimulated glucose uptake (pyruvate) and insulin mediated suppression of lipolysis (glycerol).

A single microdialysis catheter (M Dialysis 63 40/30, Prospect Diagnostics ltd) was inserted under local anaesthetic (1ml of 1% lignocaine) into the subcutaneous adipose tissue 5cm to one side of the umbilicus. Using the CMA107 microdialysis pump, a microdialysate solution (physiological sterile saline solution) was introduced into the catheter (perfusion rate = 0.3μl/minute).

Microdialysis took place over the duration of the hyperinsulinaemic clamp (including the basal phase). Microdialysis samples were taken at 30-minute intervals for the duration of the 2-step clamp. Microdialysate fractions will be analyzed by mobile photometric, enzyme-kinetic, automated analyzer (CMA ISCUS flex) for glycerol, glucose, lactate and pyruvate.

RNA isolation and cDNA synthesis

The blood samples were collected into 15 ml tubes. Total RNA from blood samples was extracted using Roche High Pure PCR Template Preparation Kit (Catalog number; 11796828001) according to the manufacturer's instructions. Total RNA was reverse-transcribed into first-strand complementary DNA (cDNA) using a High Capacity cDNA Reverse Transcription Kit (Invitrogen, Life Sciences, Catalog Number: 4368814) in a tube including 2.0 µl 10X RT buffer, 0.8 µl 25X dNTP (100 mM), 2.0 µl 10X RT random primer, 1.0 µl reverse transcriptase enzyme, and 4.2 µl nuclease free water. The cycle conditions were as follows: 10 min at 25 °C, 120 min at 37 °C, and 5 min at 85 °C.

Serum insulin, glucose and free fatty acid measurements

This is a solid phase two-site enzyme immunoassay using two monoclonal antibodies (abs) against separate antigenic determinants on the insulin molecule. Each Human and Mouse insulin ELISA kit (Mercodia, Sweden) kit contains the

following:

• Mouse monoclonal anti-insulin-coated plate

• Calibrators 0-5 containing set concentrations of recombinant human insulin

• Enzyme Conjugate 11X (1.2ml) –mouse monoclonal anti-insulin

• Enzyme Conjugate Buffer (12ml) – added to Enzyme Conjugate 11X to make Enzyme Conjugate 1X solution

• Wash buffer 21X (50ml) – added to 1L distilled H20 to make wash buffer 1X solution

• Substrate TMB (light sensitive)

• Stop solution

Methods

Human serum was defrosted on ice at room temperature. Calibrators and samples (10µl each) in duplicate were transferred to 96-well plate. Enzyme conjugate 1X solution 100µl was added to each well, and samples incubated on a plate shaker (700-900 rpm) for 2 hours at room temperature (18-25°C). Reaction volume was discarded by inverting the microplate over a sink and plates then washed manually by adding 350µl wash buffer 1X solution to each well. Wash solution was discarded and the plate tapped firmly against absorbent paper to remove excess liquid. This step was repeated 5 times, followed by addition of Substrate TMB 200µl to each well. After incubation for 15 minutes at room temperature, 50µl Stop Solution was added and the plate placed on the shaker for 5 seconds to ensure mixing. Optical density of plates was measured at 450nm on spectrophotometer.

Serum free fatty acids (FFA)

Serum free fatty acids were measured in human serum samples using a commercially available kit (ZenBio, NC, US). Assessment of serum fatty acids is via a coupled reaction to measure non-esterified fatty acids (NEFA). The initial step is catalyzed by acyl-CoA synthetase (ACS), which produces fatty acyl-CoA thiol esters from the NEFA, ATP, magnesium and CoA in the reaction. Subsequently acyl-CoA esters react with oxygen in the presence of acyl-CoA oxidase to produce hydrogen peroxide. In the presence of peroxidase, hydrogen peroxide allows the oxidative consensation of 3-methyl-N-ethyl-N-(β-hydroxylethyl)-aniline with 4-aminoantipyrine, forming a purple product which absorbs light at 550nm. Each kit contains the following:

- Dilution buffer 100ml
- FFA standard
- FFA Diluent A
- FFA Diluent B
- FFA Reagent A
- FFA Reagent B

Methods

A standard curve was prepared using the Standard Solution by means of serial dilutions with dilution buffer, with final concentrations of 0, 1.4, 4.1, 12.3, 37, 111 and 333μM. FFA Reagent A and B was prepared by adding 50ml FFA Diluent

A and B respectively. 5µl of serum samples were added in duplicate to a 96-well plate. 45µl of dilution buffer was added to each well to give a total volume of 50µl (1:10 dilution). 100 µl of Reagent A was added to each well. The plate was placed on an orbital shaker for 10 seconds to ensure mixing, then placed in an incubator at 37°C for 10 minutes. 50 µl of Reagent B was next added to each well and the plate placed on an orbital shaker for 10 seconds to ensure mixing. The plate was then placed in an incubator at 37°C for 10 minutes. The plate was allowed to equilibrate at room temperature for 5 minutes. The optical density of each well was then measured at 540nm.

Magnetic resonance spectroscopy (MRS) of liver

Principle:- The current method for assessment of hepatic steatosis is with ultrasound or liver biopsy. These procedures are highly insensitive (ultrasound) or invasive and uncomfortable for patients (biopsy) limiting their use in clinical practice (311). Non-invasive magnetic resonance spectroscopy (MRS) protocols have already been applied for the quantification of hepatocellular lipid content in different populations and have excellent correlation with liver biopsy (312). MRS directly measures the triglyceride content in the liver cells and quantitatively analyzes the composition of fat in liver and the biochemical characteristic of lipid metabolism.

MRS protocol: MRS of the liver was performed on a Siemens Verio 3T MRI system

using single-voxel PRESS-MRS, following orthogonal T1w VIBE (3D-GRE) breath-hold localisers of the thorax and abdomen. A (20x20x20) mm^3 MRS voxel was prescribed, localised in the central right lobe of the liver, avoiding major blood vessels and bile ducts. Image-based shimming was performed over a co-localised (40x40x40) mm^3 region, with manual adjustments where necessary to achieve water linewidth < 40Hz. To allow T2-corrected fat fraction measurements, MRS was acquired without water suppression during a single breath-hold (NSA=7, TR=3s, preps=0), with 4 repeated acquisitions at each of 4 selected echo times/TE's (TE=30,40,70,100 ms). MRS with water suppression was also acquired at the same TEs to further characterise the metabolite profile. All breath-hold scans were acquired at end-expiration with patient coaching. Spectra were fitted offline using Tarquin[4] with a customised basis set containing lipid and metabolite peaks. Strict quality control (QC) criteria were applied and visual inspection of fits was performed. Exponential fitting was performed to estimate water, lipid and metabolite T2s and lipid and metabolite levels were calculated relative to water at each TE with and without T2 correction.

Dual energy absorptiometry (DXA) scan

DXA scan is recognized as the reference method to measure bone mineral density (BMD) and uses two X-ray energies to measure the presence of bone mineral, lean tissue and adipose tissue. DXA was employed for body composition assessment using Hologic Discovery/W DXA (software version Apex 3.0, Hologic

Inc.). Specific fat phenotype was measured using android, gynecoid, peripheral (arms and legs), and trunk regions of interest, with subsequent calculation of android:gynecoid and trunk:peripheral fat ratios (Gregson et al., 2013).

6.3.3 Statistical analysis

Continuous clinical and laboratory variables are reported as means and standard error (SE) as all variables had parametric distribution on D'Agostino and Pearson Omnibus Normality testing. Categorical variables are reported as number and percentages. Area under the curve (AUC) analysis was performed using the trapezoidal method for interstitial glycerol release during the clamp. For comparison of single variables, unpaired Student t-tests were used (or non-parametric equivalents where data were not normally distributed). Where repeated samples were taken repeated-measures one-way ANOVA was used, incorporating the Dunnett's test for multiple comparisons. The significance level was set at $p<0.05$. All analysis was performed using the GraphPad Prism 5.0 software package.

Storage of clinical samples

Serum and plasma samples and adipose biopsies collected were stored frozen in 1ml aliquots at -80C at the Institute of Biomedical Research, University of Birmingham. The specimen storage banks hold a license from the Human Tissue Authority to store tissue for research purposes.

Data handling, quality assurance, record keeping and retention

Data management was undertaken according to the standard operating procedures of the CRCTU at the University of Birmingham, UK. The CRCTU was fully compliant with the Data Protection Act 1998 and the International Conference on Harmonisation Good Clinical Practice (ICH GCP). The CRCTU was responsible for monitoring the study and providing annual reports to the MHRA. The trial was registered with the Data Protection Act website at the University of Birmingham. Participant identifiable data were shared only within the clinical team on a need-to-know basis to provide clinical care, and to ensure good and appropriate follow-up. Patient identifiable data were also shared with approved auditors from the NRES, Competent authorities (including MHRA, EMA and FDA), Sponsor (University of Birmingham), NHS R&D departments and the primary care practitioner. All participants provided specific written-consent at trial entry to enable data to be shared with the above. Otherwise, confidentiality was maintained throughout the trial and thereafter. On completion of the trial, data will be transferred to a secure archiving facility at the University of Birmingham,

where data will be held for a minimum of 10 years and then destroyed.

Sponsorship, Indemnity and Monitoring

The University of Birmingham acted as the sponsor of the trial. As sponsor the University was responsible for the general conduct of the study and indemnified the trial centre against any claims, arising from any negligent act or omission by the University in fulfilling the sponsor role in respect of the study.

Sources of funding

The HCV trial was funded by the Medical Research Council (Clinical Research Fellowship awarded to Lim TR, 2012), and the NIHR liver BRU. The LEAN trial was funded by the Wellcome Trust (Clinical Research Fellowship awarded to Armstrong MJ, 2009), Novo Nordisk Ltd and the NIHR liver BRU. The FindIT trial was funded by Medical Research Council (Senior Clinical Fellowship awarded to Tomlinson JW, 2009).

5.4 RESULTS

5.4.1 Patient characteristics and clinical parameters

13 patients with CHC (nine patients with genotype 1, four patients with genotype 3), 16 patients with NASH and 12 healthy controls were included in the analysis for this chapter [Table 5-1]. All healthy volunteers were male. 83.3% of patients from FindIT were Caucasian, compared to 69.2% in the HCV cohort and 100% in the NASH cohort. Median age was comparable between the three groups. BMI, total fat mass, truncal fat mass and blood parameters such as total cholesterol, HDL, triglycerides and creatinine were significantly different within the groups. Post hoc analysis showed that the significant variance in total cholesterol was between all groups, and the significant variance in BMI, total fat mass, truncal fat mass, HDL and triglycerides were only between NASH and HCV or NASH and control.

	Control n=12	CHC n=13	NASH n=16	p value (bold=significant)
Male sex, n (%)	12 (100)	8 (61.5)	11 (68.8)	
Age (years)	38.67 (14.53)	42.08 (12.93)	54.44 (8.37)	
Caucasian, n(%)	10 (83.3)	9 (69.2)	16 (100.00)	
BMI (kg/m2)	26.89 (4.33)	25.96 (4.87)	34.26 (4.16)	**<0.0001**
Total fat mass (kg)	17.63 (9.39)	21.08 (9.19)	35.76 (10.57)	**<0.0001**
Truncal fat mass (kg)	10.53 (5.77)	8.99 (5.24)	20.28 (5.79)	**<0.0001**
Fasting glucose (mmol/L)	4.39 (0.33)	4.63 (0.33)	5.34 (0.97)	**0.0014**
Fasting insulin (pmol/L)	20.844 (14.606)	46.67 (6.50)	125.8 (83.22)	**0.0003**
Total cholesterol (mmol/L)	5.52 (1.60)	4.01 (0.62)	4.51 (0.80)	**0.0038**
HDL (mmol/L)	1.46 (0.24)	1.44 (0.42)	1.11 (0.26)	**0.0086**
Triglycerides (mmol/L)	1.03 (0.28))	0.78 (0.30)	1.95 (1.05)	**0.0002**
Creatinine (umol/L)	89.18 (11.69)	71.7 (18.0)	71.31 (13.86)	**0.0070**
HOMA-IR	0.60 (0.46)	1.26 (0.76)	4.39 (3.25)	**0.0003**
M/I (step 1) (mg/kg/min/pmol/L)	0.033 (0.023)	0.020 (0.097)	0.004 (0.001)	**<0.0001**
M/I (step 2) (mg/kg/min/pmol/L)	0.01311 (0.00564)	0.00824 (0.00254)	0.00397 (0.00125)	**<0.0001**
%fat on MRS	1.483 (3.103)	2.34 (3.82)	n/a	0.814

Table 5-1. Demographics and clinical parameters of healthy subjects, patients with CHC and NASH. Blood parameters were fasted. Mean (SE), unless stated. One-way ANOVA.

5.4.2 Systemic insulin resistance

An analysis of variance (ANOVA) yielded significant variation in fasting glucose, fasting insulin and homeostatic model assessment-insulin resistance (HOMA-IR) within the groups [Table 5-1]. During the 2-step hyperinsulinaemic clamp, there was significant variation in M/I (weight-adjusted glucose infusion rates in response to low-dose [$F=14.87$, $p<0.0001$] and high-dose [$F=24.27$, $p<0.0001$] insulin infusions) [Fig 5-3A & B]. Post hoc analysis showed that the differences were significant between control and NASH (0.033±0.023 vs. 0.004±0.001

mg/kg/min; p<0.0001; and between CHC and NASH (0.020±0.097 vs. 0.004±0.001 mg/kg/min; p<0.0001) at low dose insulin infusion. At high dose insulin infusion, it was significant between all groups (0.0131±0.00564 vs. 0.00824±0.0025 vs. 0.00397±0.0012 mg/kg/min; p<0.0001 for control, CHC and NASH respectively).

3A.

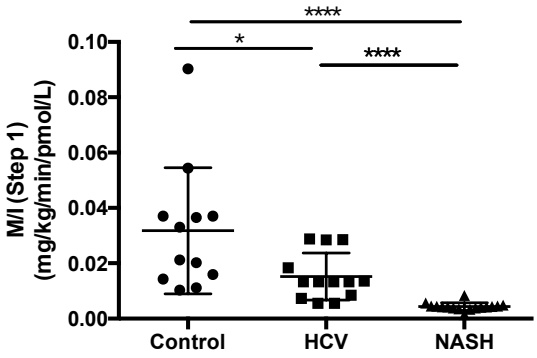

3B.

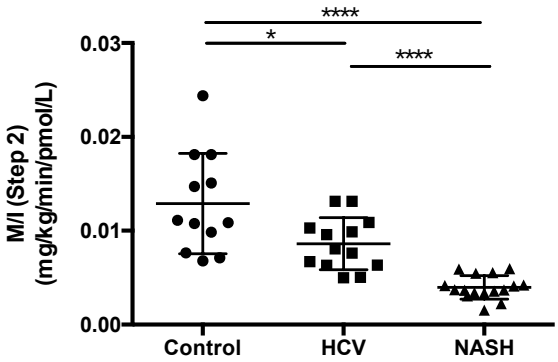

Fig 5-3. Significant variation in weight-adjusted glucose infusion rates in response to low dose, M/I (Step 1) and high dose, M/I (Step 2) values. M/I values were measured in control (n=12), HCV (n=13) and NASH (n=16) patients over 120-240min [A] and 240-360min [B] of the euglycaemic hyperinsulinaemic clamp. *p<0.05, ****p<0.0001. One-way ANOVA

5.4.3 Hepatic and Peripheral (muscle) insulin resistance

From the 2-step hyperinsulinaemic clamp, body weight-adjusted rate of glucose appearance, Ra and glucose disposal rates, Gd, were calculated. There were significant differences in the rate of appearance of glucose at basal [$F=42.16$, $p<0.0001$) and at low-dose insulin infusion, ie. endogenous glucose production, EGP [$F=8.76$, $p<0.001$] [Fig 5-4A to C], as well as glucose disposal at low-dose [$F=7.54$, $p=0.0018$] and at high-dose insulin infusions [$F=7.64$, $p=0.0017$] between groups [Fig 5-4D to F]. The significance for Gd during low-dose insulin infusion was lost when genotype 3 patients were excluded from the analysis [Fig 5-4E]. Post hoc analysis showed that CHC and NASH differed significantly for EGP (0.71 ± 0.35 vs. 1.29 ± 0.56 mg/kg/min; $p<0.005$) and Gd during insulin infusions [low dose: 1.81 ± 1.35 vs. 0.77 ± 0.28 mg/kg/min; $p<0.05$, high dose: 6.59 ± 3.24 vs. 4.44 ± 2.30mg/kg/min; $p<0.005$]. There was no difference in EGP and Gd between CHC and controls.

4A.

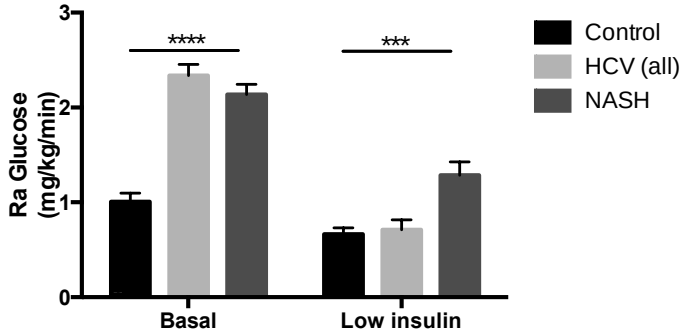
Ra Glucose (mg/kg/min)
3
2
1
0
****
***
Basal
Low insulin
Control
HCV (all)
NASH

4B.

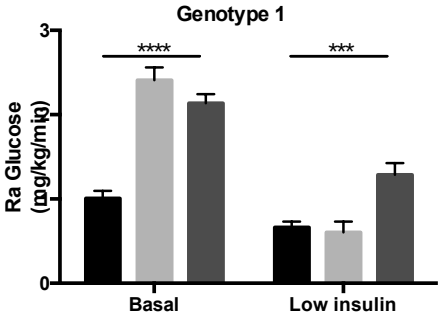
Genotype 1
Ra Glucose (mg/kg/min)
3
0
****
***
Basal
Low insulin

4C.

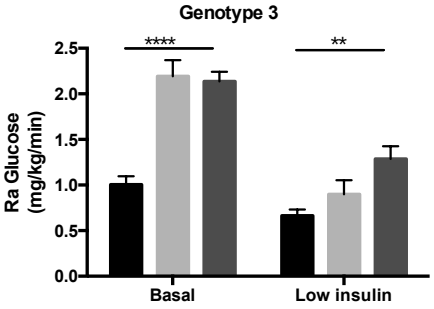
Genotype 3
Ra Glucose (mg/kg/min)
2.5
2.0
1.5
1.0
0.5
0.0
****
**
Basal
Low insulin

4D.

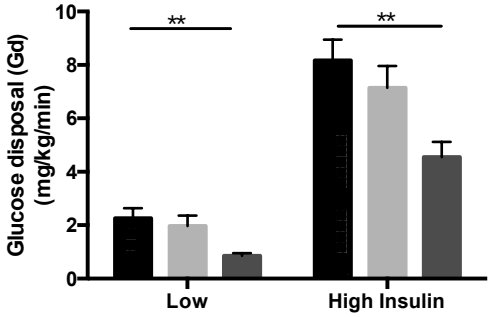

4E.

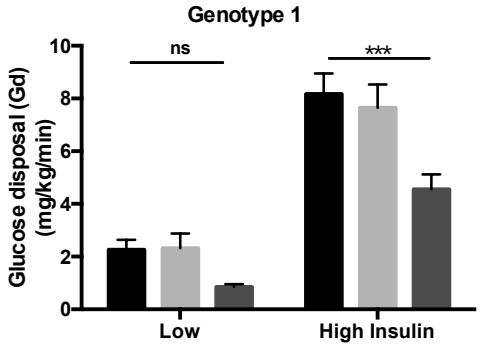

4F.

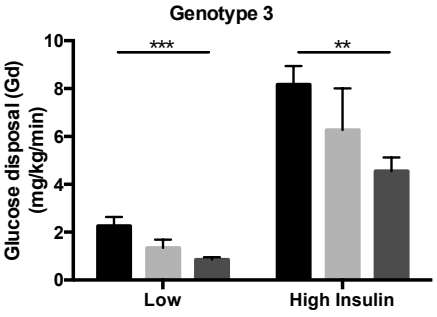

Fig 5-4. Significant difference in hepatic and peripheral (skeletal) insulin resistance within control, CHC and NASH groups. The degree of hepatic and muscle insulin sensitivity was determined by suppression of hepatic glucose production [A] and glucose disposal [D], respectively. Sub-analysis of Ra and Gd performed according to genotypes 1, n=9 [B&E] or 3, n=4 [C&F]. *p<0.05, **p<0.005, ***p<0.001, ****p<0.0001. Black bar=control group, light grey bar= HCV group, dark grey bar=NASH group. One-way ANOVA.

5.4.4 Hepatic lipid content and *de novo* lipogenesis

Proton density fat fraction (single echo time) measured by mass resonance spectrometry was significantly different between controls and patients with genotype 3 CHC (0.86±0.32 vs. 5.21±2.44, p=0.011). There was no difference between controls and genotype 1 CHC (0.86±0.32 vs. 0.83±0.20, p=0.93) [Fig 5-5A]. No comparison was made with NASH as MRS was not part of the clinical protocol in the study (LEAN).

The percentage contribution of *de novo* synthesized palmitate to plasma triglycerides was similar between genotype 1 and 3 CHC (6.45±1.78 vs. 5.64±3.03, p=0.819) [Fig 5-5B]. DNL was not compared between CHC and control or NASH groups as the enrichment analysis was performed in different centres.

5A.

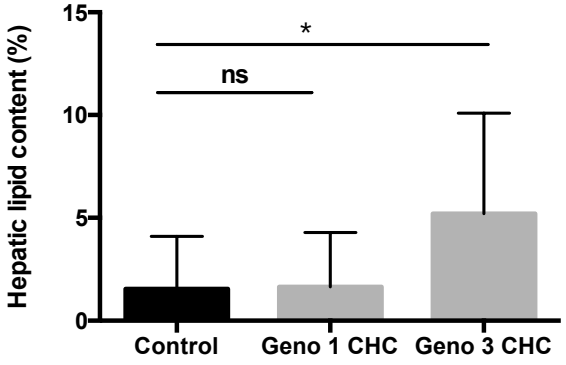

5B.

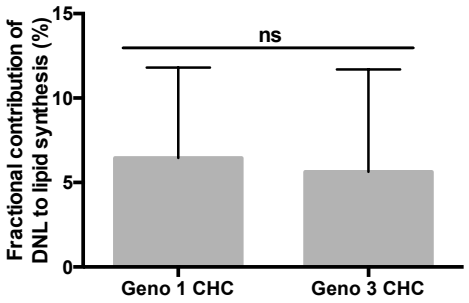

Fig 5-5. Increased hepatic lipid content in genotype 3 CHC. Hepatic lipid content as measured by magnetic resonance spectrometry (MRS), in control, genotype 1 CHC, n=9 and genotype 3 CHC, n=4 [A]. DNL as measured by deuterated water incorporation into plasma triglyceride palmitate between genotype 1 and 3 CHC [B]. Black bar=control group, light grey bar= HCV group. *$p<0.05$, ns=non significant. Unpaired Student's t-test

5.4.5 Global adipose tissue insulin resistance

Basal circulating NEFA levels were similar across all 3 groups [F=0.158, p=0.855]. However, following low dose insulin infusion, NEFA levels were higher in patients with NASH when compared to controls and CHC, consistent with adipose tissue insulin resistance [F=6.93, p=0.003]. After high dose insulin infusion there were no significant differences between groups [F=1.45, p=0.246]. Post hoc analysis of serum NEFA levels at low dose insulin infusion showed a significant difference between CHC and NASH (52.56±36.49 vs. 135.50±68.10 μmol/L, p<0.0001) and control and NASH (76.60±69.31 vs. 135.50±68.10 μmol/L, p<0.0001). No difference was observed between control and HCV groups (76.60±69.31 vs. 52.56±36.49 μmol/L, p=0.289) [Fig 5-6A].

In order to determine insulin sensitivity, using regression analysis, the insulin concentrations causing half-maximal suppression of serum NEFA was calculated for each subject [Fig 5-6B]. There were significant differences in insulin concentrations causing half-maximal suppression of serum NEFA between the groups [F=11.58, p=0.0001]. Post hoc analysis revealed that insulin-1/2-maximal NEFA was 3-fold higher in NASH subjects compared to HCV patients (226.89±140.79μmol vs. 77.29±89.03 μmol/L; p<0.005). No significant difference was seen between control and HCV groups (65.21±54.11 vs. 77.29±89.03 μmol/L; p=0.67).

Glycerol rate of appearance (Ra glycerol), which measures the global lipolytic rate, was suppressed by insulin in all groups. Ra glycerol was higher in CHC compared to control; at basal (1.811±0.880μmol/kg/min vs. 0.26±0.11μmol/kg/min; p<0.001), low (0.14±0.17μmol/kg/min vs. 0.68±0.38μmol/kg/min; p<0.001) and high insulin (0.12±0.15μmol/kg/min vs. 0.62±0.31μmol/kg/min; p<0.001) [Fig 5-7]. No comparison was made between CHC and NASH as the patients in the latter group did not receive $^{2}H_{5}$-glycerol infusion in the study.

6A.

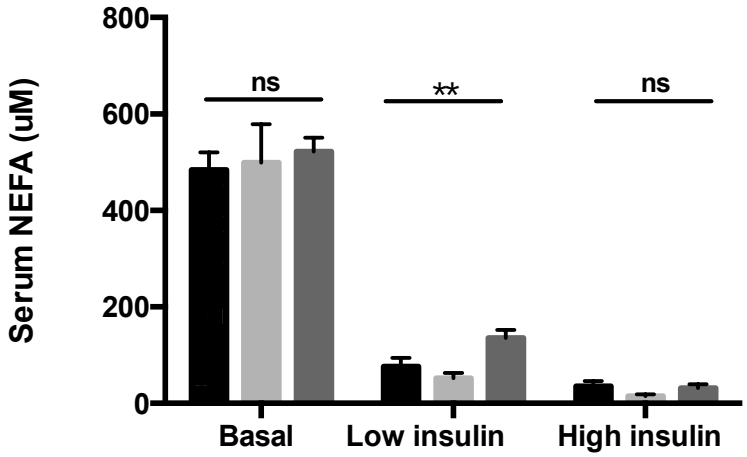

6B.

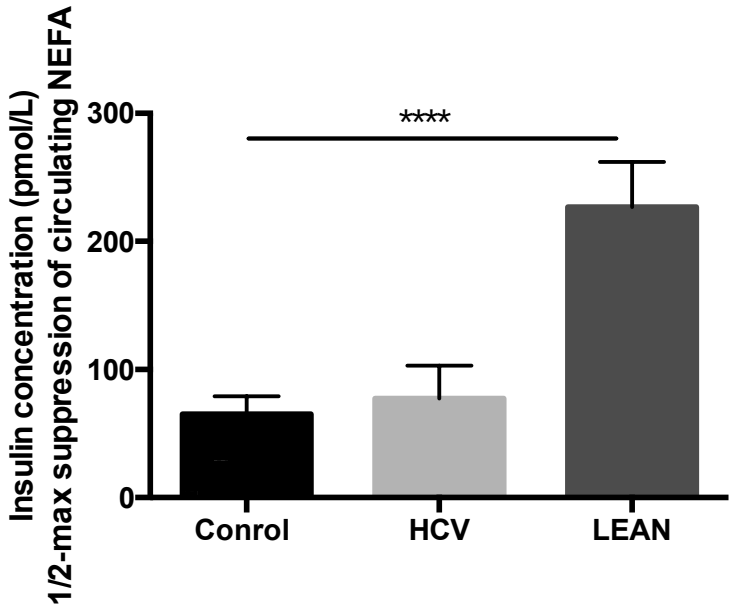

Fig 5-6. Significant variation in global lipolysis within the three groups. Mean circulating NEFA concentrations at basal and hyperinsulinaemic phases of euglycaemic clamp were measured in control, CHC and NASH [A]. Concentration of circulating insulin concentrations (pmol/L) causing ½-maximal suppression of circulating NEFA [B]. Key: Black bar=control group, light grey bar= HCV group, dark grey bar=NASH group. ***p<0.01, ***p<0.0001, ns=non significant. One-way ANOVA.

7.

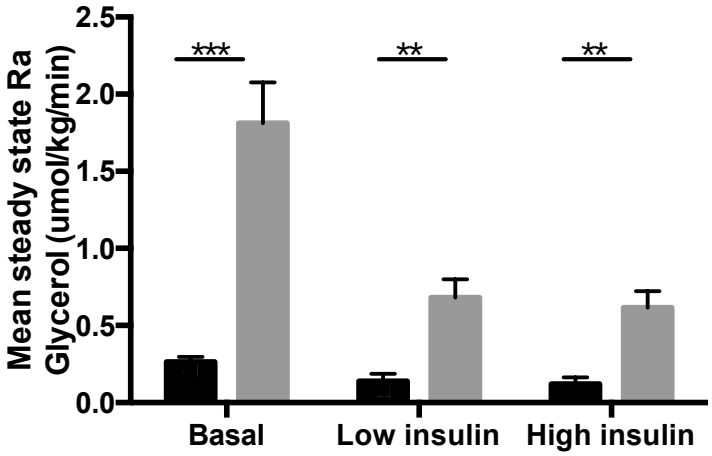

Fig 5-7. CHC increases global insulin suppressed lipolysis at basal, low and high insulin levels. Whole body lipolysis was assessed by measuring glycerol rate of appearance (Gly Ra) in 12 healthy controls and 13 patients with CHC (nine patients with genotype 1, four with genotype 3). Insulin decreased Gly Ra consistent with decreased lipolysis and CHC increased Gly Ra consistent with increased lipolysis. Key: Black bar=control group, light grey bar= HCV group. **p<0.005, ***p<0.001. Unpaired Student's t-test.

5.4.6 Abdominal subcutaneous adipose tissue (SAT) insulin resistance

Interstitial glycerol release assessed using microdialysis, was used as a direct measure of abdominal SAT function [Fig 5-8A & B]. During fasting and low dose insulin infusion, there was no variation in the rate of interstitial glycerol release between the groups [basal: $F=2.21$ $p=0.12$; low dose: $F=3.13$ $p=0.059$]. The differences within the groups became significant at high-dose insulin [$F=7.240$, $p=0.003$).

In post-hoc analysis, the difference in SAT glycerol level at high dose insulin was observed between control and NASH (102.94±61.80 vs. 175.25±82.68 umol/kg/min, $p=0.002$) and between CHC and NASH (109.58±55.50 vs. 175.25±82.68 umol/kg/min, $p=0.0451$). Even though no difference was seen between control and CHC collectively, significant difference was seen when comparing control and genotype 3, n=4 (102.94±61.8 vs. 160.38±45.79 umol/kg/min $p=0.019$) [Fig 5-8C]. Insulin half maximal glycerol in NASH patients was 7-fold higher than that of CHC patients (115.48±44.42; 682.55±32.87 $p<0.005$) [Fig 5-8D].

8A.

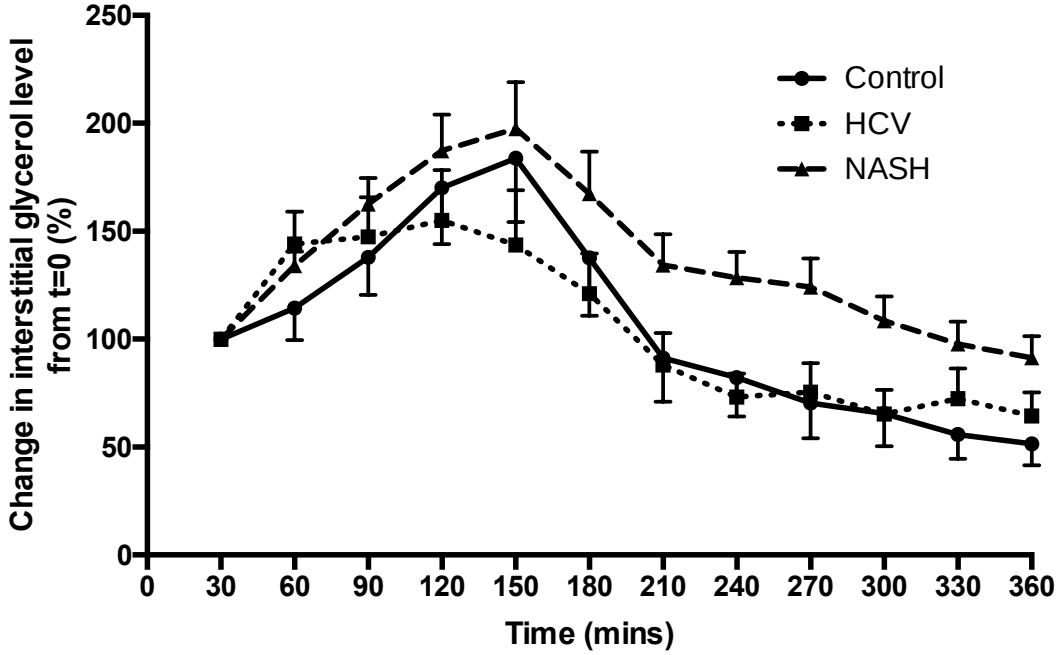
Change in interstitial glycerol level from t=0 (%)
250
200
150
100
50
0
0
30
60
90
120
150
180
210
240
270
300
330
360
Time (mins)
Control
HCV
NASH

8B.

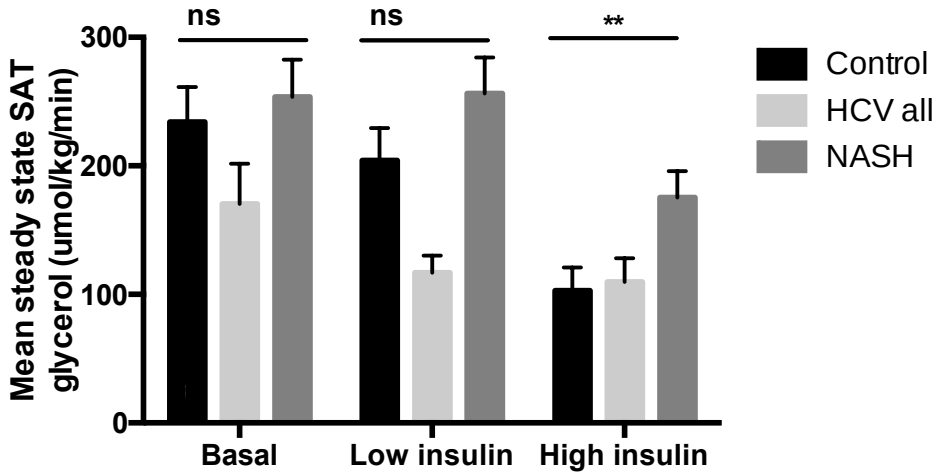
Mean steady state SAT glycerol (umol/kg/min)
300
200
100
0
ns
ns
**
Basal
Low insulin
High insulin
Control
HCV all
NASH

8C.

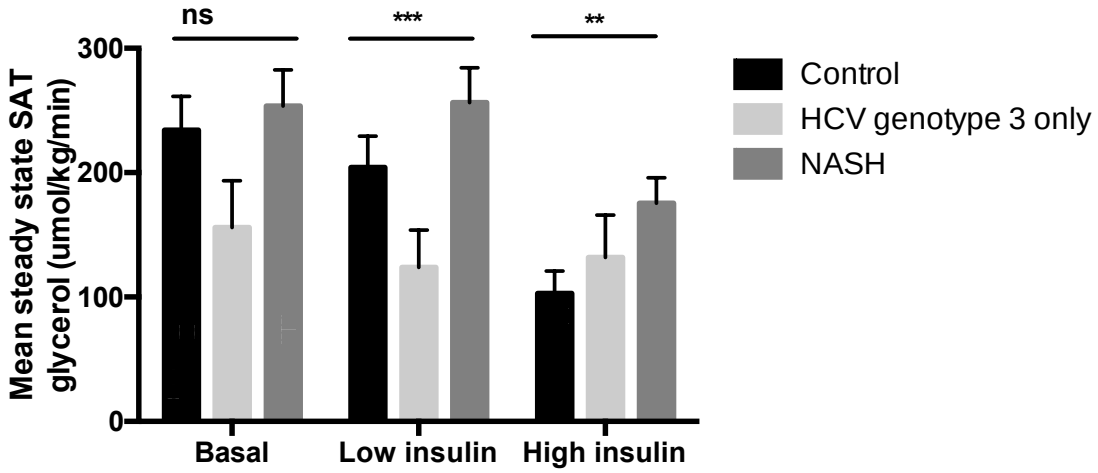

8D.

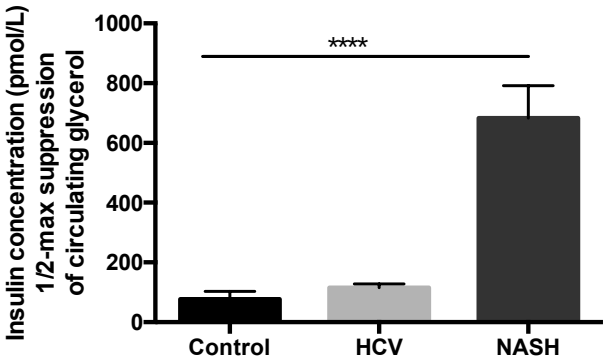

Fig 5-8. Patients with genotype 3 CHC and NASH have increased abdominal subcutaneous adipose tissue (SAT) insulin resistance. SAT interstitial fluid concentration of glycerol (%) during the 2-step hyperinsulinaemic euglycaemic clamp [A]. Mean levels of glycerol release during steady state were determined to quantify the rate of lipolysis in SAT under basal and hyperinsulinaemic conditions in all patients [B & C]. Concentration of circulating insulin concentration (pmol/L) causing ½-maximal suppression of circulating NEFA [D]. Key: Black bar=control group, light grey bar= HCV group, dark grey bar=NASH group. **p<0.01, ***p<0.001, ****p<0.0001, ns=non significant. One-way ANOVA.

5.5 DISCUSSION

We demonstrated that there was a modest increase in systemic and adipose tissue insulin resistance in patients with CHC. Unlike NASH, hepatic and peripheral insulin resistance in CHC was comparable to that of healthy controls. Whether the lack of effect of HCV on hepatic and muscle insulin sensitivity in this analysis was due to the study being underpowered or experimental design is unclear at this point in time. Another explanation may be that more patients with genotype 1 CHC were included in this analysis, and a higher prevalence of insulin resistance has been linked to genotype 3 CHC (144). However, exclusion of either genotype from the analysis did not change these observations, suggesting an alternative explanation to the lack of difference in insulin resistance seen between the CHC and controls.

Obesity may have contributed to the marked differences seen between CHC and NASH, as mean BMI was significantly higher in the NASH group. Obesity is known to be associated with an increased risk of developing insulin resistance and type 2 diabetes. In obese individuals, adipose tissue releases increased amounts of NEAAs, glycerol, hormones including leptin and adiponectin and pro-inflammatory cytokines, all of which are involved in the development of insulin resistance (313-315). It also increases the activity of hormone-sensitive lipase, which enhances lipolysis in visceral adipose tissue, thus resulting in the release of NEFAs. NEFAs are preferentially converted to triglycerides within hepatocytes. The triglycerides are then hydrolyzed to release FA and glycerol.

The increased NEFA load can thus lead to hepatic steatosis and insulin resistance (316, 317). In support of these findings, Tirado *et al.* demonstrated that bariatric surgery improved insulin resistance in morbidly obese subjects (318).

So does hepatic steatosis *per se* cause insulin resistance? Addressing the relationship between steatosis and insulin resistance poses considerable challenges. Several murine (192, 319) and human (44, 320) studies did not associate steatosis to insulin resistance. A recent study of the phosphoproteome of mouse livers treated with insulin showed hundreds of changes in phosphorylation in cellular proteins, many of which have not been described as parts of the insulin signaling network (321). It is also impossible to study the accumulation of a specific lipid in isolation. Any change in a lipid metabolic pathway induced by an experimental intervention may result in compensatory changes in other pathways affecting discrete lipid pools. In this study, hepatic and peripheral insulin resistance as well as DNL, were increased in the NASH cohort. Patients with genotype 3 CHC had increased baseline hepatic lipid content and adipose tissue insulin resistance when compared to genotype 1 CHC and controls. This suggests that hepatic steatosis, at least in genotype 3 CHC, may be the main driving force for the development of peripheral (adipose) insulin resistance seen in some patients with CHC.

There is a growing body of evidence to suggest that adipose insulin resistance is linked to the onset of peripheral and hepatic insulin resistance (322, 323) in NASH. However, this has not been established in CHC. Despite having no effect on peripheral and hepatic IR, CHC resulted in an increase in Ra glycerol, indicating a

lack of suppression of global lipolysis by insulin. However, only those with genotype 3 CHC developed SAT insulin resistance and this occurred only during high dose insulin infusion (chapter 6). The apparent discrepancy in the Ra glycerol and glycerol from SAT microdialysis in the CHC cohort is explained by the fact that Ra glycerol measures the rate of turnover ie. balance between generation and utilization of glycerol. Therefore, concentrations can remain the same if Ra and Rd change in parallel. In addition, other fat depots may contribute to Ra glycerol. On the other hand, glycerol from microdialysis measures glycerol concentration in SAT and reflects depot-specific SAT insulin resistance. It may be that other depot such as visceral adipose tissue, plays a more significant role in the development of insulin resistance in CHC, especially during fasting and low insulin infusions. In contrast to this, patients with NASH exhibited profound abdominal SAT insulin resistance at basal, low and high insulin infusion. There is also evidence to suggest that skeletal muscle dysfunction associated with NAFLD plays a role in its pathogenesis. In morbidly obese patients, intramyocelluar lipids predicts NASH and advanced fibrosis (324). However, Cuthbertson *et al.* showed that despite the higher hepatic lipid content, intramyocellular lipid contents and muscle mitochondrial function were similar between NAFLD and control groups (325).

This study is not without limitations. The numbers are small and the NASH arm was unmatched for body weight and BMI. In addition, patients from the three groups were recruited at different time points. Even though a standardized protocol was used, direct comparison between the studies may have been affected by factors such as operator and time variability etc. The pathogenesis of

insulin resistance in CHC may differ according to the virus genotype. Therefore, future studies concentrating on different genotypes ought to be studied.

5.6 CONCLUSION

We showed that patients with CHC have modest elevation in systemic, global and abdominal subcutaneous adipose tissue IR, with the latter only seen in genotype 3. These observations were also “milder” than that seen in NASH. Due to small sample sizes, further studies and validation are required. The genotype-specific effect of HCV on insulin resistance and how this differs from the mechanisms involved in the development of insulin resistance in NASH remain to be elucidated.

6.0 HCV ERADICATION IMPROVES HEPATIC AND ADIPOSE TISSUE INSULIN RESISTANCE

6.1 INTRODUCTION

Despite the fact that liver is the predominant replication site for HCV, the sites of insulin resistance in patients with HCV infection remain elusive, with some studies suggesting the liver as the primary site (137, 326) while others suggesting extra-hepatic sites, namely adipose tissue and skeletal muscle (138). The mechanisms underlying the cross talk between liver and extra-hepatic sites also remain largely unknown.

Clearance of hepatitis C virus with antiviral therapy improves insulin resistance (327, 328). However, most studies to date utilized homeostatic model assessment-insulin resistance (HOMA-IR) to quantify insulin resistance in patients with CHCs (329-334). This measurement does not determine hepatic vs. peripheral effects (335). Studies aimed to dissect the sites of insulin resistance are also limited (137, 138). Some have hinted at the association between HCV infection and alterations in adipocytokines but data have been inconclusive (280, 336, 337). It has been suggested that the presence of adipose insulin resistance is associated with failed suppression of NEFA levels resulting in an increase in NEFA delivery and availability in the liver. We elected to study the metabolic effects of genotypes 1 and 3 patients with CHC with no features of metabolic syndrome or evidence of cirrhosis, as each of these conditions in themselves is

associated with insulin resistance. Genotypes 1 and 3 are also common, have worldwide distribution, and differ substantially in hepatic lipid accumulations.

6.2 HYPOTHESIS AND AIMS

Hypothesis: *Adipose tissue insulin resistance is the cardinal feature of the metabolic abnormalities associated with chronic hepatitis C and this improves following viral eradication.*

Aim:

To define global and tissue specific changes in insulin sensitivity in chronic hepatitis C before and after viral eradication by measuring:-

1. Change in systemic insulin sensitivity
2. Change in liver fat and insulin sensitivity
3. Change in adipose tissue insulin sensitivity and gene expression profiles

6.3 METHODS

The clinical protocol received full ethical approval from the National Research Ethics Service (NRES) Committee West Midlands, Solihull (East Midlands REC Centre) [REC reference 12/WM/0281].

6.3.1 Study subjects

Of the 13 patients in CHC group described in the previous chapters, 8 underwent antiviral treatment and 7 achieved viral eradication, and were included in this analysis [see patient flow chart below]. The main reasons for screening failure for the remaining patients were ineligibility to participate in clinical trials offering directly acting antiviral treatment (90.8%), patient's refusal to participate in the study (7.9%) and little understanding of English (1.3%). HCV infection was confirmed with a positive anti-HCV antibody and detectable HCV RNA by PCR. Patients received either interferon-containing or interferon-free regimen, which was decided by the clinician following discussion with the individual involved. The decision was largely dependent on the genotype, the presence of co-morbidity and contra-indication to treatment, and the availability/suitability of the patients for clinical trial participation (if available) at the time of recruitment to the study.

The metabolic phenotype was studied at 2 time points:- at baseline (prior to anti-viral treatment) and 3 to 6 months following end of treatment, to allow wash-out

period of the medication. Inclusion and exclusion criteria were described in the previous chapter.

Patient Flow Chart

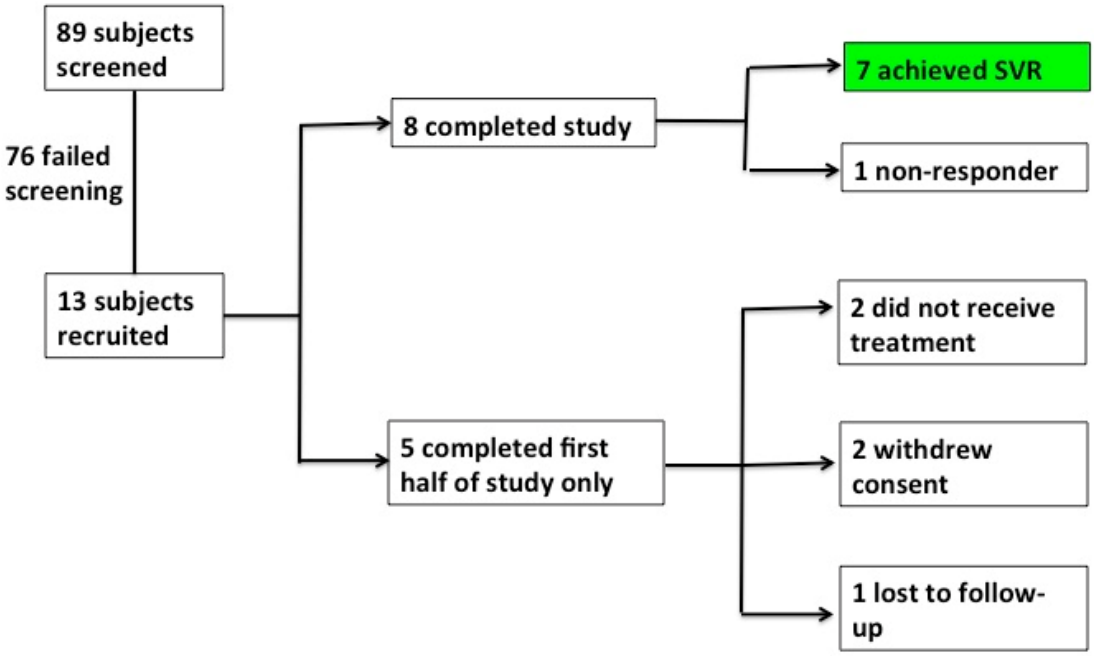

6.3.2 Study design

All patients were invited to visit the Welcome Trust Clinical Research Unit for the second time following viral eradication. Patient demographics, clinical and biochemical measures and metabolic studies carried out prior to antiviral therapy were repeated in patients with successful viral eradication. Schematic of experimental design [Fig 1] and metabolic study [Fig 1 of chapter 5] are illustrated below.

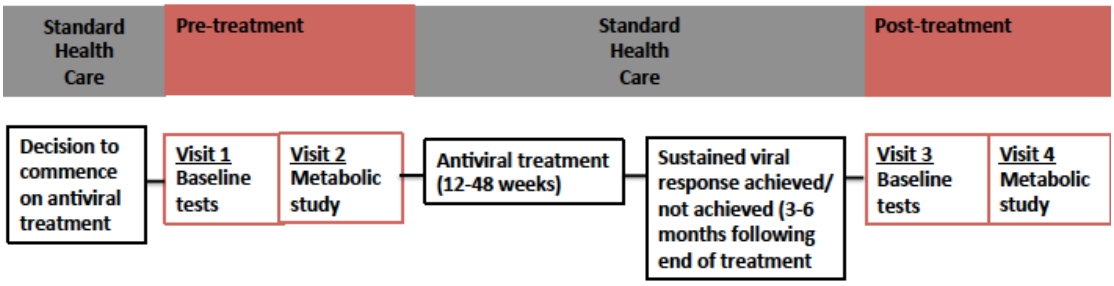

Fig 6-1. Schematics of experimental design (Visits 1 to 4)

SAT biopsy

30 minutes into commencement of low-dose insulin infusion, a subcutaneous adipose tissue biopsy was performed in the abdomen using aseptic technique. Following local anaesthetic, a small incision was made on the contralateral side to the microdialysis catheter of the abdomen and 1cm^2 tissue is obtained. Metabolic gene expression will be performed using quantitative RT-PCR. The value of the biopsy is that we can then compare the lipid metabolic gene profile for the 2-time points (during HCV infection and upon successful antiviral treatment).

RNA isolation and cDNA synthesis

The blood samples were collected into 15 ml tubes. Total RNA from blood

samples was extracted using Roche High Pure PCR Template Preparation Kit (Catalog number; 11796828001) according to the manufacturer's instructions. Total RNA was reverse-transcribed into first-strand complementary DNA (cDNA) using a High Capacity cDNA Reverse Transcription Kit (Invitrogen, Life Sciences, Catalog Number: 4368814) in a tube including 2.0 µl 10X RT buffer, 0.8 µl 25X dNTP (100 mM), 2.0 µl 10X RT random primer, 1.0 µl reverse transcriptase enzyme, and 4.2 µl nuclease free water. The cycle conditions were as follows: 10 min at 25 °C, 120 min at 37 °C, and 5 min at 85 °C.

High-throughput quantitative PCR

qRT-PCR is performed in two steps after total RNA purification and conversion to single stranded cDNA using polyT priming: the targeted genes are pre-amplified in a single 14-cycle PCR reaction for each sample by combining 100 ng cDNA with the pooled primers and TaqMan Pre-Amp Mastermix (Fluidigm BioMark™) following conditions recommended in the manufacturer's protocol, and 21 Å~ 84 (samples Å~ primers) qRT-PCR reactions are performed for each primer pair on each sample on a 96.96 array. We used the EvaGreen detection assay following standard Fluidigm protocols. Primer sets amplifying the mRNAs of the relevant genes are presented in Table 1. Ct values were calculated from the system software [BioMark Real-Time PCR Analysis, Fluidigm].

Table 6-1. List of 84 genes involved in metabolism or inflammation and the primer sets amplifying the mRNAs of the relevant genes.

Target	Gene Full Name	FP	RP
ABHD5	abhydrolase domain containing 5	GCAGCATTGACTCCCTTTAACC	AGGCCTTAAACGC
ACACA	acetyl-CoA carboxylase alpha	ATCCCAGCTGATCCAGCAAA	GCAGAATCTGGGA
ADIPOQ	adiponectin, C1Q and collagen domain containing	CCTGGTGAGAAGGGTGAGAAA	GGTTTCACCGATG
ADRB2	adrenoceptor beta 2	ATGGACTCCGCAGATCTTCC	AAGTGCCCATGAT
AKT1	v-akt murine thymoma viral oncogene homolog 1	CACACACTCACCGAGAACC	TCGTGGGTCTGGA
AKT2	v-akt murine thymoma viral oncogene homolog 2	ACGGGGCCACCATGAAAA	GGCCATAGTCATT
ANGPTL4	angiopoietin like 4	TCCACTTGGGACCAGGATCA	AATGGCTGCAGGT
APOB	apolipoprotein B	AAGCCATCTGCAAGGAGCAA	AGTCTGTGTCACT
APOE	apolipoprotein E	CCCAGGTCACCCAGGAAC	TGTTCCTCCAGTT
AQP7	aquaporin 7	GACAAAACATGGTTCAAGCATCC	CTATCACGGACCA
ARNT	aryl hydrocarbon receptor nuclear translocator	CTGTGTGGCTACTGTTGGCTA	GCTGGTCTTCAGG
ATF6	activating transcription factor 6	TTGGCAAAGCAGCAACCAA	ACAGTAGGCTGAG
CCL2	chemokine (C-C motif) ligand 2	TAGCAGCCACCTTCATTCCC	CCTCTGCACTGAG
CCL28	chemokine (C-C motif) ligand 28	GAGCTGATGGGGATTGTGAC	TTGGCAGCTTGCA
CD36	CD36 molecule (thrombospondin receptor)	AGCAGCAACATTCAAGTTAAGCA	GCGTCCTGGGTTA
CD81	CD81 molecule	GGCAGCAACATCATCAGCAA	AGCAATGCCGATG
CIDEC	cell death inducing DFFA like effector c	TTGGCTGCCTGAACGTGAA	TGTGGCCTGCATG
CLDN1	claudin 1	TATGACCCTATGACCCCAGTCA	CCAGAAGGCAGA
CPT1A	carnitine palmitoyltransferase 1A (liver)	TCCATGCCATCCTGCTTTACA	AGTGGAATCGTGG
CXCR2	chemokine (C-X-C motif) receptor 2	ATCGGTGGCCACTCCAATAA	GGTCGCTGGGCTT
IL8	chemokine (C-X-C motif) receptor 2	TCTGGAGGTGTCCTACAGGT	CTTCAAAGCTGTC
DGAT1	diacylglycerol O-acyltransferase 1	ACTACCGTGGCATCCTGAAC	GAAATAACCGGGC
DUSP1	dual specificity phosphatase 1	AGACATCAGCTCCTGGTTCA	CAGTGGACAAACA
ERN1	endoplasmic reticulum to nucleus signaling 1	AGATAGTCTCTGCCCATCAACC	TCGGGTTTTGGTG
FABP3	fatty acid binding protein 3	CTGGAAGCTAGTGGACAGCAA	CCACCTGCCTGGT
FABP4	fatty acid binding protein 4	ATGTGTGATGCTTTTGTAGGTAC	CCACTTTCCTGGT
FABP5	fatty acid binding protein 5	GACGCAGACCCCTCTCTG	TTCCTTCCAGCTG
FASN	fatty acid synthase	GGAGGGGACAGTGCATCAA	GTTTACACTCCTC
G6PC	glucose-6-phosphatase, catalytic subunit	TCAGGAAGCTGTGGGCATTA	GCACGGAAGTGTT
G6PD	glucose-6-phosphate dehydrogenase	GGCAAGGAGATGGTGCAGAA	GTGCCAAAGGGCT
GAPDH	glyceraldehyde-3-phosphate dehydrogenase	GAACGGGAAGCTTGTCATCAA	ATCGCCCCACTTG
GLUL	glutamate-ammonia ligase	GTCAAGATTGCGGGGACTAA	CCCATGCTGATTC
HIF1A	hypoxia inducible factor 1, alpha subunit	CAGTCGACACAGCCTGGATA	TTCTTCTGGCTCA
HIF3A	hypoxia inducible factor 3, alpha subunit	CTCCTTGCGCATGAAGAGTA	CTCATATGTCCAG
HK1	hexokinase 1	TCATTTCCCTGCCAGCAGAC	CGCAGTCTGTTGC
HSD11B1	hydroxysteroid (11-beta) dehydrogenase 1	GAAGCAGAGCAATGGAAGCA	TTGCAGAATAGGC
IFNA1	interferon, alpha 1	TGACTCATACACCAGGTCAC	CAGGGGTGAGAG
IFNG	interferon, gamma	ACTGCCAGGACCCATATGTAA	GTTCCATTATCCG
IL10	interleukin 10	CCGTGGAGCAGGTGAAGAA	GTCAAACTCACTC
IFNL3	interferon, lambda 3	CTGCCACATAGCCCAGTTCAA	CGGCACTTGCAGT
IL4	interleukin 4	CAGCTGATCCGATTCCTGAAA	GTTGGCTTCCTTC
IL5RA	interleukin 5 receptor subunit alpha	GATCAGCTGTTTGCCCTTCA	TTCCTTCAATCTCT
IL6	interleukin 6	AGAGCTGTGCAGATGAGTACAA	GTTGGGTCAGGG
IRS1	insulin receptor substrate 1	CAGAAGCAGCCAGAGGAC	AGAGGATTTGCTG
IRS2	insulin receptor substrate 2	TGTCCCACCACTTGAAGGAG	TGACATGTGACAT
JAK2	Janus kinase 2	TCTGCAGTGGAGGAGATAAACC	TGCAGGAAGCTGA
LDLR	low density lipoprotein receptor	CCACGGTGGAGATAGTGACAA	TCTCATTTCCTCTG
LEP	leptin	CACCAAAACCCTCATCAAGACAA	AGCCCAGGAATGA
LIPE	lipase, hormone-sensitive	AGTTAAGTGGGCGCAAGTCC	GCCAGTGCTGCTT
LOX	lysyl oxidase	ATCCAGGCGTCCACGTAC	AGCAGCACCCTGT
LPL	lipoprotein lipase	TGGCCGAGAGTGAGAACA	AGCTTCAACATGA
LRP10	LDL receptor related protein 10	GCAGCAAGGAACAGACTGTCA	GAGAGGGGAGCG
MAPK1	mitogen-activated protein kinase 1	TTGGTACAGGGCTCCAGAAA	TCTGCCAGAATGC
MTOR	mechanistic target of rapamycin (serine/threonine kinase)	CCAAACCCAGGTGTGATCAA	TCCTCATTTCCAG
NFKB1	nuclear factor of kappa light polypeptide gene enhancer in B-cells 1	CTACCTGGTGCCTCTAGTGAAA	ACCTTTGCTGGTC
NOX4	NADPH oxidase 4	TCCAGCTGTACCTCAGTCAA	GGACGTCCTATAA

NR3C1	nuclear receptor subfamily 3 group C member 1	GCAGCAGTGAAATGGGCAAA	CAGTAGGGTCATT
OCLN	occludin	AACTGGCGGCGAGTCC	TCCTGTAGGCCAG
PDHA1	pyruvate dehydrogenase (lipoamide) alpha 1	GTGCTGGTAGCATCCCGTAA	CCTTCTTCCAGCC
PDK1	pyruvate dehydrogenase kinase 1	ACCAAGACCTCGTGTTGAGAC	AAGACGTGATATG
PDK4	pyruvate dehydrogenase kinase, isozyme 4	CTACTCGGATGCTGATGAACCA	CCAATGTGGCTTG
PDP1	pyruvate dehyrogenase phosphatase catalytic subunit 1	TCCTGAAGAGCTTGCTCGAA	ACGCCCCTACAAC
PER1	period circadian clock 1	TGATTGCAGAGCGCATCCA	TGTGTGCCGCGTA
PER2	period circadian clock 2	GCCTGATGATGGCAAAATCTGAA	GTGTGTGTCCACT
PGK1	phosphoglycerate kinase 1	GTGGAATGGCTTTTACCTTCC	CTTGGCTCCCTCT
PIK3CA	phosphatidylinositol-4,5-bisphosphate 3-kinase catalytic subunit alpha	CTGCAGTTCAACAGCCACAC	ACAGGTCAATGGC
PLG	plasminogen	AGCTGGGAGCAGGAAGTATA	CTGTTTTCAGCCA
PLIN1	perilipin 1	TCACCTTGCTGGATGGAGAC	ATTCGCAGGTGCC
PLIN2	perilipin 2	CCTCTCATGGGTAGAGTGGAA	GCAATTGCAAGAG
PNPLA1	patatin like phospholipase domain containing 1	TGGAGGAACTAGGCCAAGAAC	GACGGTTTCCTTC
PPARA	peroxisome proliferator-activated receptor alpha	GACAAGGCCTCAGGCTATCA	TCATACACCAGCT
PPARG	peroxisome proliferator-activated receptor gamma	TAGATGACAGCGACTTGGCAATA	TGGGCTTCACATT
PPARGC1A	PPARG coactivator 1 alpha	ACTTTTGTGGACGCAAGCAA	TGGAAGCAGGGT
PPIA	peptidylprolyl isomerase A (cyclophilin A)	TCTGGTTCCTTCTGCGTGAA	CCAGGGAATACGT
PRKAA1	protein kinase, AMP-activated, alpha 1 catalytic subunit	CCAACTATGCTGCACCAGAA	AGAATAACCCCAC
RAB18	RAB18, member RAS oncogene family	GCTAACCACCCTGAAGATCC	TGCAAGTTCTGGA
RXRA	retinoid X receptor alpha	AGGAAACATGGCTTCCTTCAC	TCGCAGCTGTACA
SCARB1	scavenger receptor class B member 1	GAGATCCTGAAGGGCGAGAA	GATGTTGCTTTTG
SIRT1	sirtuin 1	ACAAAGTTGACTGTGAAGCTGTAC	GTTCATCAGCTGG
SLC2A1	solute carrier family 2 (facilitated glucose transporter), member 1	ATTGTGGGCATGTGCTTCC	AGAACCAGGAGC
SLC2A4	solute carrier family 2 (facilitated glucose transporter), member 4	TTCTCCAACTGGACGAGCAA	GGACCGCAAATAG
SOCS1	suppressor of cytokine signaling 1	CATCCGCGTGCACTTTCA	GCTCGAAGAGGC
SOCS3	suppressor of cytokine signaling 3	TTCAGCTCCAAGAGCGAGTA	TCACTGCGCTCCA
SRD5A1	steroid-5-alpha-reductase, alpha polypeptide 1	GCCATGTTCCTCGTCCACTA	CAACAGTGGCATA
SRD5A2	steroid-5-alpha-reductase, alpha polypeptide 2	TGATGGGTGGTACACAGACA	AGCTGGCGCAATA
SREBF1	sterol regulatory element binding transcription factor 1	CAGCAACCAGAAACTCAAGCA	GCCGACACCAGAT
TLR3	toll-like receptor 3	TCTCATGTCCAACTCAATCCA	CAGCTGAACCTGA
TNF	tumor necrosis factor	CTTCTCGAACCCCGAGTGAC	ACTGGAGCTGCCC
UCP2	uncoupling protein 2 (mitochondrial, proton carrier)	TTCCTCTGGATACTGCTAAAGTCC	TCAGAATGGTGCC
VEGFA	vascular endothelial growth factor A	GAGGAGGGCAGAATCATCAC	GTCTCGATTGGAT
VLDLR	very low density lipoprotein receptor	CCTAGCTCATCCTCTTGCACTA	TGGCACCATAGAC

6.3.3 Statistical analysis

Sample size justification

This is an observational pilot study with no pharmacological intervention. The aim is to study insulin resistance and lipid metabolism during their routine NHS care. Assuming a difference in insulin resistance response (as measured by glucose infusion rate mg/kg/min) after anti-viral treatment is normally distributed with a standard deviation of 1.4, we will be able to detect a true difference in the mean response of at least 1.393 mg/kg/min. To reliably detect this significant 1.393 mg/kg/min change in HCV patients, with 80% power, at a significance level of 0.05, 20 patients would be required. However, if we allow for 20% drop out rate in each group, 24 patients would be required to achieve a significant primary outcome.

Sources of funding

The trial was funded by the Medical Research Council (Clinical Research Fellowship awarded to Lim T, 2010), and the liver BRU.

6.4 RESULTS

6.4.1 Patient characteristics and clinical parameters

Seven patients achieved sustained viral response (SVR) following antiviral treatment, and are therefore included in the analysis in this chapter. SVR was confirmed with an undetectable HCV RNA three months after the end of antiviral treatment. The types and duration of antiviral treatment for each subject were listed in Table 5-2. In brief, five patients received pegylated-interferon containing regimen and the remaining two patients received pegylated-interferon-free directly acting antiviral agents, either as routine NHS prescription [patient 1,2 and 7] or as part of a clinical trial [patient 5 & 6 ION-1; patients 9 & 11 –PEDESTAL]. ION-1 was a phase 3, multicenter, randomized, open-label study to investigate the efficacy and safety of Harvoni® (Sofosbuvir/Ledipasvir) Fixed-Dose Combination (FDC) +/- Ribavirin for 12 and 24 weeks in treatment-naive subjects with CHC genotype. PEDESTAL was a phase 3, blinded randomized study of peg-interferon Lambda-1a and ribavirin compared to peg-interferon alfa-2a and ribavirin, each administered with telaprevir in subjects with genotype 1 CHC who are treatment-naïve or relapsed on treatment with peg-interferon alfa and ribavirin. The duration of treatment varied between 12 to 48 weeks [median 24 weeks].

Baseline demographics were male sex (85.7%), median age of 55.3 years, Caucasian (85.6%), genotype 1 (57.1%) and genotype 3 (42.9%) HCV infection. Viral, metabolic and liver parameters were measured before and 3 months following the end of antiviral treatment. BMI and total fat mass remained unaltered during the period of the study. Android/gynoid fat mass ratio decreased but this did not achieve statistical significance. Other metabolic parameters such as fasting glucose and insulin levels, total cholesterol and %fat on MRS were unchanged. As expected, liver parameters ie AST and ALT improved following viral eradication [Table 3].

Table 6-2. **Types and duration of antiviral treatment.** Peg=pegylated, SVR=sustained virological response. Telaprevir=protease inhibitor, Sofosbuvir=NS5B polymerase inhibitor, Ledipasvir=NS5A inhibitor.

Patient ID	Types of antiviral treatment	Duration of treatment (weeks)
01	Peg-Interferon + Ribavirin	48
02	Peg-Interferon + Ribavirin	16
05	Sofosbuvir + Ledipasvir + Ribavirin	12
06	Sofosbuvir + Ledipasvir + Ribavirin	24
07	Telaprevir + Peg-Interferon + Ribavirin	24
09	Telaprevir + Peg-Interferon + Ribavirin	24
11	Telaprevir + Peg-Interferon + Ribavirin	24

Table 6-3. **Demographics and clinical parameters** of patients who completed antiviral treatment and achieved sustained virological clearance (SVR). Mean (SE), unless stated. Blood parameters were fasted. Comparisons of continuous variables with paired Student's t test.

Demographics	**Pre-treatment**	**Post-treatment**	**P-value**
Male sex	6 (85.7)		
Age (years)	55.3 (9.6)	56.3 (9.6)	
Caucasian, n(%)	6 (85.7)		
Viral parameters	**Pre-treatment**		
Genotype 1, n(%)	4 (57.1)		
Genotype 3, n(%)	3 (42.9)		
HCV RNA (mean±SD)	2,109,727(4,125,315)		
IFN-containing antiviral treatment	5 (71.4)		
Duration of treatment in months, range [med]	12-48 [24]		
Metabolic parameters	**Pre-treatment**	**Post-treatment**	**P-value**
BMI (kg/m2)	25.4 (4.7)	24.6 (3.9)	0.723
Weight (kg)	80.1 (19.5)	77.2 (16.4)	0.772
Total fat mass (kg)	23.5 (10.0)	21.0 (7.8)	0.613
Android/Gynoid fat mass	1.01 (0.28)	0.95 (0.30)	0.745
Fasting glucose (mmol/L)	4.65 (0.38)	4.71 (0.39)	0.811
Fasting insulin (pmol/L)	35.67 (15.52)	35.32 (31.47)	0.975
HOMA-IR	1.11 (1.05)	1.06 (0.97)	0.917
Total cholesterol (mmol/L)	3.9 (0.6)	4.1 (0.8)	0.473
HDL (mmol/L)	1.4 (0.4)	1.5 (0.3)	0.799
Triglycerides (mmol/L)	0.8 (0.3)	1.1 (0.7)	0.259
Creatinine (umol/L)	75.0 (12.6)	71.6 (8.8)	0.565
%fat on MRS (PDFF)	2.25 (3.22)	1.55 (1.88)	0.62
M/I (step 1) (mg/kg/min/pmol/L)	0.018 (0.011)	0.031 (0.020)	0.142
M/I (step 2) (mg/kg/min/pmol/L)	0.008 (0.003)	0.029 (0.037)	0.172
Liver parameters	**Pre-treatment**	**Post-treatment**	**P-value**
AST (IU/L)	34.9 (13.6)	20.0 (5.4)	**0.019**
ALT (IU/L)	52.3 (24.4)	20.9 (14.9)	**0.013**
GGT (IU/L)	49.0 (39.0)	16 (2.3)	0.092
Bilirubin (umol/L)	13.7 (8.1)	12.0 (7.5)	0.689
Albumin (g/L)	42.7 (3.4)	45.1 (3.2)	0.193

6.4.2 Systemic insulin resistance

Fasting serum glucose, insulin and homeostasis model assessment of insulin resistance (HOMA-IR) did not alter significantly following HCV eradication with antiviral therapy. There was also no difference in M/I values (weight-adjusted glucose infusion rates in response to low-dose and high-dose insulin) between those with viraemia and those without (low-dose 0.018±0.01 mg/kg/min vs 0.031±0.020 mg/kg/min; p=0.133; high-dose 0.008±0.003 mg/kg/min vs. 0.029±0.037 mg/kg/min, p=0.204)[Fig 6-2A & B]. This remained so after excluding patients who received pegylated-interferon (peg-IFN) as part of their antiviral regimen [Fig 6-2D & F]. The two patients who received peg-IFN free regimen showed an upward trend in M/I values during low and high insulin infusions but statistical analysis was no performed due to the small number of patients in the group [Fig 6-2C & 4E].

2A.

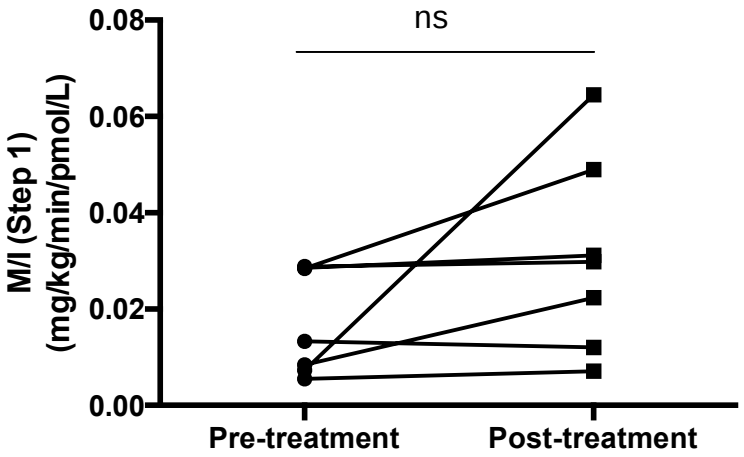
ns
0.08
0.06
0.04
0.02
0.00
M/I (Step 1)
(mg/kg/min/pmol/L)
Pre-treatment
Post-treatment

2B.

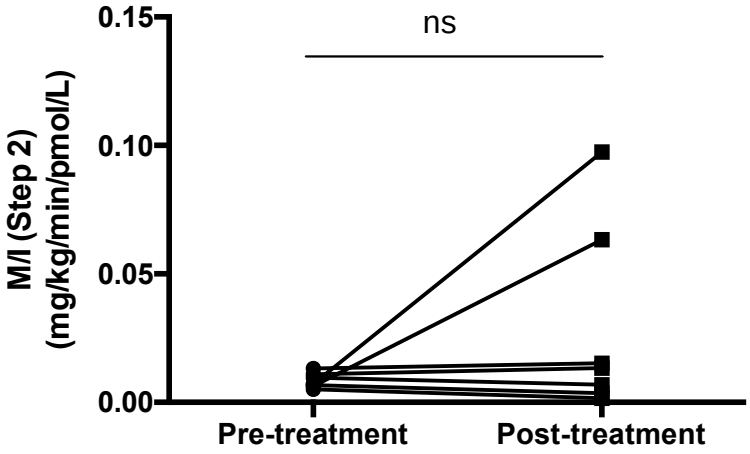
ns
0.15
0.10
0.05
0.00
M/I (Step 2)
(mg/kg/min/pmol/L)
Pre-treatment
Post-treatment

2C.

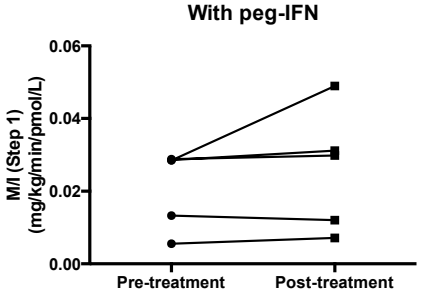

2D.

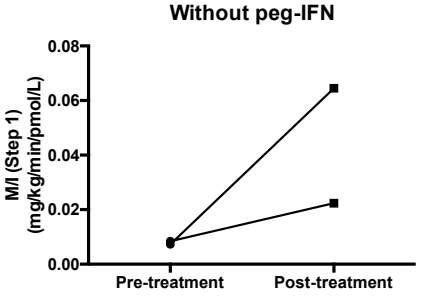

2E.

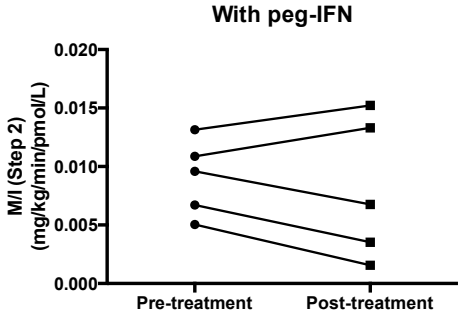

2F.

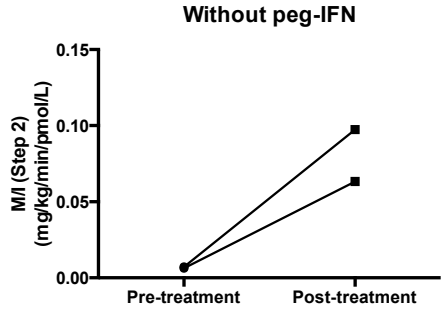

Fig 6-2. No significant changes in M/I values before and after antiviral treatment in patients with CHC. Collective (genotype 1 & 3) M/I values were measured over 120-240min [A] and 240-360 [B] min of the euglycaemic hyperinsulinaemic clamp, and in patients who received pegylated interferon (peg-IFN) containing regimen, n=5 [C] & [E] or without peg-IFN regimen, n=2 [D] & [F]. ns=non-significant. Paired Student's t-test.

6.4.3 Hepatic and Peripheral (muscle) insulin resistance

From the 2-step hyperinsulinaemic clamp, body weight-adjusted rate of glucose appearance, Ra and glucose disposal rates, Gd, were calculated. Endogenous glucose production, EGP was significantly lower following SVR (0.994±0.166 vs. 0.718±0.180 mg/kg/min; p=0.049) [Fig 6-3C]. There was no difference in Ra at fasting (2.36±0.06 vs. 2.21±0.14 mg/kg/min), Gd at low insulin (1.612±1.345 vs. 2.948±1.612 mg/kg/min; p=0.237) or at high insulin [5.972±2.601 vs. 8.069±3.432 mg/kg/min;p=0.557) before and after SVR [Fig 6-3D]. In the sub-analysis according to genotypes, the improvement in Ra at low insulin following SVR was only seen in genotype 3 CHC [Fig 6-4A & B]. Interestingly, when genotype 3 patients were excluded, Gd at high dose insulin infusion significantly increased following SVR [Fig 6-4C & D].

3A.

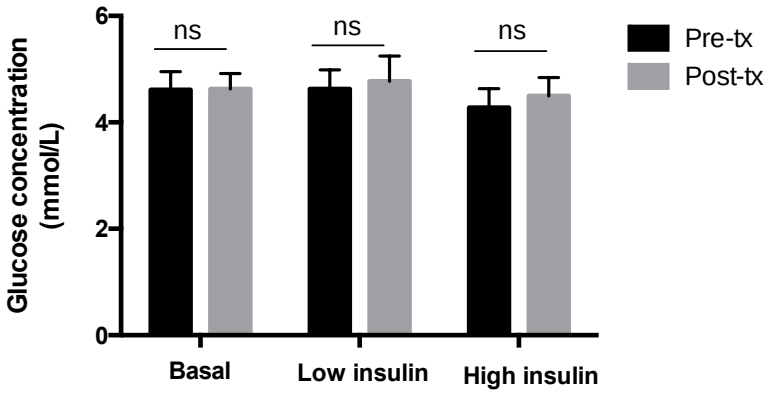

3B.

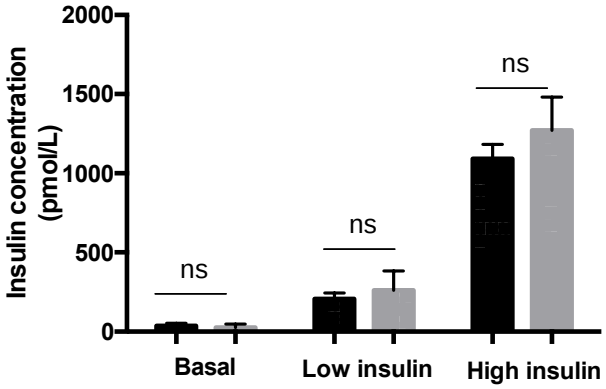

3C.

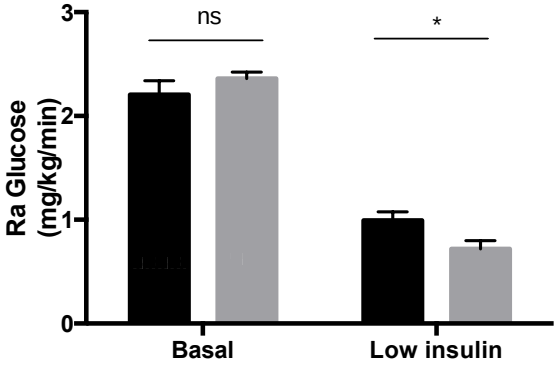

3D.

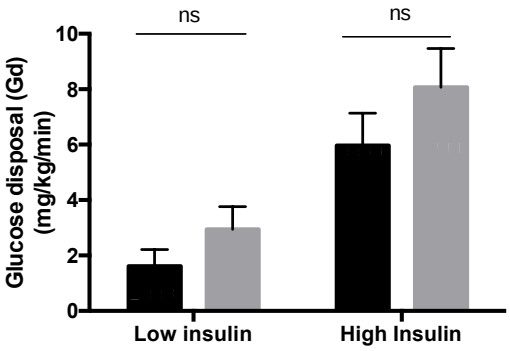

Fig 6-3. HCV eradication improves endogenous glucose production, EGP (hepatic insulin sensitivity) and glucose disposal, Gd (skeletal insulin sensitivity) at low insulin. Circulating glucose [A] and insulin [B] concentrations during the 2-step hyperinsulinaemic euglycaemic clamp. The degree of hepatic and skeletal insulin sensitivity was determined by suppression of hepatic glucose production, Ra [C] and glucose disposal, Gd [D], respectively following viral eradication. Key: Black bar=prior to antiviral treatment, grey bar= after antiviral treatment. *p<0.05, ns=non-significant. Paired Student's t-test.

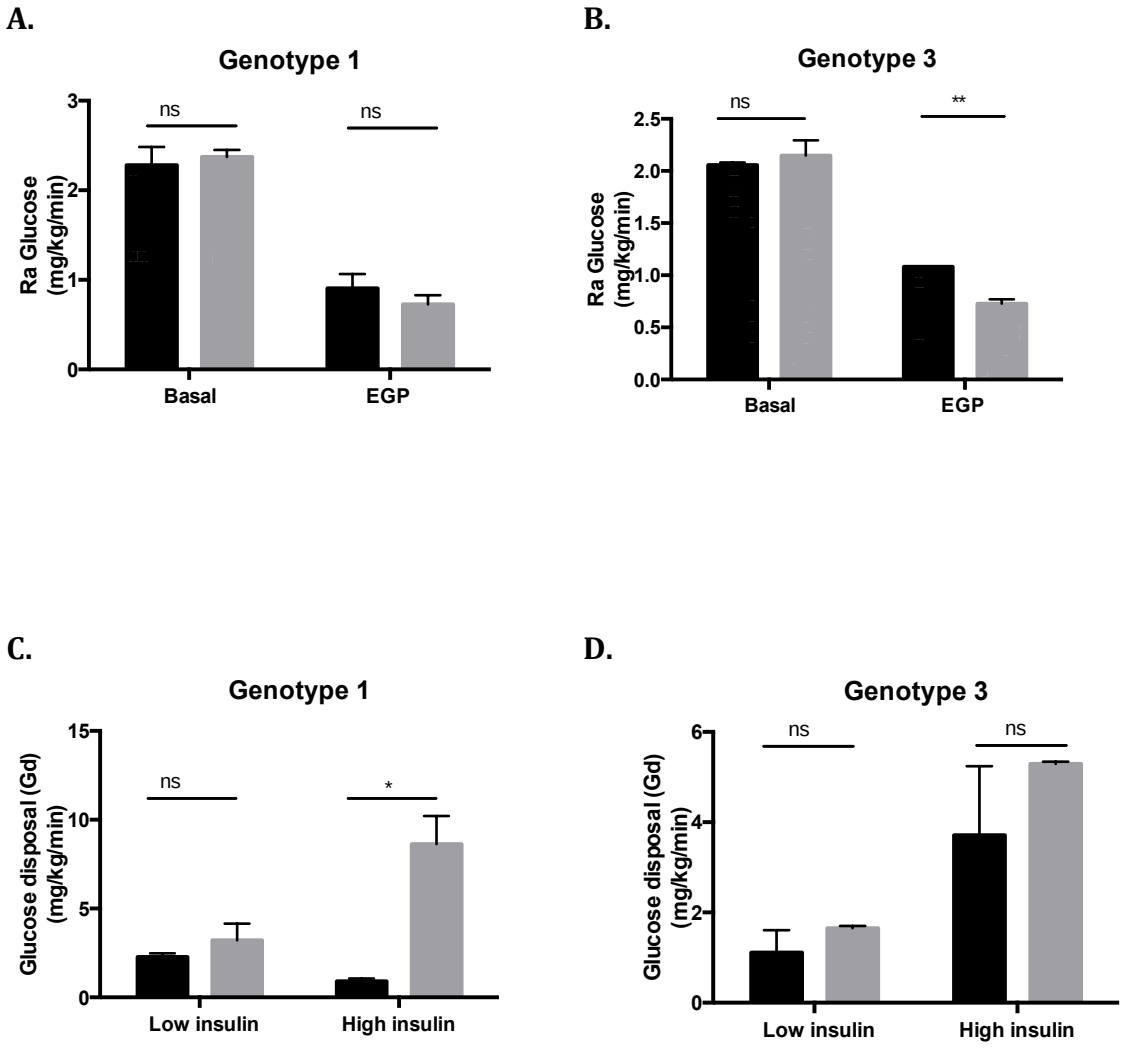

Fig 6-4. Viral eradication improves hepatic insulin sensitivity in genotype 3 and peripheral insulin sensitivity in genotype 1 CHC. The degree of hepatic and skeletal insulin sensitivity was determined by suppression of hepatic glucose production in genotype 1, n=4 [A] and genotype 3, n=3 [B] and glucose disposal in genotype 1 [C] and 3 [D], respectively. Key: Black bar=prior to antiviral treatment, grey bar= after antiviral treatment. ns=non-significant. *p<0.05, **p<0.01, ns=non-significant. Paired Student's t-test.

6.4.4 Hepatic *de novo* lipogenesis and lipid content

The percentage contribution of DNL to total endogenous palmitate synthesis was unchanged following SVR [5.62±4.27 vs. 4.31±4.72, p=0.68] [Fig 6-5A]. This remained unchanged when analyzing for genotype 1 only [1.95±0.53 vs. 5.73±3.18, p=0.11] [Fig 6-5B] or genotype 3 [10.52±7.52 vs. 8.72±5.73, p=0.84] [Fig 6-5C] groups.

There was no change in hepatic lipid and choline content following viral eradication as measured by magnetic resonance spectroscopy (MRS). Mean baseline % fat was within normal limits (ie. <5%) and was unaltered by viral eradication (2.26±3.22 vs. 1.55±1.88 p=0.38) [Fig 6-4D]. Choline/water ratios were also unchanged before and after antiviral treatment (3.24±1.39 vs. 3.72±1.98; p=0.92) [Fig 6-5E]. An example of an axial, sagittal and coronal 3D-GE T1-weighted images of the abdomen showing typical MRS voxel placement in the right lobe of liver of one of the patients is shown in Fig 6-5F.

5A.

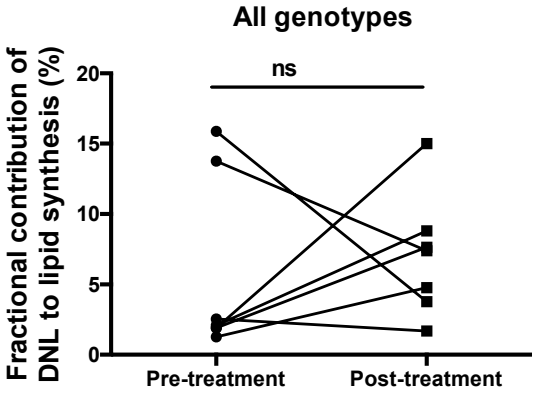
All genotypes
ns
Fractional contribution of DNL to lipid synthesis (%)
20
15
10
5
0
Pre-treatment
Post-treatment

5B.

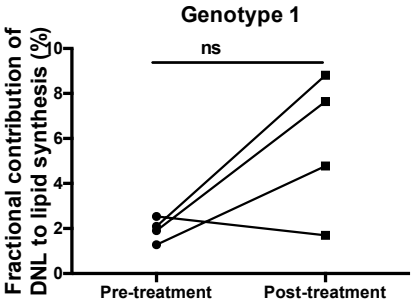
Genotype 1
ns
Fractional contribution of DNL to lipid synthesis (%)
10
8
6
4
2
0
Pre-treatment
Post-treatment

5C.

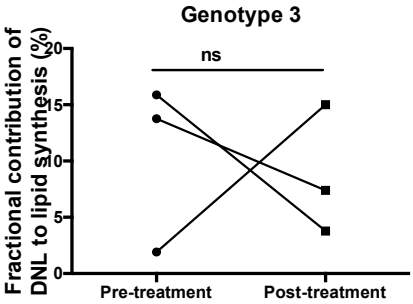
Genotype 3
ns
Fractional contribution of DNL to lipid synthesis (%)
20
15
10
5
0
Pre-treatment
Post-treatment

5D.

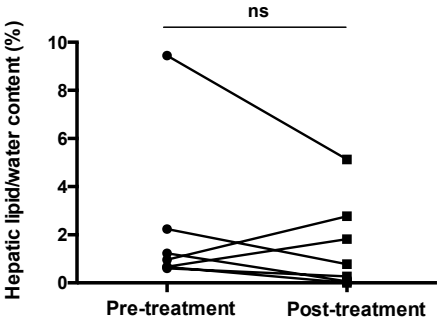
ns
Hepatic lipid/water content (%)
10
8
6
4
2
0
Pre-treatment
Post-treatment

5E.

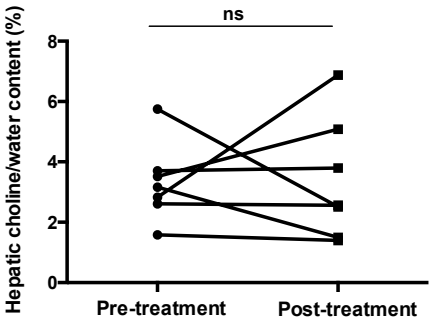
ns
Hepatic choline/water content (%)
8
6
4
2
0
Pre-treatment
Post-treatment

5F.

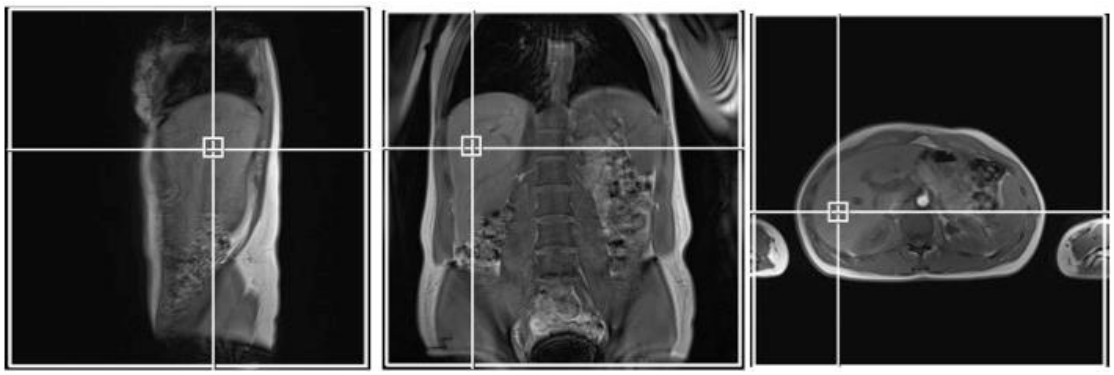

Fig 6-5. No significant impact of HCV eradication on *de novo* lipogenesis (DNL) and hepatic lipid/water & choline/water content on MRS. DNL as measured by deuterated water incorporation into plasma triglyceride palmitate. in all patients [A], genotype 1 [B] or genotype 3 [C]. Hepatic lipid content percentage [D] and choline/water ratio [E] as measured by magnetic resonance spectrometry (MRS). Axial, sagittal and coronal 3D-GE T1-weighted images of the abdomen showing typical MRS voxel placement in the right lobe of liver [F] circles=pre-treatment, squares=post-treatment. ns=non-significant. Paired Student's t-test.

6.4.5 Global adipose tissue insulin resistance

Mean fasting circulating non-essential fatty acid (NEFA) levels was significantly lower following viral eradication (112±41.87μmol/L vs. 80.40±38.83μmol/L; p<0.001). NEFA levels were suppressed in the presence of insulin although the low and high dose insulin-suppressed circulating NEFA levels were unchanged before and after SVR (low insulin: 12.85±7.91μmol vs. 10.41±8.42μmol/L; p=0.16; high insulin: 4.09±4.26μmol vs. 3.46±4.45μmol/L; p=0.84) [Fig 6-6A & B].

Glycerol rate of appearance (Ra glycerol) is a measure of global lipolytic rate and is suppressed by insulin. There was no difference in Ra glycerol at basal (2.11±1.12μmol/kg/min vs. 2.23±1.16μmol/kg/min; p=0.64), low (0.75±0.53μmol/kg/min vs. 0.75±0.34μmol/kg/min; p-0.66) or high insulin (0.61±0.38μmol/kg/min vs. 0.54±0.22μmol/kg/min; p=0.83) infusion before and after antiviral treatment, pan-genotypically [Fig 6-7A], or in genotypes 1 and 3 alone [Fig 6-7B & C].

6A.

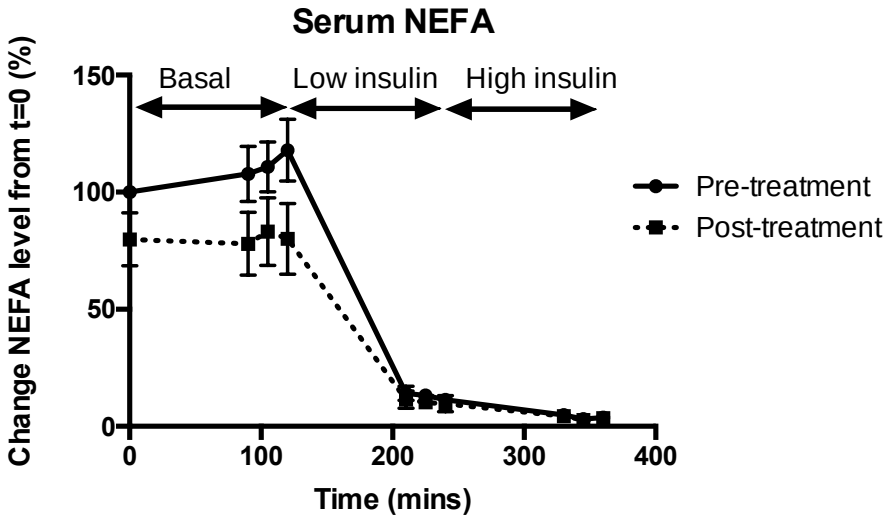

6B.

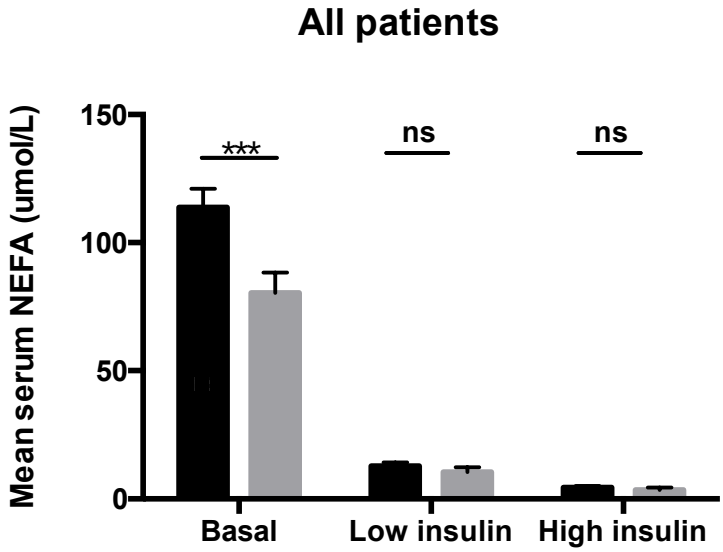

Fig 6-6. HCV eradication improves mean fasting circulating serum NEFA levels. Circulating NEFA concentrations at basal and hyperinsulinaemic phases of euglycaemic clamp before and after antiviral treatment [A]. To determine adipose insulin resistance at basal and hyperinsulinaemic conditions, mean circulating serum NEFA levels at steady states were measured [B]. Key: Black bar=prior to antiviral treatment, grey bar= after antiviral treatment. ***p<0.001, ns=non-significant. Paired Student's t-test.

7A.

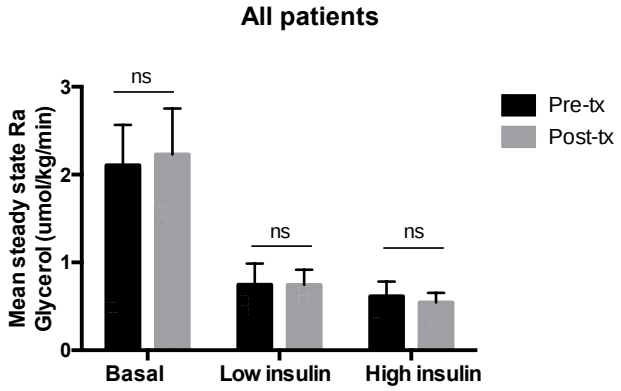

7B.

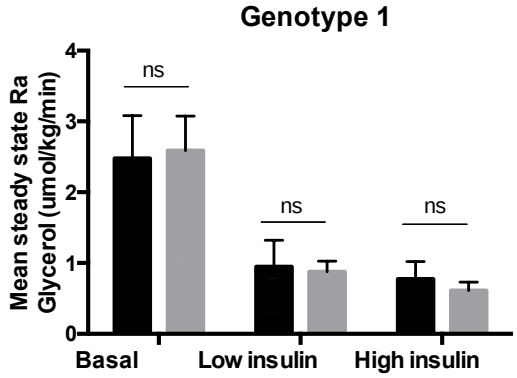

7C.

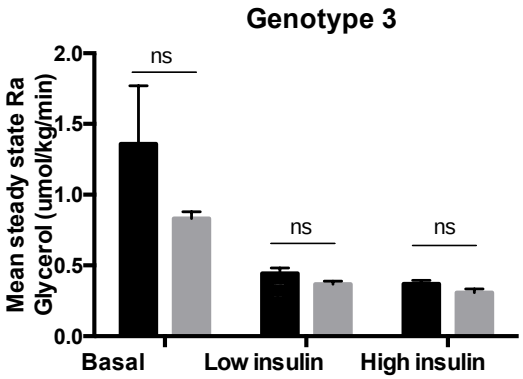

Fig 6-7. No impact of sustained virological response (SVR) rates on whole body lipolysis measured by glycerol rate of appearance (Gly Ra). Whole body lipolysis was assessed by measuring glycerol rate of appearance (Gly Ra) in all patients, n=7 [A], and in patients with genotype 1, n=4 [B] and genotype 3, n=3 [C]. Insulin decreased Gly Ra consistent with decreased lipolysis but no differences before and after SVR or across genotype. Black bar= pre-antiviral treatment. Grey bar=post-antiviral treatment. ns= non-significant. Paired Student's t-test.

6.4.6 Abdominal subcutaneous adipose tissue (SAT) insulin resistance

Interstitial glycerol release assessed using microdialysis, was used as a direct measure of abdominal SAT function [Fig 6-8A & B]. During fasting, the rate of interstitial glycerol release was lower following viral eradication (260.63±128.15μmol/kg/min vs. 193.69±42.85μmol/kg/min; $p<0.05$). During low-insulin infusion, there was no difference in abdominal SAT function before and after viral eradication (147.93±56.83μmol/kg/min vs. 145.21±61.93μmol/kg/min; $p=0.23$). Both these observations were comparable to the changes seen in serum NEFA levels and Ra Gly in our previous data [Fig 6-6 & 6-7]. However, there was a significant improvement in low dose insulin suppressed interstitial glycerol release when genotype 1 was excluded [Fig 6-8D]. High dose insulin suppressed interstitial glycerol release was significantly lower following viral eradication (98.72±22.28μmol/kg/min vs. 70.59±25.49μmol/kg/min; $p<0.05$), suggesting that even though global lipolysis did not change, abdominal SAT function improved with viral eradication. This remained significant when analyzing individually genotype 3 [Fig 6-8C] or genotype 1 [Fig 6-8D].

8A.

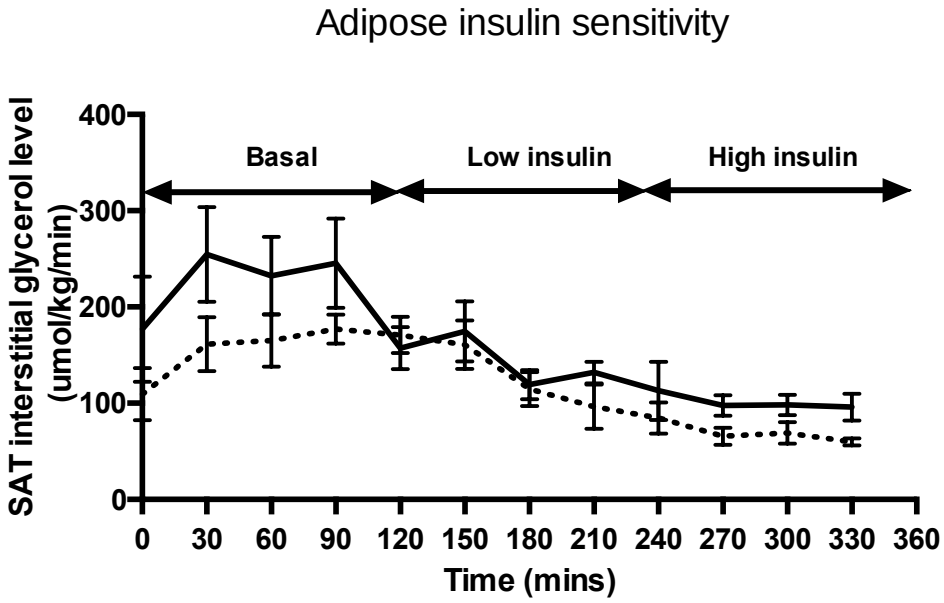
Adipose insulin sensitivity
SAT interstitial glycerol level (umol/kg/min)
400
300
200
100
0
Basal
Low insulin
High insulin
0
30
60
90
120
150
180
210
240
270
300
330
360
Time (mins)

8B.

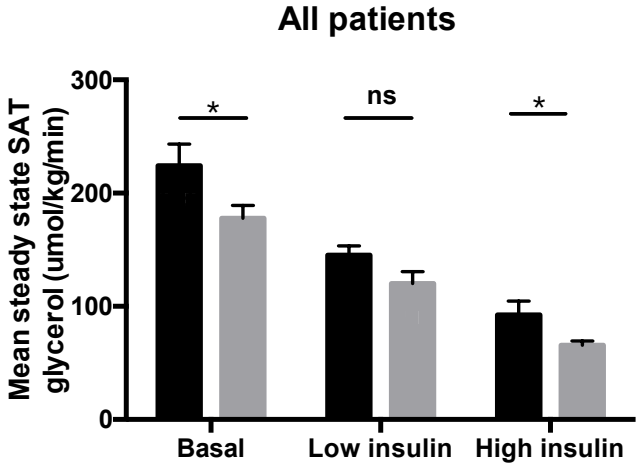
All patients
Mean steady state SAT glycerol (umol/kg/min)
300
200
100
0
*
ns
*
Basal
Low insulin
High insulin

8C. **8D.**

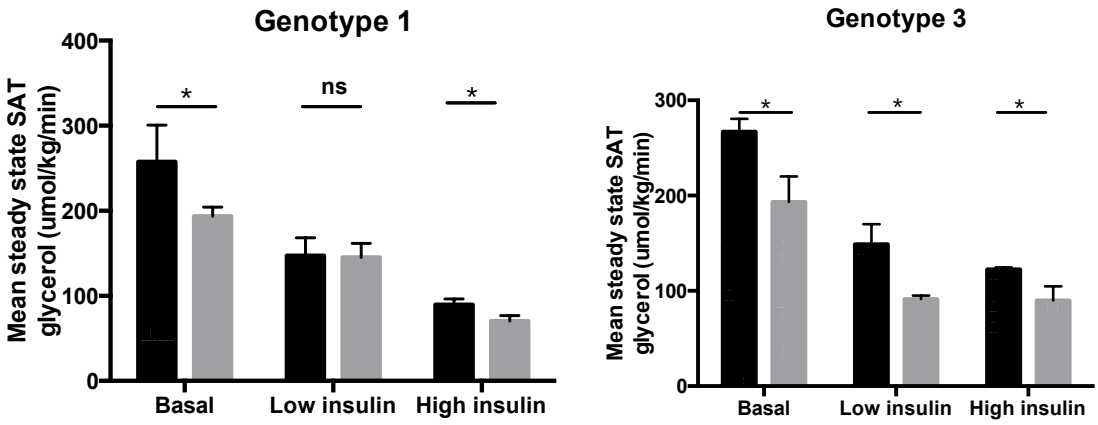

Fig 6-8. SVR rates following antiviral treatment improve abdominal subcutaneous adipose tissue (SAT) insulin resistance. [A] SAT interstitial fluid concentration of glycerol during the 2-step hyperinsulinaemic euglycaemic clamp. [B] Mean levels of glycerol release during steady state were determined to quantify the rate of lipolysis in SAT under basal and hyperinsulinaemic conditions in all patients n=7 [B], in genotype 1 n=4 [C] and genotype 3 n=3 [D]. Continuous black line or black bar= pre-antiviral treatment. Dotted black line or grey bar=post-antiviral treatment. *p<0.05, ns=non-significant. Paired student's t-test.

6.4.7 Metabolic genes

The expression levels of several genes involved in the metabolic pathway were analyzed in this study using Fluidigm BioMark™ HD System 96.96 Dynamic Array. We selected 84 genes involved in cellular lipid and carbohydrate metabolism as well as inflammatory response (Table 6-1). 15 out of 84 genes showed significant differences in expression levels before and after viral eradication. Of the fifteen genes, eight were involved in lipid synthesis [fatty acid binding protein 3 (FABP3), aquaporin 7 (AQP7), pyruvate dehydrogenase alpha 1 (PDHA1), protein kinase AMP-activated catalytic subunit alpha 1 (PRKAA1), very low density lipoprotein receptor (VLDLR), perilipin 1 (PLIN1), diacylglycerol O-acyltransferase 1 (DGAT1), sterol regulatory element binding transcription factor 1 (SREBF1)] (Fig 6-9A); and four in insulin signaling [hexokinase 1 (HK1), insulin receptor substrate 2 (IRS2), v-akt murine thymoma viral oncogene homolog 2 (AKT2) and pyruvate dehydrogenase kinase 1 (PDK1) (Fig. 6-9B). All but PDK1 gene was upregulated following viral eradication.

A.

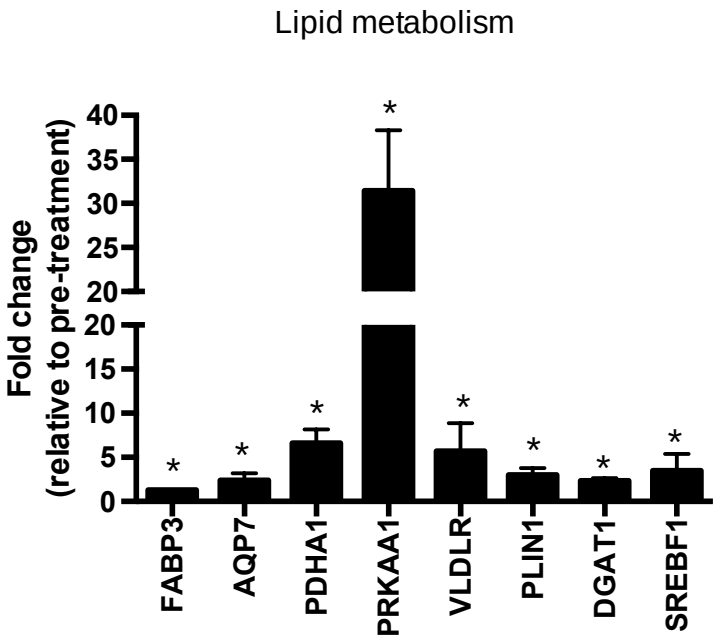

B.

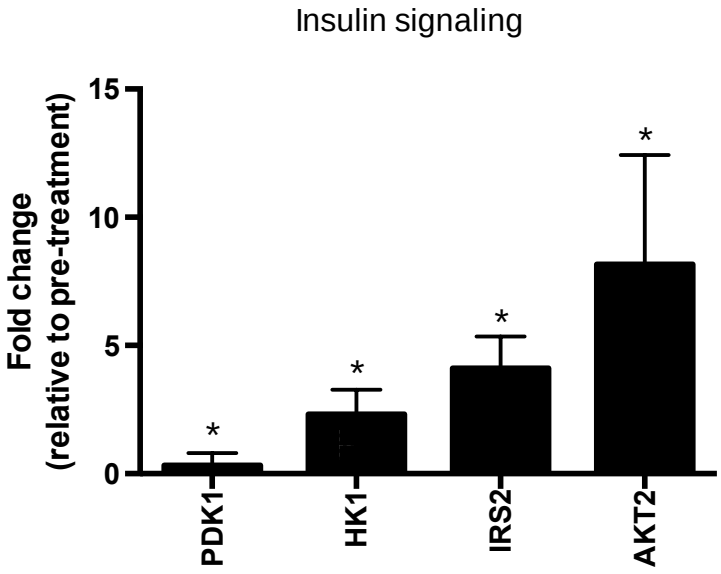

Fig 6-9. HCV eradication regulates the mRNA expression of lipogenic (A) and insulin signaling (B) genes. Fold change of 8 lipogenic genes and 4 insulin signaling genes, which showed significant differences in expression levels in pre and post viral eradication in HCV patients. Data are presented as mean ± se fold induction compared to untreated cells and quantified relative to GAPDH. *$p<0.05$. Unpaired Student's t test

6.5 DISCUSSION

This is the first longitudinal study measuring both carbohydrate and lipid flux before and after viral eradication in patients with CHC. We have used a variety of assessments including ^{13}C-glucose infusion, $^{2}H_5$-glycerol infusion, adipose tissue microdialysis and metabolic gene mRNA expression from adipose tissue biopsy to quantify peripheral, hepatic, and adipose tissue function and their response to insulin. We identified that the improvement in insulin resistance upon successful viral eradication was not systemic, but tissue specific, ie. hepatic and subcutaneous adipose tissue. This was not accompanied by alterations in body weight or in hepatic lipid content.

Despite inducing more steatosis and fibrosis, it is unclear whether the degree of insulin resistance is linked to certain HCV genotype. Evidence presented is controversial, with some suggesting higher insulin resistance among patients with genotype 1 (338) while others showing a higher prevalence in genotype 3 CHC (144). Some authors also presented data showing similar prevalence of insulin resistance in both genotypes (138, 339). Even though our study was not powered to compare the two groups, we observed no difference in baseline hepatic or skeletal IR between genotypes 1 and 3 CHC.

However, the improvement in hepatic IR following viral eradication was more pronounced in genotype 3, which was perhaps unsurprising, as genotype 3 HCV is known to be more pro-steatogenic and therefore, its eradication should

improve hepatic steatosis and hence hepatic IR. More interestingly, in our study, the improvement in skeletal IR was only observed in genotype 1 CHC. This is the first study to show the genotype-specific impact of genotype 1 and genotype 3 infection on steatosis and insulin resistance by studying both lipid and carbohydrate flux. The distinct pattern of lipid alteration between different genotypes has only been studied previously using patients' serological markers for lipid metabolism (257). *Chang et. al* showed that post-SVR HDL and apolipoprotein A1 levels increased in genotype 2 but not in genotype 1 CHC. In their cohort, baseline steatosis and insulin resistance, as well as significantly different viral load may have different impact on the metabolic profile post SVR. However, as the baseline metabolic features and viral load were comparable between the two genotypes in our study, there may yet be an unrevealed mechanism of action of HCV proteins in inducing IR.

We also detected no difference in hepatic DNL and hepatic lipid content in patients with CHC before and after viral eradication. This is different from the study by Lambert *et.al* (335) who noticed improvement in DNL in patients who were cured from CHC. However, his study is conducted in patients with cirrhosis, which in itself, may induce insulin resistance. Low baseline hepatic lipid content in our patients may also mask the possible improvement seen with viral eradication. Previous MRS studies involving HCV patients have suggested that levels of lipid and choline containing compounds in the liver are related to disease severity and choline/lipid or choline/water ratios are predictive of response to treatment (340, 341). As predicted, we did not detect any changes in

these measurements before and after antiviral therapy as all patients in our study are in early/pre-cirrhotic stage.

To the best of our knowledge, only one other study had explored the effect of HCV infection on whole body lipolysis (137). Vanni *et al.* measured serum NEFA levels and mean steady state of appearance of glycerol (Glycerol Ra) following $^{2}H_{5}$-glycerol infusion and found no difference in whole body lipolysis between healthy volunteers and patients with CHC. We demonstrated a reduction in fasting serum NEFA levels but no change in Ra Glycerol following viral eradication. Direct comparison between the two studies is confounded by the different phenotypic and metabolic profile of the subjects in both studies.

We know that both mean level of serum NEFA and $^{2}H_{5}$-Glycerol tracer measurements detect whole body lipolysis and are unable to correlate whole body lipolysis to a specific tissue. By pairing these with abdominal SAT microdialysis (a reduction in mean steady state glycerol) and biopsies (increased expression of lipogenic and glycolytic genes), we showed an improvement in abdominal SAT-specific insulin sensitivity with viral eradication in CHC. Interestingly, genotype 3 CHC seem to show more significant improvement (at basal, low and high insulin infusions) compared to genotype 1 CHC (at basal and high insulin infusions). This supports a genotype specific mechanism underlying SAT IR in patients with CHC. In fact, there are clinical observations supporting a "fat-independent" mechanism in the development of IR in CHC, whereby patients with genotype 3 CHC have more extensive hepatic steatosis but a lower incidence of IR (144). SAT adipose tissue dysfunction has been linked to other

liver conditions, especially non-alcoholic fatty liver disease (306), but this is the first study demonstrating its importance in patients with CHC.

Our study is not without limitations. 13 out of the intended 24 patients with CHC were recruited into the study. This is largely due to the introduction of the new directly acting antivirals (DAAs), which meant that most patients with CHC were not commenced on the conventional interferon-based antiviral treatment between 2011-2013. Thus, the numbers were small, making it difficult to extrapolate the relevance of genotype 1 vs. genotype 3 in inducing insulin resistance and hepatic steatosis. We were unable to directly compare subcutaneous and visceral adipose tissue function, as real-time assessment of dynamic, specific visceral adipose tissue function is not currently feasible in human studies. Insulin resistance likely exacerbates the HCV-induced influence on lipogenesis, and may explain the association between insulin resistance, disease progression, and nonresponse to therapy in HCV (342). One factor that may influence this is the use of pegylated interferon in patients with CHC, which has been shown to alter insulin sensitivity both *in vivo* and *in vitro* (343, 344). Indeed, even though a wash out period of 3 to 6 months was included in our design to try and eliminate the effect of interferon treatment, we still observed a more dramatic improvement in systemic insulin sensitivity in patients who did not received interferon, compared to those who did as part of their antiviral regimen suggesting that the effect(s) of interferon on insulin signaling may be more long lasting. Furthermore, treatment typically induces weight loss and reduced food intake, both of which can alter insulin sensitivity. However, in our

study, there was no change in BMI, weight or fat mass before and after viral eradication.

6.6 CONCLUSION

This study suggests that chronic hepatitis C (CHC) is intricately linked to insulin resistance and hepatic steatosis. Using state-of-the-art metabolic assessments, we have demonstrated that both hepatic and adipose tissue insulin sensitivity improved after viral eradication. The identification of extra-hepatic effects of HCV infection, especially in the adipose tissue is novel and has important clinical relevance. Further studies are needed to evaluate the potential interaction between HCV and adipose tissue in inducing insulin resistance and the genotype-specific mechanisms involved, to allow for novel and targeted therapies.

7.0 GENERAL DISCUSSION AND CONCLUSION

7.1 Low oxygen induces hepatic lipid accumulation via HIFs

Whilst some studies proposed that hypoxia-induced hepatic lipid accumulation is either predominantly driven by HIF1α (5, 66, 67, 245) or HIF2α (7, 229, 242), we showed that both HIFs play major roles in inducing hepatic lipid accumulation. In addition to the type of HIF stabilization, the degree of HIF stabilization also determines the metabolic outcomes in liver diseases. Murine models with whole-body PHD1 knock out developed hepatic steatosis but not the deleterious metabolic effects of high fat diet (345). Liver specific stabilization of HIF2α by acute PHD3 deletion did not lead to hepatic steatosis, suggesting that low level of hepatic HIF2α stabilization, as found in the HIF-PHD2$^{gt/gt}$ mice, has beneficial effects (346), whereas extensive hepatic HIF2α stabilization leads to steatosis (229). The HIF-PHD2$^{gt/gt}$ mice had decreased serum cholesterol and acetyl-CoA levels, postulating that the latter may have contributed to the low serum cholesterol level seen (346). In addition, liver specific stabilization of HIF1α and HIF2α appeared to have no effect on hepatic triglyceride synthesis, but extensive HIF2α stabilization increases hepatic and serum cholesterol levels (229, 347). Taken together, the isoform and degree of HIF stabilization seem to determine the metabolic phenotype in liver diseases.

Significant efforts have been made to discover PHD inhibitors using a wide variety of methods. However, deleterious effects caused by PHD inhibition meant that tissue-specific delivery of PHD inhibition is more desirable. Since the expression and function of individual PHD has been shown to vary, isoform-selective PHD inhibitors are also desirable. Future studies should identify the distinct roles of HIF isoforms because inhibition of specific PHDs could give rise to differential responses of HIF1α and HIF2α (348).

7.2 Hepatic steatosis and insulin resistance in CHC

In the clinical studies, patients with CHC demonstrated increased hepatic lipid content (genotype 3 only) and DNL, when compared to control, which contradicted the *in vitro* findings. There are several reasons for the disparity seen between the *in vitro* and clinical observations. Apart from DNL, FFA uptake and β-oxidation, liver fat volume is also determined by the export of TG as VLDL into the bloodstream, and the flux of fatty acids released from adipose tissue through lipolysis. Both of these were not measured in the *in vitro* study. Secondly, laboratory cultured HCV viruses are diverse and may affect the host metabolism differently compared to human viruses. The relative contribution of virus and immune response on host metabolism remains to be dissected. Other groups have also made claims based on evidence gathered *in vitro,* which are also in conflict with the observations made in humans. For example, although transcription factors responsible for DNL, such as SREBF1 and SREBF2 are increased in HCV infected cells (266, 349-352), their levels in the liver of infected individual inversely correlate with steatosis severity (101). This suggests that their activation, albeit necessary for the HCV life cycle, may not be sufficient to bring about steatosis *in vivo*.

Interaction between HCV, lipid metabolism and insulin signaling is complex and to some extent, genotype-specific. It is not possible to determine whether the increased lipogenesis seen in some patients with CHC, is due to elevated insulin, HCV, or a combination, but ample evidence from cellular models exists to suggest a primary role for HCV on lipogenesis. In this study, patients with genotype 3

CHC appeared to be more steatotic and insulin resistant (SAT-specific) than genotype 1 CHC. Hepatic steatosis has been linked to insulin resistance in human studies and this phenomenon is not specific to CHC (287, 288, 353). However, despite an increase in hepatic steatosis in genotype 3, serum triglyceride levels and systemic insulin resistance do not differ in genotypes 1 and 3 infections (354), as was found in this study. *In vivo* data suggested skeletal muscle (137, 138) and visceral adipose tissue (355) as the primary sites of insulin resistance in CHC. We have now identified the liver and subcutaneous adipose tissue as the predominant sites of insulin resistance in CHC.

Even though HCV eradication improved hepatic and adipose tissue insulin resistance, when we compared baseline metabolic parameters between 12 healthy subjects and 13 patients with CHC, only those with genotype 3 CHC were more 'adipose-insulin resistant'. It may be that patients with CHC, especially genotype 1, have "subclinical" hepatic insulin resistance, which improves with successful antiviral treatment. Indeed lower cut off values for HOMA-IR have been used in certain subgroup of patients to identify those with glucose intolerance (356). This concept has not been validated in patients with CHC. In addition, HOMA-IR measures systemic insulin resistance and does not differentiate hepatic vs. peripheral insulin resistance. The hyperinsulinaemic euglycaemic clamp is the gold standard for assessing insulin resistance [1]. The question of what is a "normal" M value that rules out insulin resistance is largely unknown but is dependent on the dose of insulin infused. Several meta-analysis have tried to examine M values across various hyperinsulinaemic euglycaemic

clamps at variable insulin infusion rates resulting in different cut-off values (357, 358). This is the first study, which proposes that, in addition to SAT IR, patients with CHC may also have "subclinical" hepatic glucose intolerance, which improves with viral eradication.

Directly acting anti-viral agents (DAAs) have been shown to be less effective in genotype 3 CHC. We have now identified that patients infected with the pro-steatogenic genotype 3 HCV have increased SAT adipose tissue insulin resistance, and viral eradication improved both hepatic and adipose tissue insulin resistance in CHC. Future therapies should aim at understanding the cross talk between SAT and liver especially in genotype 3 CHC, as genotype 3 HCV is now the new villain in the era of DAAs.

7.3 Patients with CHC and NASH have different metabolic phenotypes

The presence of hepatic steatosis in the setting of another liver disease (such as CHC) is associated with liver disease progression. NAFLD and CHC are two multisystem diseases whose spectrum of clinical manifestations, seemingly as a result of them sharing hepatic steatosis and insulin resistance as prominent features, overlap (359). There are also strong arguments suggesting that the association of NAFLD and CHC is much more frequent than predicted by chance alone, proving an intricate link between the two diseases (360). There is limited data comparing the metabolic profile in those with NAFLD and CHC. From the metabolic aspect, HCV infection resembles NASH in numerous features, such as the presence of steatosis, serum dyslipidemia, and oxidative stress in the liver (361). On the other hand, there are noticeable differences between HCV and NASH, in the fact that HCV modulates cellular gene expression and intracellular signal transduction pathways, while such details have not been noted for NASH.

Our data suggest that patients with NASH are more insulin resistant than patients with CHC, and whilst the sites of insulin resistance in NASH are both in hepatic and peripheral (skeletal and SAT), the insulin resistance in CHC is mainly in SAT. As eluded previously, mean BMI was higher in the NASH group compared to CHC cohort and this may be, in part, contribute to the degree of insulin resistance observed in the NASH group. The prevalence of NAFLD is directly linked to body weight. While 10-15% of the general population has fatty liver, over 70% of obese individuals have hepatic steatosis (182, 362, 363). In CHC, obesity (BMI > 30kg/m^2) was an independent negative predictor of

response to antiviral treatment in CHC (364). Weight loss is also associated with a reduction in steatosis and an improvement in liver biochemistry and fibrosis in the absence of any antiviral effects (365). Therefore it is not surprising that in our analysis, patients with CHC were less insulin resistant, as their mean BMI was only 26 kg/m^2 vs. 34 kg/m^2 in the NASH group. However, obesity cannot be blamed entirely for the higher insulin resistance seen in NASH patients. One study suggested that adipose distributed in the visceral/abdominal region appears to convey the greatest risk in NAFLD studies, as it has been shown to strongly correlate with the severity of hepatic steatosis, irrespective of whether the individual was lean or obese (366).

This is the first study, demonstrating the differences in the degree and sites of steatosis and insulin resistance in CHC and NASH. Extrapolation of notions from NAFLD to HCV research seem relevant (256) and will pave for more studies and novel therapies in both liver disease. Future studies should include weight-matched individuals with CHC and NASH, albeit difficulty in recruiting lean NASH patients.

7.4 CONCLUSION AND FUTURE RESEARCH

Our data have increased our understanding of the impact of hypoxia and HCV infection on lipid metabolism and insulin resistance, as well delineating the metabolic entities between CHC and NASH, to allow for the development of novel therapeutic targets.

Future research can be aimed at (1) identifying the different depots of adipose tissue insulin resistance in CHC (visceral vs. abdominal subcutaneous tissue), (2) defining the genotype-specific effect of HCV on insulin resistance and (3) targeting the different roles of HIF subtypes and their roles on different cells under different physiological conditions.

8.0 BIBLIOGRAPHY

1. Wilson GK, Tennant DA, McKeating JA. Hypoxia inducible factors in liver disease and hepatocellular carcinoma: current understanding and future directions. Journal of hepatology. 2014;61(6):1397-406.
2. Jungermann K, Kietzmann T. Oxygen: modulator of metabolic zonation and disease of the liver. Hepatology. 2000;31(2):255-60.
3. Gebhardt R, Baldysiak-Figiel A, Krugel V, Ueberham E, Gaunitz F. Hepatocellular expression of glutamine synthetase: an indicator of morphogen actions as master regulators of zonation in adult liver. Progress in histochemistry and cytochemistry. 2007;41(4):201-66.
4. Arteel GE, Iimuro Y, Yin M, Raleigh JA, Thurman RG. Chronic enteral ethanol treatment causes hypoxia in rat liver tissue in vivo. Hepatology. 1997;25(4):920-6.
5. Nath B, Levin I, Csak T, Petrasek J, Mueller C, Kodys K, et al. Hepatocyte-specific hypoxia-inducible factor-1alpha is a determinant of lipid accumulation and liver injury in alcohol-induced steatosis in mice. Hepatology. 2011;53(5):1526-37.
6. Nasimuzzaman M, Waris G, Mikolon D, Stupack DG, Siddiqui A. Hepatitis C virus stabilizes hypoxia-inducible factor 1alpha and stimulates the synthesis of vascular endothelial growth factor. Journal of virology. 2007;81(19):10249-57.
7. Qu A, Taylor M, Xue X, Matsubara T, Metzger D, Chambon P, et al. Hypoxia-inducible transcription factor 2alpha promotes steatohepatitis through augmenting lipid accumulation, inflammation, and fibrosis. Hepatology. 2011;54(2):472-83.
8. Wilson GK, Brimacombe CL, Rowe IA, Reynolds GM, Fletcher NF, Stamataki Z, et al. A dual role for hypoxia inducible factor-1alpha in the hepatitis C virus lifecycle and hepatoma migration. Journal of hepatology. 2012;56(4):803-9.
9. Jungermann K, Kietzmann T. Zonation of parenchymal and nonparenchymal metabolism in liver. Annu Rev Nutr. 1996;16:179-203.
10. Katz N, Teutsch HF, Jungermann K, Sasse D. Heterogeneous reciprocal localization of fructose-1,6-bisphosphatase and of glucokinase in microdissected periportal and perivenous rat liver tissue. FEBS letters. 1977;83(2):272-6.
11. Gebhardt R, Mecke D. Heterogeneous distribution of glutamine synthetase among rat liver parenchymal cells in situ and in primary culture. The EMBO journal. 1983;2(4):567-70.
12. Gebhardt R, Matz-Soja M. Liver zonation: Novel aspects of its regulation and its impact on homeostasis. World journal of gastroenterology : WJG. 2014;20(26):8491-504.
13. Halpern KB, Shenhav R, Matcovitch-Natan O, Toth B, Lemze D, Golan M, et al. Erratum: Single-cell spatial reconstruction reveals global division of labour in the mammalian liver. Nature. 2017;543(7647):742.
14. Colnot S, Perret, P. Liver Zonation. Molecular Pathology of Liver Diseases: Springer Science; 2011. p. 7-8.

15. Benhamouche S, Decaens T, Godard C, Chambrey R, Rickman DS, Moinard C, et al. Apc tumor suppressor gene is the "zonation-keeper" of mouse liver. Developmental cell. 2006;10(6):759-70.
16. Cadoret A, Ovejero C, Terris B, Souil E, Levy L, Lamers WH, et al. New targets of beta-catenin signaling in the liver are involved in the glutamine metabolism. Oncogene. 2002;21(54):8293-301.
17. Shimazu T. Reciprocal innervation of the liver: its significance in metabolic control. Advances in metabolic disorders. 1983;10:355-84.
18. Guder WG, Schmidt U. Liver cell heterogeneity. The distribution of pyruvate kinase and phosphoenolpyruvate carboxykinase (GTP) in the liver lobule of fed and starved rats. Hoppe-Seyler's Zeitschrift fur physiologische Chemie. 1976;357(12):1793-800.
19. Katz N, Teutsch HF, Sasse D, Jungermann K. Heterogeneous distribution of glucose-6-phosphatase in microdissected periportal and perivenous rat liver tissue. FEBS letters. 1977;76(2):226-30.
20. Zierz S, Katz N, Jungermann K. Distribution of pyruvate kinase type L and M2 in microdissected periportal and perivenous rat liver tissue with different dietary states. Hoppe-Seyler's Zeitschrift fur physiologische Chemie. 1983;364(10):1447-53.
21. Vasilj A, Gentzel M, Ueberham E, Gebhardt R, Shevchenko A. Tissue proteomics by one-dimensional gel electrophoresis combined with label-free protein quantification. J Proteome Res. 2012;11(7):3680-9.
22. Chafey P, Finzi L, Boisgard R, Cauzac M, Clary G, Broussard C, et al. Proteomic analysis of beta-catenin activation in mouse liver by DIGE analysis identifies glucose metabolism as a new target of the Wnt pathway. Proteomics. 2009;9(15):3889-900.
23. Gebhardt R. Metabolic zonation of the liver: regulation and implications for liver function. Pharmacol Ther. 1992;53(3):275-354.
24. Massimi M, Lear SR, Williams DL, Jones AL, Erickson SK. Differential expression of apolipoprotein E messenger RNA within the rat liver lobule determined by in situ hybridization. Hepatology. 1999;29(5):1549-55.
25. Braeuning A, Ittrich C, Kohle C, Hailfinger S, Bonin M, Buchmann A, et al. Differential gene expression in periportal and perivenous mouse hepatocytes. FEBS J. 2006;273(22):5051-61.
26. Berkowitz CM, Shen CS, Bilir BM, Guibert E, Gumucio JJ. Different hepatocytes express the cholesterol 7 alpha-hydroxylase gene during its circadian modulation in vivo. Hepatology. 1995;21(6):1658-67.
27. Carroll VA, Ashcroft M. Targeting the molecular basis for tumour hypoxia. Expert Rev Mol Med. 2005;7(6):1-16.
28. Kim JW, Tchernyshyov I, Semenza GL, Dang CV. HIF-1-mediated expression of pyruvate dehydrogenase kinase: a metabolic switch required for cellular adaptation to hypoxia. Cell metabolism. 2006;3(3):177-85.
29. Ginouves A, Ilc K, Macias N, Pouyssegur J, Berra E. PHDs overactivation during chronic hypoxia "desensitizes" HIFalpha and protects cells from necrosis. Proceedings of the National Academy of Sciences of the United States of America. 2008;105(12):4745-50.
30. Lofstedt T, Fredlund E, Holmquist-Mengelbier L, Pietras A, Ovenberger M, Poellinger L, et al. Hypoxia inducible factor-2alpha in cancer. Cell Cycle. 2007;6(8):919-26.

31. Hirsila M, Koivunen P, Gunzler V, Kivirikko KI, Myllyharju J. Characterization of the human prolyl 4-hydroxylases that modify the hypoxia-inducible factor. The Journal of biological chemistry. 2003;278(33):30772-80.
32. Oliver KM, Taylor CT, Cummins EP. Hypoxia. Regulation of NFkappaB signalling during inflammation: the role of hydroxylases. Arthritis Res Ther. 2009;11(1):215.
33. Vogel S, Wottawa M, Farhat K, Zieseniss A, Schnelle M, Le-Huu S, et al. Prolyl hydroxylase domain (PHD) 2 affects cell migration and F-actin formation via RhoA/rho-associated kinase-dependent cofilin phosphorylation. The Journal of biological chemistry. 2010;285(44):33756-63.
34. Lee DC, Sohn HA, Park ZY, Oh S, Kang YK, Lee KM, et al. A lactate-induced response to hypoxia. Cell. 2015;161(3):595-609.
35. Appelhoff RJ, Tian YM, Raval RR, Turley H, Harris AL, Pugh CW, et al. Differential function of the prolyl hydroxylases PHD1, PHD2, and PHD3 in the regulation of hypoxia-inducible factor. The Journal of biological chemistry. 2004;279(37):38458-65.
36. Aprelikova O, Chandramouli GV, Wood M, Vasselli JR, Riss J, Maranchie JK, et al. Regulation of HIF prolyl hydroxylases by hypoxia-inducible factors. Journal of cellular biochemistry. 2004;92(3):491-501.
37. Lando D, Peet DJ, Whelan DA, Gorman JJ, Whitelaw ML. Asparagine hydroxylation of the HIF transactivation domain a hypoxic switch. Science. 2002;295(5556):858-61.
38. Dayan F, Roux D, Brahimi-Horn MC, Pouyssegur J, Mazure NM. The oxygen sensor factor-inhibiting hypoxia-inducible factor-1 controls expression of distinct genes through the bifunctional transcriptional character of hypoxia-inducible factor-1alpha. Cancer research. 2006;66(7):3688-98.
39. Jiang BH, Jiang G, Zheng JZ, Lu Z, Hunter T, Vogt PK. Phosphatidylinositol 3-kinase signaling controls levels of hypoxia-inducible factor 1. Cell Growth Differ. 2001;12(7):363-9.
40. Semenza G. Signal transduction to hypoxia-inducible factor 1. Biochemical pharmacology. 2002;64(5-6):993-8.
41. Conrad PW, Freeman TL, Beitner-Johnson D, Millhorn DE. EPAS1 trans-activation during hypoxia requires p42/p44 MAPK. The Journal of biological chemistry. 1999;274(47):33709-13.
42. Isaacs JS, Jung YJ, Mimnaugh EG, Martinez A, Cuttitta F, Neckers LM. Hsp90 regulates a von Hippel Lindau-independent hypoxia-inducible factor-1 alpha-degradative pathway. The Journal of biological chemistry. 2002;277(33):29936-44.
43. Gradin K, McGuire J, Wenger RH, Kvietikova I, fhitelaw ML, Toftgard R, et al. Functional interference between hypoxia and dioxin signal transduction pathways: competition for recruitment of the Arnt transcription factor. Molecular and cellular biology. 1996;16(10):5221-31.
44. Cohen JC, Horton JD, Hobbs HH. Human fatty liver disease: old questions and new insights. Science. 2011;332(6037):1519-23.
45. Kersten S. Mechanisms of nutritional and hormonal regulation of lipogenesis. EMBO Rep. 2001;2(4):282-6.
46. Postic C, Girard J. Contribution of de novo fatty acid synthesis to hepatic steatosis and insulin resistance: lessons from genetically engineered mice. The Journal of clinical investigation. 2008;118(3):829-38.

47. Houten SM, Wanders RJ. A general introduction to the biochemistry of mitochondrial fatty acid beta-oxidation. J Inherit Metab Dis. 2010;33(5):469-77.
48. Olson AL, Knight JB. Regulation of GLUT4 expression in vivo and in vitro. Front Biosci. 2003;8:s401-9.
49. Lin HV, Accili D. Hormonal regulation of hepatic glucose production in health and disease. Cell metabolism. 2011;14(1):9-19.
50. Samuel VT, Shulman GI. Mechanisms for insulin resistance: common threads and missing links. Cell. 2012;148(5):852-71.
51. Ozcan U, Cao Q, Yilmaz E, Lee AH, Iwakoshi NN, Ozdelen E, et al. Endoplasmic reticulum stress links obesity, insulin action, and type 2 diabetes. Science. 2004;306(5695):457-61.
52. Tuncman G, Hirosumi J, Solinas G, Chang L, Karin M, Hotamisligil GS. Functional in vivo interactions between JNK1 and JNK2 isoforms in obesity and insulin resistance. Proceedings of the National Academy of Sciences of the United States of America. 2006;103(28):10741-6.
53. Lee AH, Heidtman K, Hotamisligil GS, Glimcher LH. Dual and opposing roles of the unfolded protein response regulated by IRE1alpha and XBP1 in proinsulin processing and insulin secretion. Proceedings of the National Academy of Sciences of the United States of America. 2011;108(21):8885-90.
54. Smith U. Impaired ('diabetic') insulin signaling and action occur in fat cells long before glucose intolerance--is insulin resistance initiated in the adipose tissue? Int J Obes Relat Metab Disord. 2002;26(7):897-904.
55. Hunter SJ, Garvey WT. Insulin action and insulin resistance: diseases involving defects in insulin receptors, signal transduction, and the glucose transport effector system. The American journal of medicine. 1998;105(4):331-45.
56. Grundy SM. What is the contribution of obesity to the metabolic syndrome? Endocrinol Metab Clin North Am. 2004;33(2):267-82, table of contents.
57. Devaraj S, Rosenson RS, Jialal I. Metabolic syndrome: an appraisal of the pro-inflammatory and procoagulant status. Endocrinol Metab Clin North Am. 2004;33(2):431-53, table of contents.
58. Thorens B, Cheng ZQ, Brown D, Lodish HF. Liver glucose transporter: a basolateral protein in hepatocytes and intestine and kidney cells. The American journal of physiology. 1990;259(6 Pt 1):C279-85.
59. Orci L, Unger RH, Ravazzola M, Ogawa A, Komiya I, Baetens D, et al. Reduced beta-cell glucose transporter in new onset diabetic BB rats. The Journal of clinical investigation. 1990;86(5):1615-22.
60. Proud CG, Denton RM. Molecular mechanisms for the control of translation by insulin. The Biochemical journal. 1997;328 (Pt 2):329-41.
61. Krauss RM, Siri PW. Metabolic abnormalities: triglyceride and low-density lipoprotein. Endocrinol Metab Clin North Am. 2004;33(2):405-15.
62. Bruder ED, Lee PC, Raff H. Lipid and fatty acid profiles in the brain, liver, and stomach contents of neonatal rats: effects of hypoxia. American journal of physiology Endocrinology and metabolism. 2005;288(2):E314-20.
63. Guzman M, Castro J. Zonation of fatty acid metabolism in rat liver. The Biochemical journal. 1989;264(1):107-13.

64. Shen GM, Zhao YZ, Chen MT, Zhang FL, Liu XL, Wang Y, et al. Hypoxia-inducible factor-1 (HIF-1) promotes LDL and VLDL uptake through inducing VLDLR under hypoxia. The Biochemical journal. 2012;441(2):675-83.
65. Liu Y, Ma Z, Zhao C, Wang Y, Wu G, Xiao J, et al. HIF-1alpha and HIF-2alpha are critically involved in hypoxia-induced lipid accumulation in hepatocytes through reducing PGC-1alpha-mediated fatty acid beta-oxidation. Toxicology letters. 2014;226(2):117-23.
66. Nishiyama Y, Goda N, Kanai M, Niwa D, Osanai K, Yamamoto Y, et al. HIF-1alpha induction suppresses excessive lipid accumulation in alcoholic fatty liver in mice. Journal of hepatology. 2012;56(2):441-7.
67. Kim WY, Safran M, Buckley MR, Ebert BL, Glickman J, Bosenberg M, et al. Failure to prolyl hydroxylate hypoxia-inducible factor alpha phenocopies VHL inactivation in vivo. The EMBO journal. 2006;25(19):4650-62.
68. Wu WT, Tsai SS, Shih TS, Lin MH, Chou TC, Ting H, et al. The Association between Obstructive Sleep Apnea and Metabolic Markers and Lipid Profiles. PloS one. 2015;10(6):e0130279.
69. Mishra P, Nugent C, Afendy A, Bai C, Bhatia P, Afendy M, et al. Apnoeic-hypopnoeic episodes during obstructive sleep apnoea are associated with histological nonalcoholic steatohepatitis. Liver international : official journal of the International Association for the Study of the Liver. 2008;28(8):1080-6.
70. Jouet P, Sabate JM, Maillard D, Msika S, Mechler C, Ledoux S, et al. Relationship between obstructive sleep apnea and liver abnormalities in morbidly obese patients: a prospective study. Obesity surgery. 2007;17(4):478-85.
71. Tanne F, Gagnadoux F, Chazouilleres O, Fleury B, Wendum D, Lasnier E, et al. Chronic liver injury during obstructive sleep apnea. Hepatology. 2005;41(6):1290-6.
72. Dorkova Z, Petrasova D, Molcanyiova A, Popovnakova M, Tkacova R. Effects of continuous positive airway pressure on cardiovascular risk profile in patients with severe obstructive sleep apnea and metabolic syndrome. Chest. 2008;134(4):686-92.
73. Tokuda F, Sando Y, Matsui H, Koike H, Yokoyama T. Serum levels of adipocytokines, adiponectin and leptin, in patients with obstructive sleep apnea syndrome. Intern Med. 2008;47(21):1843-9.
74. Robinson GV, Pepperell JC, Segal HC, Davies RJ, Stradling JR. Circulating cardiovascular risk factors in obstructive sleep apnoea: data from randomised controlled trials. Thorax. 2004;59(9):777-82.
75. Li J, Thorne LN, Punjabi NM, Sun CK, Schwartz AR, Smith PL, et al. Intermittent hypoxia induces hyperlipidemia in lean mice. Circ Res. 2005;97(7):698-706.
76. Li J, Savransky V, Nanayakkara A, Smith PL, O'Donnell CP, Polotsky VY. Hyperlipidemia and lipid peroxidation are dependent on the severity of chronic intermittent hypoxia. J Appl Physiol (1985). 2007;102(2):557-63.
77. Benotti P, Wood GC, Argyropoulos G, Pack A, Keenan BT, Gao X, et al. The impact of obstructive sleep apnea on nonalcoholic fatty liver disease in patients with severe obesity. Obesity (Silver Spring). 2016.
78. Cakmak E, Duksal F, Altinkaya E, Acibucu F, Dogan OT, Yonem O, et al. Association Between the Severity of Nocturnal Hypoxia in Obstructive Sleep

Apnea and Non-Alcoholic Fatty Liver Damage. Hepatitis monthly. 2015;15(11):e32655.
79. Li J, Nanayakkara A, Jun J, Savransky V, Polotsky VY. Effect of deficiency in SREBP cleavage-activating protein on lipid metabolism during intermittent hypoxia. Physiol Genomics. 2007;31(2):273-80.
80. Savransky V, Nanayakkara A, Vivero A, Li J, Bevans S, Smith PL, et al. Chronic intermittent hypoxia predisposes to liver injury. Hepatology. 2007;45(4):1007-13.
81. Jun J, Reinke C, Bedja D, Berkowitz D, Bevans-Fonti S, Li J, et al. Effect of intermittent hypoxia on atherosclerosis in apolipoprotein E-deficient mice. Atherosclerosis. 2010;209(2):381-6.
82. Mahat B, Chasse E, Mauger JF, Imbeault P. Effects of acute hypoxia on human adipose tissue lipoprotein lipase activity and lipolysis. Journal of translational medicine. 2016;14(1):212.
83. De Francesco R, Migliaccio G. Challenges and successes in developing new therapies for hepatitis C. Nature. 2005;436(7053):953-60.
84. Simmonds P, Bukh J, Combet C, Deleage G, Enomoto N, Feinstone S, et al. Consensus proposals for a unified system of nomenclature of hepatitis C virus genotypes. Hepatology. 2005;42(4):962-73.
85. Alvisi G, Madan V, Bartenschlager R. Hepatitis C virus and host cell lipids: an intimate connection. RNA Biol. 2011;8(2):258-69.
86. Kaplan DE, Sugimoto K, Newton K, Valiga ME, Ikeda F, Aytaman A, et al. Discordant role of CD4 T-cell response relative to neutralizing antibody and CD8 T-cell responses in acute hepatitis C. Gastroenterology. 2007;132(2):654-66.
87. Logvinoff C, Major ME, Oldach D, Heyward S, Talal A, Balfe P, et al. Neutralizing antibody response during acute and chronic hepatitis C virus infection. Proceedings of the National Academy of Sciences of the United States of America. 2004;101(27):10149-54.
88. von Hahn T, Yoon JC, Alter H, Rice CM, Rehermann B, Balfe P, et al. Hepatitis C virus continuously escapes from neutralizing antibody and T-cell responses during chronic infection in vivo. Gastroenterology. 2007;132(2):667-78.
89. Blight KJ, Kolykhalov AA, Rice CM. Efficient initiation of HCV RNA replication in cell culture. Science. 2000;290(5498):1972-4.
90. Lohmann V, Korner F, Koch J, Herian U, Theilmann L, Bartenschlager R. Replication of subgenomic hepatitis C virus RNAs in a hepatoma cell line. Science. 1999;285(5424):110-3.
91. Raney KD, Sharma SD, Moustafa IM, Cameron CE. Hepatitis C virus non-structural protein 3 (HCV NS3): a multifunctional antiviral target. The Journal of biological chemistry. 2010;285(30):22725-31.
92. Morikawa K, Lange CM, Gouttenoire J, Meylan E, Brass V, Penin F, et al. Nonstructural protein 3-4A: the Swiss army knife of hepatitis C virus. Journal of viral hepatitis. 2011;18(5):305-15.
93. Phan T, Kohlway A, Dimberu P, Pyle AM, Lindenbach BD. The acidic domain of hepatitis C virus NS4A contributes to RNA replication and virus particle assembly. Journal of virology. 2011;85(3):1193-204.
94. Gouttenoire J, Penin F, Moradpour D. Hepatitis C virus nonstructural protein 4B: a journey into unexplored territory. Reviews in medical virology. 2010;20(2):117-29.

95. den Boon JA, Ahlquist P. Organelle-like membrane compartmentalization of positive-strand RNA virus replication factories. Annu Rev Microbiol. 2010;64:241-56.
96. Schmitz U, Tan SL. NS5A--from obscurity to new target for HCV therapy. Recent Pat Antiinfect Drug Discov. 2008;3(2):77-92.
97. Behrens SE, Tomei L, De Francesco R. Identification and properties of the RNA-dependent RNA polymerase of hepatitis C virus. The EMBO journal. 1996;15(1):12-22.
98. Masaki T, Suzuki R, Murakami K, Aizaki H, Ishii K, Murayama A, et al. Interaction of hepatitis C virus nonstructural protein 5A with core protein is critical for the production of infectious virus particles. Journal of virology. 2008;82(16):7964-76.
99. Koike K, Tsutsumi T, Yotsuyanagi H, Moriya K. Lipid metabolism and liver disease in hepatitis C viral infection. Oncology. 2010;78 Suppl 1:24-30.
100. Goldwasser J, Cohen PY, Lin W, Kitsberg D, Balaguer P, Polyak SJ, et al. Naringenin inhibits the assembly and long-term production of infectious hepatitis C virus particles through a PPAR-mediated mechanism. Journal of hepatology. 2011;55(5):963-71.
101. McPherson S, Jonsson JR, Barrie HD, O'Rourke P, Clouston AD, Powell EE. Investigation of the role of SREBP-1c in the pathogenesis of HCV-related steatosis. Journal of hepatology. 2008;49(6):1046-54.
102. Enjoji M, Kohjima M, Kotoh K, Nakamuta M. Metabolic disorders and steatosis in patients with chronic hepatitis C: metabolic strategies for antiviral treatments. Int J Hepatol. 2012;2012:264017.
103. Tsutsumi T, Suzuki T, Shimoike T, Suzuki R, Moriya K, Shintani Y, et al. Interaction of hepatitis C virus core protein with retinoid X receptor alpha modulates its transcriptional activity. Hepatology. 2002;35(4):937-46.
104. Sheikh MY, Choi J, Qadri I, Friedman JE, Sanyal AJ. Hepatitis C virus infection: molecular pathways to metabolic syndrome. Hepatology. 2008;47(6):2127-33.
105. Parvaiz F, Manzoor S, Iqbal J, McRae S, Javed F, Ahmed QL, et al. Hepatitis C virus nonstructural protein 5A favors upregulation of gluconeogenic and lipogenic gene expression leading towards insulin resistance: a metabolic syndrome. Archives of virology. 2014;159(5):1017-25.
106. Shi ST, Polyak SJ, Tu H, Taylor DR, Gretch DR, Lai MM. Hepatitis C virus NS5A colocalizes with the core protein on lipid droplets and interacts with apolipoproteins. Virology. 2002;292(2):198-210.
107. Ramiere C, Rodriguez J, Enache LS, Lotteau V, Andre P, Diaz O. Activity of hexokinase is increased by its interaction with hepatitis C virus protein NS5A. Journal of virology. 2014;88(6):3246-54.
108. Castera L, Chouteau P, Hezode C, Zafrani ES, Dhumeaux D, Pawlotsky JM. Hepatitis C virus-induced hepatocellular steatosis. The American journal of gastroenterology. 2005;100(3):711-5.
109. Gastaminza P, Cheng G, Wieland S, Zhong J, Liao W, Chisari FV. Cellular determinants of hepatitis C virus assembly, maturation, degradation, and secretion. Journal of virology. 2008;82(5):2120-9.
110. Colpitts CC, Lupberger J, Doerig C, Baumert TF. Host cell kinases and the hepatitis C virus life cycle. Biochimica et biophysica acta. 2015;1854(10 Pt B):1657-62.

111. Barba G, Harper F, Harada T, Kohara M, Goulinet S, Matsuura Y, et al. Hepatitis C virus core protein shows a cytoplasmic localization and associates to cellular lipid storage droplets. Proceedings of the National Academy of Sciences of the United States of America. 1997;94(4):1200-5.
112. Moradpour D, Englert C, Wakita T, Wands JR. Characterization of cell lines allowing tightly regulated expression of hepatitis C virus core protein. Virology. 1996;222(1):51-63.
113. Moriya K, Fujie H, Shintani Y, Yotsuyanagi H, Tsutsumi T, Ishibashi K, et al. The core protein of hepatitis C virus induces hepatocellular carcinoma in transgenic mice. Nature medicine. 1998;4(9):1065-7.
114. Rubbia-Brandt L, Quadri R, Abid K, Giostra E, Male PJ, Mentha G, et al. Hepatocyte steatosis is a cytopathic effect of hepatitis C virus genotype 3. Journal of hepatology. 2000;33(1):106-15.
115. Su AI, Pezacki JP, Wodicka L, Brideau AD, Supekova L, Thimme R, et al. Genomic analysis of the host response to hepatitis C virus infection. Proceedings of the National Academy of Sciences of the United States of America. 2002;99(24):15669-74.
116. Kim KH, Hong SP, Kim K, Park MJ, Kim KJ, Cheong J. HCV core protein induces hepatic lipid accumulation by activating SREBP1 and PPARgamma. Biochemical and biophysical research communications. 2007;355(4):883-8.
117. Jackel-Cram C, Babiuk LA, Liu Q. Up-regulation of fatty acid synthase promoter by hepatitis C virus core protein: genotype-3a core has a stronger effect than genotype-1b core. Journal of hepatology. 2007;46(6):999-1008.
118. Perlemuter G, Sabile A, Letteron P, Vona G, Topilco A, Chretien Y, et al. Hepatitis C virus core protein inhibits microsomal triglyceride transfer protein activity and very low density lipoprotein secretion: a model of viral-related steatosis. FASEB journal : official publication of the Federation of American Societies for Experimental Biology. 2002;16(2):185-94.
119. Okuda M, Li K, Beard MR, Showalter LA, Scholle F, Lemon SM, et al. Mitochondrial injury, oxidative stress, and antioxidant gene expression are induced by hepatitis C virus core protein. Gastroenterology. 2002;122(2):366-75.
120. Negro F. Mechanisms and significance of liver steatosis in hepatitis C virus infection. World journal of gastroenterology : WJG. 2006;12(42):6756-65.
121. Dharancy S, Malapel M, Perlemuter G, Roskams T, Cheng Y, Dubuquoy L, et al. Impaired expression of the peroxisome proliferator-activated receptor alpha during hepatitis C virus infection. Gastroenterology. 2005;128(2):334-42.
122. Cheng Y, Dharancy S, Malapel M, Desreumaux P. Hepatitis C virus infection down-regulates the expression of peroxisome proliferator-activated receptor alpha and carnitine palmitoyl acyl-CoA transferase 1A. World journal of gastroenterology : WJG. 2005;11(48):7591-6.
123. Piccoli C, Quarato G, Ripoli M, D'Aprile A, Scrima R, Cela O, et al. HCV infection induces mitochondrial bioenergetic unbalance: causes and effects. Biochimica et biophysica acta. 2009;1787(5):539-46.
124. Sato C, Saito T, Misawa K, Katsumi T, Tomita K, Ishii R, et al. Impaired mitochondrial beta-oxidation in patients with chronic hepatitis C: relation with viral load and insulin resistance. BMC gastroenterology. 2013;13:112.
125. Aytug S, Reich D, Sapiro LE, Bernstein D, Begum N. Impaired IRS-1/PI3-kinase signaling in patients with HCV: a mechanism for increased prevalence of type 2 diabetes. Hepatology. 2003;38(6):1384-92.

126. Banerjee S, Saito K, Ait-Goughoulte M, Meyer K, Ray RB, Ray R. Hepatitis C virus core protein upregulates serine phosphorylation of insulin receptor substrate-1 and impairs the downstream akt/protein kinase B signaling pathway for insulin resistance. Journal of virology. 2008;82(6):2606-12.
127. Bose SK, Shrivastava S, Meyer K, Ray RB, Ray R. Hepatitis C virus activates the mTOR/S6K1 signaling pathway in inhibiting IRS-1 function for insulin resistance. Journal of virology. 2012;86(11):6315-22.
128. Araki E, Lipes MA, Patti ME, Bruning JC, Haag B, 3rd, Johnson RS, et al. Alternative pathway of insulin signalling in mice with targeted disruption of the IRS-1 gene. Nature. 1994;372(6502):186-90.
129. Withers DJ, Gutierrez JS, Towery H, Burks DJ, Ren JM, Previs S, et al. Disruption of IRS-2 causes type 2 diabetes in mice. Nature. 1998;391(6670):900-4.
130. Kawaguchi T, Yoshida T, Harada M, Hisamoto T, Nagao Y, Ide T, et al. Hepatitis C virus down-regulates insulin receptor substrates 1 and 2 through up-regulation of suppressor of cytokine signaling 3. The American journal of pathology. 2004;165(5):1499-508.
131. Pazienza V, Clement S, Pugnale P, Conzelman S, Foti M, Mangia A, et al. The hepatitis C virus core protein of genotypes 3a and 1b downregulates insulin receptor substrate 1 through genotype-specific mechanisms. Hepatology. 2007;45(5):1164-71.
132. Im SS, Kwon SK, Kim TH, Kim HI, Ahn YH. Regulation of glucose transporter type 4 isoform gene expression in muscle and adipocytes. IUBMB life. 2007;59(3):134-45.
133. Knobler H, Schattner A. TNF-{alpha}, chronic hepatitis C and diabetes: a novel triad. QJM : monthly journal of the Association of Physicians. 2005;98(1):1-6.
134. Hotamisligil GS, Budavari A, Murray D, Spiegelman BM. Reduced tyrosine kinase activity of the insulin receptor in obesity-diabetes. Central role of tumor necrosis factor-alpha. The Journal of clinical investigation. 1994;94(4):1543-9.
135. Ruan H, Lodish HF. Insulin resistance in adipose tissue: direct and indirect effects of tumor necrosis factor-alpha. Cytokine Growth Factor Rev. 2003;14(5):447-55.
136. Cheung AT, Wang J, Ree D, Kolls JK, Bryer-Ash M. Tumor necrosis factor-alpha induces hepatic insulin resistance in obese Zucker (fa/fa) rats via interaction of leukocyte antigen-related tyrosine phosphatase with focal adhesion kinase. Diabetes. 2000;49(5):810-9.
137. Vanni E, Abate ML, Gentilcore E, Hickman I, Gambino R, Cassader M, et al. Sites and mechanisms of insulin resistance in nonobese, nondiabetic patients with chronic hepatitis C. Hepatology. 2009;50(3):697-706.
138. Milner KL, van der Poorten D, Trenell M, Jenkins AB, Xu A, Smythe G, et al. Chronic hepatitis C is associated with peripheral rather than hepatic insulin resistance. Gastroenterology. 2010;138(3):932-41 e1-3.
139. Allison ME, Wreghitt T, Palmer CR, Alexander GJ. Evidence for a link between hepatitis C virus infection and diabetes mellitus in a cirrhotic population. Journal of hepatology. 1994;21(6):1135-9.
140. Oliveira LP, de Jesus RP, Boulhosa RS, Mendes CM, Lyra AC, Lyra LG. Metabolic syndrome in patients with chronic hepatitis C virus genotype 1

infection who do not have obesity or type 2 diabetes. Clinics (Sao Paulo). 2012;67(3):219-23.
141. Souza AF, Pace FH, Chebli JM, Ferreira LE. Insulin resistance in non-diabetic patients with chronic hepatitis C: what does it mean? Arquivos brasileiros de endocrinologia e metabologia. 2011;55(6):412-8.
142. Ahmed AM, Hassan MS, Abd-Elsayed A, Hassan H, Hasanain AF, Helmy A. Insulin resistance, steatosis, and fibrosis in Egyptian patients with chronic Hepatitis C virus infection. Saudi journal of gastroenterology : official journal of the Saudi Gastroenterology Association. 2011;17(4):245-51.
143. Stepanova M, Lam B, Younossi Y, Srishord MK, Younossi ZM. Association of hepatitis C with insulin resistance and type 2 diabetes in US general population: the impact of the epidemic of obesity. Journal of viral hepatitis. 2012;19(5):341-5.
144. Hui JM, Sud A, Farrell GC, Bandara P, Byth K, Kench JG, et al. Insulin resistance is associated with chronic hepatitis C virus infection and fibrosis progression [corrected]. Gastroenterology. 2003;125(6):1695-704.
145. Deltenre P, Louvet A, Lemoine M, Mourad A, Fartoux L, Moreno C, et al. Impact of insulin resistance on sustained response in HCV patients treated with pegylated interferon and ribavirin: a meta-analysis. Journal of hepatology. 2011;55(6):1187-94.
146. Hourigan LF, Macdonald GA, Purdie D, Whitehall VH, Shorthouse C, Clouston A, et al. Fibrosis in chronic hepatitis C correlates significantly with body mass index and steatosis. Hepatology. 1999;29(4):1215-9.
147. Kumar D, Farrell GC, Fung C, George J. Hepatitis C virus genotype 3 is cytopathic to hepatocytes: Reversal of hepatic steatosis after sustained therapeutic response. Hepatology. 2002;36(5):1266-72.
148. Adinolfi LE, Gambardella M, Andreana A, Tripodi MF, Utili R, Ruggiero G. Steatosis accelerates the progression of liver damage of chronic hepatitis C patients and correlates with specific HCV genotype and visceral obesity. Hepatology. 2001;33(6):1358-64.
149. Patton HM, Patel K, Behling C, Bylund D, Blatt LM, Vallee M, et al. The impact of steatosis on disease progression and early and sustained treatment response in chronic hepatitis C patients. Journal of hepatology. 2004;40(3):484-90.
150. Fartoux L, Poujol-Robert A, Guechot J, Wendum D, Poupon R, Serfaty L. Insulin resistance is a cause of steatosis and fibrosis progression in chronic hepatitis C. Gut. 2005;54(7):1003-8.
151. Chavin KD, Yang S, Lin HZ, Chatham J, Chacko VP, Hoek JB, et al. Obesity induces expression of uncoupling protein-2 in hepatocytes and promotes liver ATP depletion. The Journal of biological chemistry. 1999;274(9):5692-700.
152. Yang SQ, Lin HZ, Lane MD, Clemens M, Diehl AM. Obesity increases sensitivity to endotoxin liver injury: implications for the pathogenesis of steatohepatitis. Proceedings of the National Academy of Sciences of the United States of America. 1997;94(6):2557-62.
153. Walsh MJ, Vanags DM, Clouston AD, Richardson MM, Purdie DM, Jonsson JR, et al. Steatosis and liver cell apoptosis in chronic hepatitis C: a mechanism for increased liver injury. Hepatology. 2004;39(5):1230-8.

154. Yoo YG, Lee MO. Hepatitis B virus X protein induces expression of Fas ligand gene through enhancing transcriptional activity of early growth response factor. The Journal of biological chemistry. 2004;279(35):36242-9.
155. Kondo S, Seo SY, Yoshizaki T, Wakisaka N, Furukawa M, Joab I, et al. EBV latent membrane protein 1 up-regulates hypoxia-inducible factor 1alpha through Siah1-mediated down-regulation of prolyl hydroxylases 1 and 3 in nasopharyngeal epithelial cells. Cancer research. 2006;66(20):9870-7.
156. Darekar S, Georgiou K, Yurchenko M, Yenamandra SP, Chachami G, Simos G, et al. Epstein-Barr virus immortalization of human B-cells leads to stabilization of hypoxia-induced factor 1 alpha, congruent with the Warburg effect. PloS one. 2012;7(7):e42072.
157. Shin YC, Joo CH, Gack MU, Lee HR, Jung JU. Kaposi's sarcoma-associated herpesvirus viral IFN regulatory factor 3 stabilizes hypoxia-inducible factor-1 alpha to induce vascular endothelial growth factor expression. Cancer research. 2008;68(6):1751-9.
158. Liu LP, Hu BG, Ye C, Ho RL, Chen GG, Lai PB. HBx mutants differentially affect the activation of hypoxia-inducible factor-1alpha in hepatocellular carcinoma. British journal of cancer. 2014;110(4):1066-73.
159. Yoo YG, Oh SH, Park ES, Cho H, Lee N, Park H, et al. Hepatitis B virus X protein enhances transcriptional activity of hypoxia-inducible factor-1alpha through activation of mitogen-activated protein kinase pathway. The Journal of biological chemistry. 2003;278(40):39076-84.
160. Cai Q, Lan K, Verma SC, Si H, Lin D, Robertson ES. Kaposi's sarcoma-associated herpesvirus latent protein LANA interacts with HIF-1 alpha to upregulate RTA expression during hypoxia: Latency control under low oxygen conditions. Journal of virology. 2006;80(16):7965-75.
161. Deshmane SL, Mukerjee R, Fan S, Del Valle L, Michiels C, Sweet T, et al. Activation of the oxidative stress pathway by HIV-1 Vpr leads to induction of hypoxia-inducible factor 1alpha expression. The Journal of biological chemistry. 2009;284(17):11364-73.
162. Ripoli M, D'Aprile A, Quarato G, Sarasin-Filipowicz M, Gouttenoire J, Scrima R, et al. Hepatitis C virus-linked mitochondrial dysfunction promotes hypoxia-inducible factor 1 alpha-mediated glycolytic adaptation. Journal of virology. 2010;84(1):647-60.
163. Mee CJ, Farquhar MJ, Harris HJ, Hu K, Ramma W, Ahmed A, et al. Hepatitis C virus infection reduces hepatocellular polarity in a vascular endothelial growth factor-dependent manner. Gastroenterology. 2010;138(3):1134-42.
164. Liu XH, Zhou X, Zhu CL, Song H, Liu F. [Effects of HCV core protein on the expression of hypoxia-inducible factor 1 alpha and vascular endothelial growth factor]. Zhonghua Gan Zang Bing Za Zhi. 2011;19(10):751-4.
165. Zhu C, Liu X, Wang S, Yan X, Tang Z, Wu K, et al. Hepatitis C virus core protein induces hypoxia-inducible factor 1alpha-mediated vascular endothelial growth factor expression in Huh7.5.1 cells. Molecular medicine reports. 2014;9(5):2010-4.
166. Vassilaki N, Kalliampakou KI, Kotta-Loizou I, Befani C, Liakos P, Simos G, et al. Low oxygen tension enhances hepatitis C virus replication. Journal of virology. 2013;87(5):2935-48.

167. Munger J, Bajad SU, Coller HA, Shenk T, Rabinowitz JD. Dynamics of the cellular metabolome during human cytomegalovirus infection. PLoS Pathog. 2006;2(12):e132.
168. Chan EY, Qian WJ, Diamond DL, Liu T, Gritsenko MA, Monroe ME, et al. Quantitative analysis of human immunodeficiency virus type 1-infected CD4+ cell proteome: dysregulated cell cycle progression and nuclear transport coincide with robust virus production. Journal of virology. 2007;81(14):7571-83.
169. Diamond DL, Syder AJ, Jacobs JM, Sorensen CM, Walters KA, Proll SC, et al. Temporal proteome and lipidome profiles reveal hepatitis C virus-associated reprogramming of hepatocellular metabolism and bioenergetics. PLoS Pathog. 2010;6(1):e1000719.
170. Shah T, Krishnamachary B, Wildes F, Mironchik Y, Kakkad SM, Jacob D, et al. HIF isoforms have divergent effects on invasion, metastasis, metabolism and formation of lipid droplets. Oncotarget. 2015;6(29):28104-19.
171. Liu Z, Jia X, Duan Y, Xiao H, Sundqvist KG, Permert J, et al. Excess glucose induces hypoxia-inducible factor-1alpha in pancreatic cancer cells and stimulates glucose metabolism and cell migration. Cancer biology & therapy. 2013;14(5):428-35.
172. Tong Y, Yang H, Xu X, Ruan J, Liang M, Wu J, et al. Effect of a hypoxic microenvironment after radiofrequency ablation on residual hepatocellular cell migration and invasion. Cancer Sci. 2017.
173. Angulo P, Lindor KD. Non-alcoholic fatty liver disease. Journal of gastroenterology and hepatology. 2002;17 Suppl:S186-90.
174. Angulo P. Nonalcoholic fatty liver disease. The New England journal of medicine. 2002;346(16):1221-31.
175. Lonardo A, Loria P. NAFLD and cardiovascular risk: direct evidence for the tale of two ages. The American journal of gastroenterology. 2009;104(7):1851-2.
176. Falck-Ytter Y, Younossi ZM, Marchesini G, McCullough AJ. Clinical features and natural history of nonalcoholic steatosis syndromes. Seminars in liver disease. 2001;21(1):17-26.
177. Marchesini G, Brizi M, Morselli-Labate AM, Bianchi G, Bugianesi E, McCullough AJ, et al. Association of nonalcoholic fatty liver disease with insulin resistance. The American journal of medicine. 1999;107(5):450-5.
178. Lonardo A, Lombardini S, Ricchi M, Scaglioni F, Loria P. Review article: hepatic steatosis and insulin resistance. Alimentary pharmacology & therapeutics. 2005;22 Suppl 2:64-70.
179. Marchesini G, Bugianesi E, Forlani G, Cerrelli F, Lenzi M, Manini R, et al. Nonalcoholic fatty liver, steatohepatitis, and the metabolic syndrome. Hepatology. 2003;37(4):917-23.
180. Bellentani S, Marino M. Epidemiology and natural history of non-alcoholic fatty liver disease (NAFLD). Ann Hepatol. 2009;8 Suppl 1:S4-8.
181. Bjornsson E, Angulo P. Non-alcoholic fatty liver disease. Scandinavian journal of gastroenterology. 2007;42(9):1023-30.
182. Bellentani S, Saccoccio G, Masutti F, Croce LS, Brandi G, Sasso F, et al. Prevalence of and risk factors for hepatic steatosis in Northern Italy. Annals of internal medicine. 2000;132(2):112-7.
183. Bellentani S, Bedogni G, Miglioli L, Tiribelli C. The epidemiology of fatty liver. European journal of gastroenterology & hepatology. 2004;16(11):1087-93.

184. Bedogni G, Miglioli L, Masutti F, Tiribelli C, Marchesini G, Bellentani S. Prevalence of and risk factors for nonalcoholic fatty liver disease: the Dionysos nutrition and liver study. Hepatology. 2005;42(1):44-52.
185. Browning JD, Szczepaniak LS, Dobbins R, Nuremberg P, Horton JD, Cohen JC, et al. Prevalence of hepatic steatosis in an urban population in the United States: impact of ethnicity. Hepatology. 2004;40(6):1387-95.
186. Nonomura A, Mizukami Y, Unoura M, Kobayashi K, Takeda Y, Takeda R. Clinicopathologic study of alcohol-like liver disease in non-alcoholics; non-alcoholic steatohepatitis and fibrosis. Gastroenterol Jpn. 1992;27(4):521-8.
187. Browning JD. Statins and hepatic steatosis: perspectives from the Dallas Heart Study. Hepatology. 2006;44(2):466-71.
188. Rashid M, Roberts EA. Nonalcoholic steatohepatitis in children. Journal of pediatric gastroenterology and nutrition. 2000;30(1):48-53.
189. Goldberg D, Ditah IC, Saeian K, Lalehzari M, Aronsohn A, Gorospe EC, et al. Changes in the Prevalence of Hepatitis C Virus Infection, Non-alcoholic Steatohepatitis, and Alcoholic Liver Disease Among Patients with Cirrhosis or Liver Failure on the Waitlist for Liver Transplantation. Gastroenterology. 2017.
190. Donnelly KL, Smith CI, Schwarzenberg SJ, Jessurun J, Boldt MD, Parks EJ. Sources of fatty acids stored in liver and secreted via lipoproteins in patients with nonalcoholic fatty liver disease. The Journal of clinical investigation. 2005;115(5):1343-51.
191. Yamaguchi K, Yang L, McCall S, Huang J, Yu XX, Pandey SK, et al. Inhibiting triglyceride synthesis improves hepatic steatosis but exacerbates liver damage and fibrosis in obese mice with nonalcoholic steatohepatitis. Hepatology. 2007;45(6):1366-74.
192. Monetti M, Levin MC, Watt MJ, Sajan MP, Marmor S, Hubbard BK, et al. Dissociation of hepatic steatosis and insulin resistance in mice overexpressing DGAT in the liver. Cell metabolism. 2007;6(1):69-78.
193. Day CP, James OF. Steatohepatitis: a tale of two "hits"? Gastroenterology. 1998;114(4):842-5.
194. Day CP. Pathogenesis of steatohepatitis. Best Pract Res Clin Gastroenterol. 2002;16(5):663-78.
195. Belfort R, Mandarino L, Kashyap S, Wirfel K, Pratipanawatr T, Berria R, et al. Dose-response effect of elevated plasma free fatty acid on insulin signaling. Diabetes. 2005;54(6):1640-8.
196. Cusi K, Kashyap S, Gastaldelli A, Bajaj M, Cersosimo E. Effects on insulin secretion and insulin action of a 48-h reduction of plasma free fatty acids with acipimox in nondiabetic subjects genetically predisposed to type 2 diabetes. American journal of physiology Endocrinology and metabolism. 2007;292(6):E1775-81.
197. Malhi H, Gores GJ. Cellular and molecular mechanisms of liver injury. Gastroenterology. 2008;134(6):1641-54.
198. Kotronen A, Yki-Jarvinen H, Sevastianova K, Bergholm R, Hakkarainen A, Pietilainen KH, et al. Comparison of the relative contributions of intra-abdominal and liver fat to components of the metabolic syndrome. Obesity (Silver Spring). 2011;19(1):23-8.
199. Chitturi S, Abeygunasekera S, Farrell GC, Holmes-Walker J, Hui JM, Fung C, et al. NASH and insulin resistance: Insulin hypersecretion and specific association with the insulin resistance syndrome. Hepatology. 2002;35(2):373-9.

200. Marchesini G, Brizi M, Bianchi G, Tomassetti S, Bugianesi E, Lenzi M, et al. Nonalcoholic fatty liver disease: a feature of the metabolic syndrome. Diabetes. 2001;50(8):1844-50.
201. Armstrong MJ, Hazlehurst JM, Hull D, Guo K, Borrows S, Yu J, et al. Abdominal subcutaneous adipose tissue insulin resistance and lipolysis in patients with non-alcoholic steatohepatitis. Diabetes Obes Metab. 2014;16(7):651-60.
202. Kato K, Takeshita Y, Misu H, Zen Y, Kaneko S, Takamura T. Liver steatosis is associated with insulin resistance in skeletal muscle rather than in the liver in Japanese patients with non-alcoholic fatty liver disease. J Diabetes Investig. 2015;6(2):158-63.
203. Lomonaco R, Ortiz-Lopez C, Orsak B, Webb A, Hardies J, Darland C, et al. Effect of adipose tissue insulin resistance on metabolic parameters and liver histology in obese patients with nonalcoholic fatty liver disease. Hepatology. 2012;55(5):1389-97.
204. Sanyal AJ, Campbell-Sargent C, Mirshahi F, Rizzo WB, Contos MJ, Sterling RK, et al. Nonalcoholic steatohepatitis: association of insulin resistance and mitochondrial abnormalities. Gastroenterology. 2001;120(5):1183-92.
205. Bugianesi E, Gastaldelli A, Vanni E, Gambino R, Cassader M, Baldi S, et al. Insulin resistance in non-diabetic patients with non-alcoholic fatty liver disease: sites and mechanisms. Diabetologia. 2005;48(4):634-42.
206. Musso G, Cassader M, De Michieli F, Rosina F, Orlandi F, Gambino R. Nonalcoholic steatohepatitis versus steatosis: adipose tissue insulin resistance and dysfunctional response to fat ingestion predict liver injury and altered glucose and lipoprotein metabolism. Hepatology. 2012;56(3):933-42.
207. Jauregui HO, Hayner NT, Driscoll JL, Williams-Holland R, Lipsky MH, Galletti PM. Trypan blue dye uptake and lactate dehydrogenase in adult rat hepatocytes--freshly isolated cells, cell suspensions, and primary monolayer cultures. In Vitro. 1981;17(12):1100-10.
208. Hazlehurst JM, Gathercole LL, Nasiri M, Armstrong MJ, Borrows S, Yu J, et al. Glucocorticoids fail to cause insulin resistance in human subcutaneous adipose tissue in vivo. The Journal of clinical endocrinology and metabolism. 2013;98(4):1631-40.
209. Bechmann LP, Hannivoort RA, Gerken G, Hotamisligil GS, Trauner M, Canbay A. The interaction of hepatic lipid and glucose metabolism in liver diseases. Journal of hepatology. 2012;56(4):952-64.
210. Tamura S, Shimomura I. Contribution of adipose tissue and de novo lipogenesis to nonalcoholic fatty liver disease. The Journal of clinical investigation. 2005;115(5):1139-42.
211. McGarry JD, Brown NF. The mitochondrial carnitine palmitoyltransferase system. From concept to molecular analysis. European journal of biochemistry / FEBS. 1997;244(1):1-14.
212. Kler RS, Sherratt HS, Turnbull DM. The measurement of mitochondrial beta-oxidation by release of 3H2O from [9,10-3H]hexadecanoate: application to skeletal muscle and the use of inhibitors as models of metabolic disease. Biochemical medicine and metabolic biology. 1992;47(2):145-56.
213. Gathercole LL, Morgan SA, Bujalska IJ, Hauton D, Stewart PM, Tomlinson JW. Regulation of lipogenesis by glucocorticoids and insulin in human adipose tissue. PloS one. 2011;6(10):e26223.

214. Jungermann K, Thurman RG. Hepatocyte heterogeneity in the metabolism of carbohydrates. Enzyme. 1992;46(1-3):33-58.
215. Sun Z, Shen W. [Effect of intermittent hypoxia on lipid metabolism in liver cells and the underlying mechanism]. Zhonghua Gan Zang Bing Za Zhi. 2014;22(5):369-73.
216. Mylonis I, Sembongi H, Befani C, Liakos P, Siniossoglou S, Simos G. Hypoxia causes triglyceride accumulation by HIF-1-mediated stimulation of lipin 1 expression. Journal of cell science. 2012;125(Pt 14):3485-93.
217. DiStefano MT, Danai LV, Roth Flach RJ, Chawla A, Pedersen DJ, Guilherme A, et al. The Lipid Droplet Protein Hypoxia-inducible Gene 2 Promotes Hepatic Triglyceride Deposition by Inhibiting Lipolysis. The Journal of biological chemistry. 2015;290(24):15175-84.
218. Savage DB, Semple RK. Recent insights into fatty liver, metabolic dyslipidaemia and their links to insulin resistance. Curr Opin Lipidol. 2010;21(4):329-36.
219. Pyper SR, Viswakarma N, Yu S, Reddy JK. PPARalpha: energy combustion, hypolipidemia, inflammation and cancer. Nucl Recept Signal. 2010;8:e002.
220. Lee AH, Scapa EF, Cohen DE, Glimcher LH. Regulation of hepatic lipogenesis by the transcription factor XBP1. Science. 2008;320(5882):1492-6.
221. Ma L, Robinson LN, Towle HC. ChREBP*Mlx is the principal mediator of glucose-induced gene expression in the liver. The Journal of biological chemistry. 2006;281(39):28721-30.
222. Videla L, Bernstein J, Israel Y. Metabolic alterations produced in the liver by chronic ethanol administration. Increased oxidative capacity. The Biochemical journal. 1973;134(2):507-14.
223. French SW. The role of hypoxia in the pathogenesis of alcoholic liver disease. Hepatology research : the official journal of the Japan Society of Hepatology. 2004;29(2):69-74.
224. Mantena SK, Vaughn DP, Andringa KK, Eccleston HB, King AL, Abrams GA, et al. High fat diet induces dysregulation of hepatic oxygen gradients and mitochondrial function in vivo. The Biochemical journal. 2009;417(1):183-93.
225. Bardag-Gorce F, French BA, Li J, Riley NE, Yuan QX, Valinluck V, et al. The importance of cycling of blood alcohol levels in the pathogenesis of experimental alcoholic liver disease in rats. Gastroenterology. 2002;123(1):325-35.
226. Hayashi N, Kasahara A, Kurosawa K, Sasaki Y, Fusamoto H, Sato N, et al. Oxygen supply to the liver in patients with alcoholic liver disease assessed by organ-reflectance spectrophotometry. Gastroenterology. 1985;88(4):881-6.
227. Yun JW, Son MJ, Abdelmegeed MA, Banerjee A, Morgan TR, Yoo SH, et al. Binge alcohol promotes hypoxic liver injury through a CYP2E1-HIF-1alpha-dependent apoptosis pathway in mice and humans. Free Radic Biol Med. 2014;77:183-94.
228. Nath B, Szabo G. Hypoxia and hypoxia inducible factors: diverse roles in liver diseases. Hepatology. 2012;55(2):622-33.
229. Rankin EB, Rha J, Selak MA, Unger TL, Keith B, Liu Q, et al. Hypoxia-inducible factor 2 regulates hepatic lipid metabolism. Molecular and cellular biology. 2009;29(16):4527-38.
230. Baker LC, Boult JK, Walker-Samuel S, Chung YL, Jamin Y, Ashcroft M, et al. The HIF-pathway inhibitor NSC-134754 induces metabolic changes and anti-

tumour activity while maintaining vascular function. British journal of cancer. 2012;106(10):1638-47.
231. Hickin JA, Ahmed A, Fucke K, Ashcroft M, Jones K. The synthesis and structure revision of NSC-134754. Chem Commun (Camb). 2014;50(10):1238-40.
232. Hsieh MM, Linde NS, Wynter A, Metzger M, Wong C, Langsetmo I, et al. HIF prolyl hydroxylase inhibition results in endogenous erythropoietin induction, erythrocytosis, and modest fetal hemoglobin expression in rhesus macaques. Blood. 2007;110(6):2140-7.
233. Fang Y, Zhang H, Zhong Y, Ding X. Prolyl hydroxylase 2 (PHD2) inhibition protects human renal epithelial cells and mice kidney from hypoxia injury. Oncotarget. 2016.
234. Heim C, Motsch B, Jalilova S, Bernhard W, Ramsperger-Gleixner M, Burzlaff N, et al. Reduction of obliterative bronchiolitis (OB) by prolyl-hydroxylase-inhibitors activating hypoxia-inducible transcription factors in an experimental mouse model. Transplant immunology. 2016.
235. Nagamine Y, Tojo K, Yazawa T, Takaki S, Baba Y, Goto T, et al. Inhibition of Prolyl Hydroxylase Attenuates Fas Ligand-induced Apoptosis and Lung Injury in Mice. Am J Respir Cell Mol Biol. 2016.
236. Kim SY, Yang EG. Recent Advances in Developing Inhibitors for Hypoxia-Inducible Factor Prolyl Hydroxylases and Their Therapeutic Implications. Molecules. 2015;20(11):20551-68.
237. Bruegge K, Jelkmann W, Metzen E. Hydroxylation of hypoxia-inducible transcription factors and chemical compounds targeting the HIF-alpha hydroxylases. Curr Med Chem. 2007;14(17):1853-62.
238. Mamede AC, Abrantes AM, Pedrosa L, Casalta-Lopes JE, Pires AS, Teixo RJ, et al. Beyond the limits of oxygen: effects of hypoxia in a hormone-independent prostate cancer cell line. ISRN Oncol. 2013;2013:918207.
239. Yang Y, Sun F, Zhang C, Wang H, Wu G, Wu Z. Hypoxia promotes cell proliferation by modulating E2F1 in chicken pulmonary arterial smooth muscle cells. J Anim Sci Biotechnol. 2013;4(1):28.
240. Gwak GY, Yoon JH, Kim KM, Lee HS, Chung JW, Gores GJ. Hypoxia stimulates proliferation of human hepatoma cells through the induction of hexokinase II expression. Journal of hepatology. 2005;42(3):358-64.
241. Xu Z, Liu E, Peng C, Li Y, He Z, Zhao C, et al. Role of hypoxia-inducible-1alpha in hepatocellular carcinoma cells using a Tet-on inducible system to regulate its expression in vitro. Oncology reports. 2012;27(2):573-8.
242. Liu Y, Ma Z, Zhao C, Wang Y, Wu G, Xiao J, et al. HIF-1alpha and HIF-2alpha are critically involved in hypoxia-induced lipid accumulation in hepatocytes through reducing PGC-1alpha-mediated fatty acid beta-oxidation. Toxicology letters. 2014;226(2):117-23.
243. Minamishima YA, Moslehi J, Padera RF, Bronson RT, Liao R, Kaelin WG, Jr. A feedback loop involving the Phd3 prolyl hydroxylase tunes the mammalian hypoxic response in vivo. Molecular and cellular biology. 2009;29(21):5729-41.
244. Scortegagna M, Ding K, Oktay Y, Gaur A, Thurmond F, Yan LJ, et al. Multiple organ pathology, metabolic abnormalities and impaired homeostasis of reactive oxygen species in Epas1-/- mice. Nature genetics. 2003;35(4):331-40.
245. Gimm T, Wiese M, Teschemacher B, Deggerich A, Schodel J, Knaup KX, et al. Hypoxia-inducible protein 2 is a novel lipid droplet protein and a specific

target gene of hypoxia-inducible factor-1. FASEB journal : official publication of the Federation of American Societies for Experimental Biology. 2010;24(11):4443-58.
246. Barnholt KE, Hoffman AR, Rock PB, Muza SR, Fulco CS, Braun B, et al. Endocrine responses to acute and chronic high-altitude exposure (4,300 meters): modulating effects of caloric restriction. American journal of physiology Endocrinology and metabolism. 2006;290(6):E1078-88.
247. Farias JG, Osorio J, Soto G, Brito J, Siques P, Reyes JG. Sustained acclimatization in Chilean mine workers subjected to chronic intermittent hypoxia. High Alt Med Biol. 2006;7(4):302-6.
248. Muratsubaki H, Enomoto K, Ichijoh Y, Yamamoto Y. Hypertriglyceridemia associated with decreased post-heparin plasma hepatic triglyceride lipase activity in hypoxic rats. Arch Physiol Biochem. 2003;111(5):449-54.
249. Jun JC, Shin MK, Yao Q, Bevans-Fonti S, Poole J, Drager LF, et al. Acute hypoxia induces hypertriglyceridemia by decreasing plasma triglyceride clearance in mice. American journal of physiology Endocrinology and metabolism. 2012;303(3):E377-88.
250. Koivunen P, Hirsila M, Gunzler V, Kivirikko KI, Myllyharju J. Catalytic properties of the asparaginyl hydroxylase (FIH) in the oxygen sensing pathway are distinct from those of its prolyl 4-hydroxylases. The Journal of biological chemistry. 2004;279(11):9899-904.
251. Peet DJ, Lando D, Whelan DA, Whitelaw ML, Gorman JJ. Oxygen-dependent asparagine hydroxylation. Methods Enzymol. 2004;381:467-87.
252. Bartenschlager R, Lohmann V. Replication of hepatitis C virus. The Journal of general virology. 2000;81(Pt 7):1631-48.
253. Lindenbach BD, Rice CM. Unravelling hepatitis C virus replication from genome to function. Nature. 2005;436(7053):933-8.
254. Pawlotsky JM. Pathophysiology of hepatitis C virus infection and related liver disease. Trends in microbiology. 2004;12(2):96-102.
255. Lavanchy D. The global burden of hepatitis C. Liver international : official journal of the International Association for the Study of the Liver. 2009;29 Suppl 1:74-81.
256. Lonardo A, Adinolfi LE, Loria P, Carulli N, Ruggiero G, Day CP. Steatosis and hepatitis C virus: mechanisms and significance for hepatic and extrahepatic disease. Gastroenterology. 2004;126(2):586-97.
257. Chang ML, Tsou YK, Hu TH, Lin CH, Lin WR, Sung CM, et al. Distinct patterns of the lipid alterations between genotype 1 and 2 chronic hepatitis C patients after viral clearance. PloS one. 2014;9(8):e104783.
258. Negro F. Abnormalities of lipid metabolism in hepatitis C virus infection. Gut. 2010;59(9):1279-87.
259. Farquhar MJ, McKeating JA. Primary hepatocytes as targets for hepatitis C virus replication. Journal of viral hepatitis. 2008;15(12):849-54.
260. Wilson GK, Stamataki Z. In vitro systems for the study of hepatitis C virus infection. Int J Hepatol. 2012;2012:292591.
261. Crabb DW, Liangpunsakul S. Alcohol and lipid metabolism. Journal of gastroenterology and hepatology. 2006;21 Suppl 3:S56-60.
262. Li M, Wang Q, Liu SA, Zhang JQ, Ju W, Quan M, et al. MicroRNA-185-5p mediates regulation of SREBP2 expression by hepatitis C virus core protein. World journal of gastroenterology : WJG. 2015;21(15):4517-25.

263. Loizides-Mangold U, Clement S, Alfonso-Garcia A, Branche E, Conzelmann S, Parisot C, et al. HCV 3a core protein increases lipid droplet cholesteryl ester content via a mechanism dependent on sphingolipid biosynthesis. PloS one. 2014;9(12):e115309.
264. Camus G, Schweiger M, Herker E, Harris C, Kondratowicz AS, Tsou CL, et al. The hepatitis C virus core protein inhibits adipose triglyceride lipase (ATGL)-mediated lipid mobilization and enhances the ATGL interaction with comparative gene identification 58 (CGI-58) and lipid droplets. The Journal of biological chemistry. 2014;289(52):35770-80.
265. Yu JW, Sun LJ, Liu W, Zhao YH, Kang P, Yan BZ. Hepatitis C virus core protein induces hepatic metabolism disorders through down-regulation of the SIRT1-AMPK signaling pathway. International journal of infectious diseases : IJID : official publication of the International Society for Infectious Diseases. 2013;17(7):e539-45.
266. Waris G, Felmlee DJ, Negro F, Siddiqui A. Hepatitis C virus induces proteolytic cleavage of sterol regulatory element binding proteins and stimulates their phosphorylation via oxidative stress. Journal of virology. 2007;81(15):8122-30.
267. Lerat H, Kammoun HL, Hainault I, Merour E, Higgs MR, Callens C, et al. Hepatitis C virus proteins induce lipogenesis and defective triglyceride secretion in transgenic mice. The Journal of biological chemistry. 2009;284(48):33466-74.
268. Horton JD, Goldstein JL, Brown MS. SREBPs: activators of the complete program of cholesterol and fatty acid synthesis in the liver. The Journal of clinical investigation. 2002;109(9):1125-31.
269. McRae S, Iqbal J, Sarkar-Dutta M, Lane S, Nagaraj A, Ali N, et al. The Hepatitis C Virus-induced NLRP3 Inflammasome Activates the Sterol Regulatory Element-binding Protein (SREBP) and Regulates Lipid Metabolism. The Journal of biological chemistry. 2016;291(7):3254-67.
270. Moriishi K, Mochizuki R, Moriya K, Miyamoto H, Mori Y, Abe T, et al. Critical role of PA28gamma in hepatitis C virus-associated steatogenesis and hepatocarcinogenesis. Proceedings of the National Academy of Sciences of the United States of America. 2007;104(5):1661-6.
271. Tanaka N, Moriya K, Kiyosawa K, Koike K, Gonzalez FJ, Aoyama T. PPARalpha activation is essential for HCV core protein-induced hepatic steatosis and hepatocellular carcinoma in mice. The Journal of clinical investigation. 2008;118(2):683-94.
272. Shimoike T, Koyama C, Murakami K, Suzuki R, Matsuura Y, Miyamura T, et al. Down-regulation of the internal ribosome entry site (IRES)-mediated translation of the hepatitis C virus: critical role of binding of the stem-loop IIId domain of IRES and the viral core protein. Virology. 2006;345(2):434-45.
273. Akil A, Wedeh G, Zahid Mustafa M, Gassama-Diagne A. SUMO1 depletion prevents lipid droplet accumulation and HCV replication. Archives of virology. 2016;161(1):141-8.
274. Bose SK, Kim H, Meyer K, Wolins N, Davidson NO, Ray R. Forkhead box transcription factor regulation and lipid accumulation by hepatitis C virus. Journal of virology. 2014;88(8):4195-203.
275. Douglas DN, Pu CH, Lewis JT, Bhat R, Anwar-Mohamed A, Logan M, et al. Oxidative Stress Attenuates Lipid Synthesis and Increases Mitochondrial Fatty

Acid Oxidation in Hepatoma Cells Infected with Hepatitis C Virus. The Journal of biological chemistry. 2016;291(4):1974-90.
276. Nelson HB, Tang H. Effect of cell growth on hepatitis C virus (HCV) replication and a mechanism of cell confluence-based inhibition of HCV RNA and protein expression. Journal of virology. 2006;80(3):1181-90.
277. Li Q, Pene V, Krishnamurthy S, Cha H, Liang TJ. Hepatitis C virus infection activates an innate pathway involving IKK-alpha in lipogenesis and viral assembly. Nature medicine. 2013;19(6):722-9.
278. Wu JM, Skill NJ, Maluccio MA. Evidence of aberrant lipid metabolism in hepatitis C and hepatocellular carcinoma. HPB : the official journal of the International Hepato Pancreato Biliary Association. 2010;12(9):625-36.
279. Choi SS, Bradrick S, Qiang G, Mostafavi A, Chaturvedi G, Weinman SA, et al. Up-regulation of Hedgehog pathway is associated with cellular permissiveness for hepatitis C virus replication. Hepatology. 2011;54(5):1580-90.
280. Peta V, Torti C, Milic N, Foca A, Abenavoli L. Adiponectin serum level in chronic hepatitis C infection and therapeutic profile. World J Hepatol. 2015;7(1):44-52.
281. Amako Y, Munakata T, Kohara M, Siddiqui A, Peers C, Harris M. Hepatitis C virus attenuates mitochondrial lipid beta-oxidation by downregulating mitochondrial trifunctional-protein expression. Journal of virology. 2015;89(8):4092-101.
282. Abid K, Pazienza V, de Gottardi A, Rubbia-Brandt L, Conne B, Pugnale P, et al. An in vitro model of hepatitis C virus genotype 3a-associated triglycerides accumulation. Journal of hepatology. 2005;42(5):744-51.
283. Leandro G, Mangia A, Hui J, Fabris P, Rubbia-Brandt L, Colloredo G, et al. Relationship between steatosis, inflammation, and fibrosis in chronic hepatitis C: a meta-analysis of individual patient data. Gastroenterology. 2006;130(6):1636-42.
284. Goossens N, Negro F. Is genotype 3 of the hepatitis C virus the new villain? Hepatology. 2014;59(6):2403-12.
285. Zimmerman HJ, Mac MF, Rappaport H, Alpert LK. Studies on the liver in diabetes mellitus. II. The significance of fatty metamorphosis and its correlation with insulin sensitivity. J Lab Clin Med. 1950;36(6):922-8.
286. Ballestri S, Nascimbeni F, Romagnoli D, Lonardo A. The independent predictors of non-alcoholic steatohepatitis and its individual histological features.: Insulin resistance, serum uric acid, metabolic syndrome, alanine aminotransferase and serum total cholesterol are a clue to pathogenesis and candidate targets for treatment. Hepatology research : the official journal of the Japan Society of Hepatology. 2016;46(11):1074-87.
287. Zhang Y, Zhang T, Zhang C, Tang F, Zhong N, Li H, et al. Identification of reciprocal causality between non-alcoholic fatty liver disease and metabolic syndrome by a simplified Bayesian network in a Chinese population. BMJ Open. 2015;5(9):e008204.
288. Musso G, Gambino R, Cassader M, Pagano G. Meta-analysis: natural history of non-alcoholic fatty liver disease (NAFLD) and diagnostic accuracy of non-invasive tests for liver disease severity. Ann Med. 2011;43(8):617-49.
289. Lonardo A, Ballestri S, Marchesini G, Angulo P, Loria P. Nonalcoholic fatty liver disease: a precursor of the metabolic syndrome. Digestive and liver disease :

official journal of the Italian Society of Gastroenterology and the Italian Association for the Study of the Liver. 2015;47(3):181-90.
290. Negro F, Forton D, Craxi A, Sulkowski MS, Feld JJ, Manns MP. Extrahepatic morbidity and mortality of chronic hepatitis C. Gastroenterology. 2015;149(6):1345-60.
291. Clark JM, Brancati FL, Diehl AM. Nonalcoholic fatty liver disease. Gastroenterology. 2002;122(6):1649-57.
292. Rubbia-Brandt L, Fabris P, Paganin S, Leandro G, Male PJ, Giostra E, et al. Steatosis affects chronic hepatitis C progression in a genotype specific way. Gut. 2004;53(3):406-12.
293. Monto A, Alonzo J, Watson JJ, Grunfeld C, Wright TL. Steatosis in chronic hepatitis C: relative contributions of obesity, diabetes mellitus, and alcohol. Hepatology. 2002;36(3):729-36.
294. Zaitoun AM, Al Mardini H, Awad S, Ukabam S, Makadisi S, Record CO. Quantitative assessment of fibrosis and steatosis in liver biopsies from patients with chronic hepatitis C. Journal of clinical pathology. 2001;54(6):461-5.
295. Doyle MA, Singer J, Lee T, Muir M, Cooper C. Improving treatment and liver fibrosis outcomes with metformin in HCV-HIV co-infected and HCV mono-infected patients with insulin resistance: study protocol for a randomized controlled trial. Trials. 2016;17(1):331.
296. Oliveira LP, Jesus RP, Boulhosa RS, Mendes CM, Lyra AC, Lyra LG. Metabolic syndrome in patients with chronic hepatitis C virus genotype 1 infection who do not have obesity or type 2 diabetes. Clinics (Sao Paulo). 2012;67(3):219-23.
297. Charlton MR, Burns JM, Pedersen RA, Watt KD, Heimbach JK, Dierkhising RA. Frequency and outcomes of liver transplantation for nonalcoholic steatohepatitis in the United States. Gastroenterology. 2011;141(4):1249-53.
298. El-Serag HB, Tran T, Everhart JE. Diabetes increases the risk of chronic liver disease and hepatocellular carcinoma. Gastroenterology. 2004;126(2):460-8.
299. Kowdley KV, Caldwell S. Nonalcoholic steatohepatitis: a twenty-first century epidemic? Journal of clinical gastroenterology. 2006;40 Suppl 1:S2-4.
300. Gholam PM, Flancbaum L, Machan JT, Charney DA, Kotler DP. Nonalcoholic fatty liver disease in severely obese subjects. The American journal of gastroenterology. 2007;102(2):399-408.
301. De Ridder RJ, Schoon EJ, Smulders JF, van Hout GC, Stockbrugger RW, Koek GH. Review article: Non-alcoholic fatty liver disease in morbidly obese patients and the effect of bariatric surgery. Alimentary pharmacology & therapeutics. 2007;26 Suppl 2:195-201.
302. Dowman JK, Tomlinson JW, Newsome PN. Pathogenesis of non-alcoholic fatty liver disease. QJM : monthly journal of the Association of Physicians. 2010;103(2):71-83.
303. Cusi K. Role of obesity and lipotoxicity in the development of nonalcoholic steatohepatitis: pathophysiology and clinical implications. Gastroenterology. 2012;142(4):711-25 e6.
304. Ortiz-Lopez C, Lomonaco R, Orsak B, Finch J, Chang Z, Kochunov VG, et al. Prevalence of prediabetes and diabetes and metabolic profile of patients with nonalcoholic fatty liver disease (NAFLD). Diabetes care. 2012;35(4):873-8.

305. Hazlehurst JM, Oprescu AI, Nikolaou N, Di Guida R, Grinbergs AE, Davies NP, et al. Dual-5alpha-Reductase Inhibition Promotes Hepatic Lipid Accumulation in Man. The Journal of clinical endocrinology and metabolism. 2016;101(1):103-13.
306. Armstrong MJ, Gaunt P, Aithal GP, Barton D, Hull D, Parker R, et al. Liraglutide safety and efficacy in patients with non-alcoholic steatohepatitis (LEAN): a multicentre, double-blind, randomised, placebo-controlled phase 2 study. Lancet. 2016;387(10019):679-90.
307. Finegood DT, Bergman RN, Vranic M. Estimation of endogenous glucose production during hyperinsulinemic-euglycemic glucose clamps. Comparison of unlabeled and labeled exogenous glucose infusates. Diabetes. 1987;36(8):914-24.
308. Steele R. Influences of glucose loading and of injected insulin on hepatic glucose output. Annals of the New York Academy of Sciences. 1959;82:420-30.
309. Folch J, Lees M, Sloane Stanley GH. A simple method for the isolation and purification of total lipides from animal tissues. The Journal of biological chemistry. 1957;226(1):497-509.
310. Lepage G, Roy CC. Direct transesterification of all classes of lipids in a one-step reaction. Journal of lipid research. 1986;27(1):114-20.
311. Fontana RJ, Lok AS. Noninvasive monitoring of patients with chronic hepatitis C. Hepatology. 2002;36(5 Suppl 1):S57-64.
312. Orlacchio A, Bolacchi F, Cadioli M, Bergamini A, Cozzolino V, Angelico M, et al. Evaluation of the severity of chronic hepatitis C with 3-T1H-MR spectroscopy. AJR American journal of roentgenology. 2008;190(5):1331-9.
313. Wellen KE, Hotamisligil GS. Inflammation, stress, and diabetes. The Journal of clinical investigation. 2005;115(5):1111-9.
314. Scherer PE. Adipose tissue: from lipid storage compartment to endocrine organ. Diabetes. 2006;55(6):1537-45.
315. Shoelson SE, Lee J, Goldfine AB. Inflammation and insulin resistance. The Journal of clinical investigation. 2006;116(7):1793-801.
316. Hotamisligil GS, Arner P, Caro JF, Atkinson RL, Spiegelman BM. Increased adipose tissue expression of tumor necrosis factor-alpha in human obesity and insulin resistance. The Journal of clinical investigation. 1995;95(5):2409-15.
317. Younossi ZM, McCullough AJ, Ong JP, Barnes DS, Post A, Tavill A, et al. Obesity and non-alcoholic fatty liver disease in chronic hepatitis C. Journal of clinical gastroenterology. 2004;38(8):705-9.
318. Tirado R, Masdeu MJ, Vigil L, Rigla M, Luna A, Rebasa P, et al. Impact of Bariatric Surgery on Heme Oxygenase-1, Inflammation, and Insulin Resistance in Morbid Obesity with Obstructive Sleep Apnea. Obesity surgery. 2017.
319. Hoy AJ, Bruce CR, Turpin SM, Morris AJ, Febbraio MA, Watt MJ. Adipose triglyceride lipase-null mice are resistant to high-fat diet-induced insulin resistance despite reduced energy expenditure and ectopic lipid accumulation. Endocrinology. 2011;152(1):48-58.
320. Hooper AJ, Adams LA, Burnett JR. Genetic determinants of hepatic steatosis in man. Journal of lipid research. 2011;52(4):593-617.
321. Monetti M, Nagaraj N, Sharma K, Mann M. Large-scale phosphosite quantification in tissues by a spike-in SILAC method. Nat Methods. 2011;8(8):655-8.

322. Kashyap S, Belfort R, Gastaldelli A, Pratipanawatr T, Berria R, Pratipanawatr W, et al. A sustained increase in plasma free fatty acids impairs insulin secretion in nondiabetic subjects genetically predisposed to develop type 2 diabetes. Diabetes. 2003;52(10):2461-74.
323. Boden G. Fatty acid-induced inflammation and insulin resistance in skeletal muscle and liver. Current diabetes reports. 2006;6(3):177-81.
324. Machado MV, Ferreira DM, Castro RE, Silvestre AR, Evangelista T, Coutinho J, et al. Liver and muscle in morbid obesity: the interplay of fatty liver and insulin resistance. PloS one. 2012;7(2):e31738.
325. Cuthbertson DJ, Irwin A, Sprung VS, Jones H, Pugh CJ, Daousi C, et al. Ectopic lipid storage in non-alcoholic fatty liver disease is not mediated by impaired mitochondrial oxidative capacity in skeletal muscle. Clin Sci (Lond). 2014;127(12):655-63.
326. Shintani Y, Fujie H, Miyoshi H, Tsutsumi T, Tsukamoto K, Kimura S, et al. Hepatitis C virus infection and diabetes: direct involvement of the virus in the development of insulin resistance. Gastroenterology. 2004;126(3):840-8.
327. Chien CH, Lin CL, Hu CC, Chang JJ, Chien RN. Clearance of Hepatitis C Virus Improves Insulin Resistance During and After Peginterferon and Ribavirin Therapy. Journal of interferon & cytokine research : the official journal of the International Society for Interferon and Cytokine Research. 2015;35(12):981-9.
328. Kawaguchi Y, Mizuta T, Oza N, Takahashi H, Ario K, Yoshimura T, et al. Eradication of hepatitis C virus by interferon improves whole-body insulin resistance and hyperinsulinaemia in patients with chronic hepatitis C. Liver international : official journal of the International Association for the Study of the Liver. 2009;29(6):871-7.
329. Miyaaki H, Ichikawa T, Taura N, Miuma S, Honda T, Shibata H, et al. Significance of Hepatic Insulin Clearance in Patients with Chronic Hepatitis C and Non-alcoholic Fatty Liver Disease. Intern Med. 2016;55(9):1049-54.
330. Oliveira LP, de Jesus RP, Boulhosa RS, Onofre T, Mendes CM, Vinhas L, et al. Factors Associated with Insulin Resistance in Patients with Chronic HCV Genotype 1 Infection without Obesity or Type 2 Diabetes. J Am Coll Nutr. 2016;35(5):436-42.
331. Desouky DE, Kasemy Z, Abdel-Hamid AE, Omar MS. Insulin resistance and prediabetes in hepatitis C virus patients. Am J Med Sci. 2015;350(2):77-80.
332. Grasso A, Malfatti F, Andraghetti G, Marenco S, Mazzucchelli C, Labanca S, et al. HOMA, BMI, and Serum Leptin Levels Variations during Antiviral Treatment Suggest Virus-Related Insulin Resistance in Noncirrhotic, Nonobese, and Nondiabetic Chronic Hepatitis C Genotype 1 Patients. Gastroenterol Res Pract. 2015;2015:975695.
333. Pais R, Rusu E, Zilisteanu D, Circiumaru A, Micu L, Voiculescu M, et al. Prevalence of steatosis and insulin resistance in patients with chronic hepatitis B compared with chronic hepatitis C and non-alcoholic fatty liver disease. European journal of internal medicine. 2015;26(1):30-6.
334. Hashemi SM, van der Poorten D, Barrera F, Bandara P, Lux O, Kench J, et al. Oxidative stress is closely associated with insulin resistance in genotypes 1 and 3 chronic hepatitis C. Hepatol Int. 2013;7(2):516-23.
335. Lambert JE, Bain VG, Ryan EA, Thomson AB, Clandinin MT. Elevated lipogenesis and diminished cholesterol synthesis in patients with hepatitis C viral infection compared to healthy humans. Hepatology. 2013;57(5):1697-704.

336. Cua IH, Hui JM, Bandara P, Kench JG, Farrell GC, McCaughan GW, et al. Insulin resistance and liver injury in hepatitis C is not associated with virus-specific changes in adipocytokines. Hepatology. 2007;46(1):66-73.
337. Jonsson JR, Moschen AR, Hickman IJ, Richardson MM, Kaser S, Clouston AD, et al. Adiponectin and its receptors in patients with chronic hepatitis C. Journal of hepatology. 2005;43(6):929-36.
338. Moucari R, Asselah T, Cazals-Hatem D, Voitot H, Boyer N, Ripault MP, et al. Insulin resistance in chronic hepatitis C: association with genotypes 1 and 4, serum HCV RNA level, and liver fibrosis. Gastroenterology. 2008;134(2):416-23.
339. Peres DP, Cheinquer H, Wolf FH, Cheinquer N, Falavigna M, Peres LD. Prevalence of insulin resistance in chronic hepatitis C genotype 1 and 3 patients. Ann Hepatol. 2013;12(6):871-5.
340. Orlacchio A, Bolacchi F, Angelico M, Mancini A, Cozzolino V, Cadioli M, et al. In vivo, high-field, 3-Tesla 1H MR spectroscopic assessment of liver fibrosis in HCV-correlated chronic liver disease. La Radiologia medica. 2008;113(2):289-99.
341. Forton DM, Thomas HC, Murphy CA, Allsop JM, Foster GR, Main J, et al. Hepatitis C and cognitive impairment in a cohort of patients with mild liver disease. Hepatology. 2002;35(2):433-9.
342. Bridge SH, Sheridan DA, Felmlee DJ, Nielsen SU, Thomas HC, Taylor-Robinson SD, et al. Insulin resistance and low-density apolipoprotein B-associated lipoviral particles in hepatitis C virus genotype 1 infection. Gut. 2011;60(5):680-7.
343. Imano E, Kanda T, Ishigami Y, Kubota M, Ikeda M, Matsuhisa M, et al. Interferon induces insulin resistance in patients with chronic active hepatitis C. Journal of hepatology. 1998;28(2):189-93.
344. Platanias LC, Uddin S, Yetter A, Sun XJ, White MF. The type I interferon receptor mediates tyrosine phosphorylation of insulin receptor substrate 2. The Journal of biological chemistry. 1996;271(1):278-82.
345. Thomas A, Belaidi E, Aron-Wisnewsky J, van der Zon GC, Levy P, Clement K, et al. Hypoxia-inducible factor prolyl hydroxylase 1 (PHD1) deficiency promotes hepatic steatosis and liver-specific insulin resistance in mice. Sci Rep. 2016;6:24618.
346. Taniguchi CM, Finger EC, Krieg AJ, Wu C, Diep AN, LaGory EL, et al. Cross-talk between hypoxia and insulin signaling through Phd3 regulates hepatic glucose and lipid metabolism and ameliorates diabetes. Nature medicine. 2013;19(10):1325-30.
347. Ramakrishnan SK, Taylor M, Qu A, Ahn SH, Suresh MV, Raghavendran K, et al. Loss of von Hippel-Lindau protein (VHL) increases systemic cholesterol levels through targeting hypoxia-inducible factor 2alpha and regulation of bile acid homeostasis. Molecular and cellular biology. 2014;34(7):1208-20.
348. Keith B, Johnson RS, Simon MC. HIF1alpha and HIF2alpha: sibling rivalry in hypoxic tumour growth and progression. Nat Rev Cancer. 2011;12(1):9-22.
349. Oem JK, Jackel-Cram C, Li YP, Zhou Y, Zhong J, Shimano H, et al. Activation of sterol regulatory element-binding protein 1c and fatty acid synthase transcription by hepatitis C virus non-structural protein 2. The Journal of general virology. 2008;89(Pt 5):1225-30.
350. Park CY, Jun HJ, Wakita T, Cheong JH, Hwang SB. Hepatitis C virus nonstructural 4B protein modulates sterol regulatory element-binding protein

signaling via the AKT pathway. The Journal of biological chemistry. 2009;284(14):9237-46.
351. Jackel-Cram C, Qiao L, Xiang Z, Brownlie R, Zhou Y, Babiuk L, et al. Hepatitis C virus genotype-3a core protein enhances sterol regulatory element-binding protein-1 activity through the phosphoinositide 3-kinase-Akt-2 pathway. The Journal of general virology. 2010;91(Pt 6):1388-95.
352. Xiang Z, Qiao L, Zhou Y, Babiuk LA, Liu Q. Hepatitis C virus nonstructural protein-5A activates sterol regulatory element-binding protein-1c through transcription factor Sp1. Biochemical and biophysical research communications. 2010;402(3):549-53.
353. Ballestri S, Zona S, Targher G, Romagnoli D, Baldelli E, Nascimbeni F, et al. Nonalcoholic fatty liver disease is associated with an almost twofold increased risk of incident type 2 diabetes and metabolic syndrome. Evidence from a systematic review and meta-analysis. Journal of gastroenterology and hepatology. 2016;31(5):936-44.
354. Kotronen A, Juurinen L, Tiikkainen M, Vehkavaara S, Yki-Jarvinen H. Increased liver fat, impaired insulin clearance, and hepatic and adipose tissue insulin resistance in type 2 diabetes. Gastroenterology. 2008;135(1):122-30.
355. Petta S, Amato M, Cabibi D, Camma C, Di Marco V, Giordano C, et al. Visceral adiposity index is associated with histological findings and high viral load in patients with chronic hepatitis C due to genotype 1. Hepatology. 2010;52(5):1543-52.
356. Aiba N, Hotta K, Yokoyama M, Wang G, Tabata M, Kamiya K, et al. Usefulness of pet ownership as a modulator of cardiac autonomic imbalance in patients with diabetes mellitus, hypertension, and/or hyperlipidemia. Am J Cardiol. 2012;109(8):1164-70.
357. Tam CS, Xie W, Johnson WD, Cefalu WT, Redman LM, Ravussin E. Defining insulin resistance from hyperinsulinemic-euglycemic clamps. Diabetes care. 2012;35(7):1605-10.
358. Bergman RN, Finegood DT, Ader M. Assessment of insulin sensitivity in vivo. Endocrine reviews. 1985;6(1):45-86.
359. Loria P, Marchesini G, Nascimbeni F, Ballestri S, Maurantonio M, Carubbi F, et al. Cardiovascular risk, lipidemic phenotype and steatosis. A comparative analysis of cirrhotic and non-cirrhotic liver disease due to varying etiology. Atherosclerosis. 2014;232(1):99-109.
360. Bedossa P, Moucari R, Chelbi E, Asselah T, Paradis V, Vidaud M, et al. Evidence for a role of nonalcoholic steatohepatitis in hepatitis C: a prospective study. Hepatology. 2007;46(2):380-7.
361. Bugianesi E, Manzini P, D'Antico S, Vanni E, Longo F, Leone N, et al. Relative contribution of iron burden, HFE mutations, and insulin resistance to fibrosis in nonalcoholic fatty liver. Hepatology. 2004;39(1):179-87.
362. Galambos JT, Wills CE. Relationship between 505 paired liver tests and biopsies in 242 obese patients. Gastroenterology. 1978;74(6):1191-5.
363. Nomura H, Kashiwagi S, Hayashi J, Kajiyama W, Ikematsu H, Noguchi A, et al. Prevalence of gallstone disease in a general population of Okinawa, Japan. American journal of epidemiology. 1988;128(3):598-605.
364. Lam NP, DeGuzman LJ, Pitrak D, Layden TJ. Clinical and histologic predictors of response to interferon-alpha in patients with chronic hepatitis C viral infection. Digestive diseases and sciences. 1994;39(12):2660-4.

365. Hickman IJ, Clouston AD, Macdonald GA, Purdie DM, Prins JB, Ash S, et al. Effect of weight reduction on liver histology and biochemistry in patients with chronic hepatitis C. Gut. 2002;51(1):89-94.
366. Eguchi Y, Eguchi T, Mizuta T, Ide Y, Yasutake T, Iwakiri R, et al. Visceral fat accumulation and insulin resistance are important factors in nonalcoholic fatty liver disease. Journal of gastroenterology. 2006;41(5):462-9.